Summer 2021

Characterization of a High Affinity Glutathione Transporter and Its Impact on Glutathione Depleted *Saccharomyces Cerevisiae*

Tirthankar Bandyopadhyay

CHARACTERIZATION OF A HIGH AFFINITY GLUTATHIONE TRANSPORTER AND ITS IMPACT ON GLUTATHIONE DEPLETED *SACCHAROMYCES CEREVISIAE*

by

Tirthankar Bandyopadhyay

Master of Science
University of Calcutta, 2011

Master of Science
University of South Carolina, 2015

Submitted in Partial Fulfillment of the Requirements

For the Degree of Doctor of Philosophy in

Chemistry

College of Arts and Sciences

University of South Carolina

2021

Accepted by:

Caryn E. Outten, Major Professor

Maksymilian Chruszcz, Committee Member

Andrew B. Greytak, Committee Member

Shannon Davis, Committee Member

Tracey L. Weldon, Interim Vice Provost and Dean of the Graduate School

DEDICATION

I would like to dedicate this dissertation to my parents, my “Ma” and “Babai”, Mrs. Rita Banerjee and Mr. Ram Jiban Bandyopadhyay. They have been a constant source of support, affection, courage, and inspiration during my growing up years. Because of them, I was able to nurture my creative abilities and a voracious appetite for having a good education. They also taught me to be kind and empathetic towards other people.

ACKNOWLEDGEMENTS

As I near the end of my graduate school tenure, I have nothing but gratitude for the people who have helped me on this journey. First, I would like to thank my personal support system, my parents back in India, Mrs. Rita Banerjee, and Mr. Ram Jiban Bandyopadhyay, without them my life would have probably run in a completely different direction. My best friend and my wife Dr. Malini Gupta, without whom I would not be here in the US and be in graduate school. I would also like to thank my in-laws, Mrs. Manikuntala Gupta, Mr. Tarun Ranjan Gupta and Mr. N. N. Sen for their continuous encouragement.

Besides my personal support system, I would also like to wholeheartedly thank my advisor and mentor Dr. Caryn E. Outten for providing me the opportunity to be a part of her lab. Not only has she taught me the nitty gritty of research-oriented lab work, but she has also provided moral support during some of the toughest phase of my graduate school journey. I would also like to thank my lab members (past and present) with whom I have shared a great camaraderie. I would like to specifically mention Dr. Angela Nadia Albetel, whom I have asked so many trivial questions, and she has patiently answered them all.

Graduate school has taught me perseverance and has given me a unique ability to handle stress and has made me a calmer person. These qualities, I will forever cultivate, and I believe they have prepared me to face and conquer newer challenges.

ABSTRACT

Thiol-disulfide redox homeostasis is integral for maintaining the redox status of proteins and other thiol-containing molecules within the cell. Among the many antioxidants and detoxifying enzymes and small peptides, glutathione (GSH) has proven to be critical for the preservation of function and structural integrity of the cell due to its functionality in areas like oxidative protein folding, thiol redox control, reactive oxygen species (ROS) and xenobiotics removal as well as iron regulation and Fe-S cluster biogenesis. Therefore, our studies are aimed at elucidating the factors that control GSH trafficking and metabolism in the model eukaryote *Saccharomyces cerevisiae* (baker's yeast). Using genetic modifications combined with targeted redox-sensitive and pH-sensitive green fluorescent protein probes, we have monitored GSH mediated pH changes and subsequently, changes in the redox potential, in the cytosol and mitochondrial matrix in response to fluctuating GSH levels in live yeast cells. These studies reveal that increased uptake of GSH or GSSG via overexpression of *HGT1*, which encodes a high affinity glutathione transporter, leads to significant changes in the intracellular pH in the cytosol and mitochondrial matrix, which, in turn, strongly impacts the redox state of GSH:GSSG pools. High intracellular GSH is known to be toxic for the cells, but it has not been shown how cells depleted of GSH (*gsh1Δ*) respond to increased GSH uptake. By expressing *HGT1* in GSH-depleted *gsh1*Δ cells, we show that *HGT1* overexpression partially rescues the inviability of GSH-deficient cells. Analysis of iron regulation and Fe-S cluster enzyme

activity demonstrates that *HGT1* overexpression reverses some of the Fe-S cluster biogenesis and iron homeostasis related defects in *gsh1*Δ strains. We also demonstrate that cysteine is a key amino acid for this rescue, suggesting that cysteine may partially substitute for GSH in *gsh1Δ* cells.

TABLE OF CONTENTS

LIST OF TABLES

LIST OF FIGURES

CHAPTER 1

INTRODUCTION AND SCOPE OF THESIS

Thiol redox regulation

Thiol redox biochemistry is assumed to play a pivotal role in understanding the cellular processes such as oxidant-dependent signaling and cell fate decisions (1). Oxidants in the form of reactive oxygen species (ROS) have potentially toxic effects and are linked to neurodegenerative disorders, aging and cancer. To prevent hyper-oxidation, cells depend on the concerted efforts of antioxidants and detoxifying enzymes (2).

The members of the thioredoxin (Trx) and glutaredoxins (Grx) families make up an extensive array of proteins, which execute central roles in redox biology, including the antioxidant response to oxygen and ROS. The yeast *Saccharomyces cerevisiae* encodes three thioredoxins, Trx1, Trx2 and Trx3, and four class I dithiol glutaredoxins, Grx1, Grx2, Grx8 and Mgp12 (3). These proteins facilitate the reduction of other proteins by cysteine thiol-disulfide exchange. They harbor an active site with a dithiol CxxC motif which is essential for function. Trxs further act as electron donors, for example, to peroxidases thereby linking cellular redox control with oxidative stress response. The related dithiol Grxs share many of the functions of Trxs but are reduced by the tripeptide glutathione (GSH) which functions as a central reservoir for upholding the cellular thiol redox balance (Figure 1.1) (4-9). GSH furthermore cooperates with, for example, glutathione peroxidases (Gpx) and glutathione-S-transferases and thus contributes significantly to the cellular

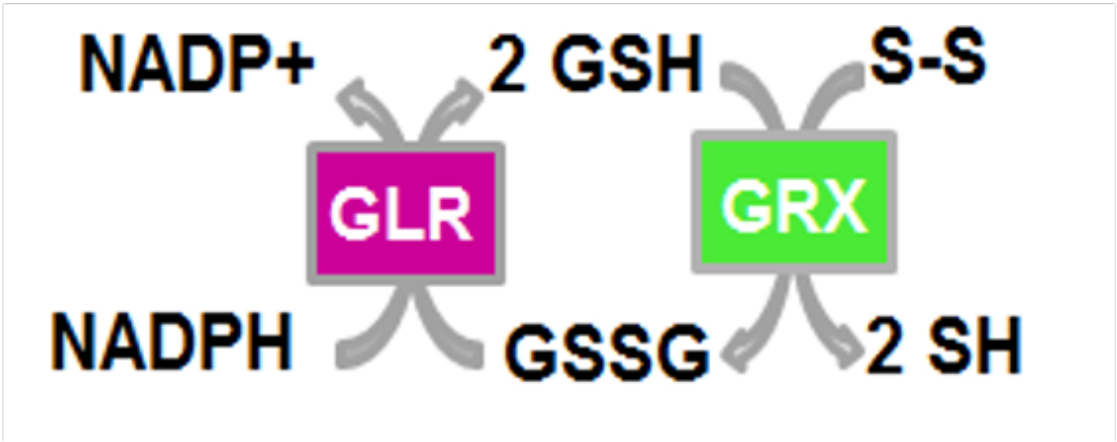

Figure 1.1: GSH-Dependent Thiol-Disulfide Redox System. Model illustrating the GSH/GRX redox regulatory pathway. GLR = Glutathione reductase, GRX = Glutaredoxin.

response to ROS. Oxidized glutathione (GSSG) and Trxs are reduced by cognate NADPH-dependent reductases. Simple eukaryotes such as *S. cerevisiae* tolerate the deletion of either glutathione reductase (Glr) or thioredoxin reductases (Trr), indicating that these proteins have partially overlapping functions. Yet, the simultaneous deletion of all genes encoding Trrs and Glrs, just like deletion of all Trx- and Grx- encoding genes, is lethal for *S. cerevisiae* (3,10).

Several members of the cellular thiol redox systems play central roles in the biosynthesis of iron-sulfur (Fe-S) proteins. GSH is an indispensable compound for the maturation of cytosolic and nuclear Fe-S proteins (11-16). Moreover, the mitochondrial glutaredoxin Grx5 and the cytosolic Grx3 serve as intermediate Fe-S cluster trafficking proteins in the mitochondrial iron-sulfur cluster (ISC) assembly and the cytosolic iron-sulfur assembly (CIA) systems (17-20). These proteins belong to the class II Grxs with a conserved monothiol CGFS active site motif and are, in contrast to most dithiol Grxs, not active in catalyzing dithiol-disulfide redox reactions (8,17). Additionally, *S. cerevisiae* contains the two cis-Golgi-localized monothiol Grx6 and Grx7 with yet ill-defined cellular roles (21-23).

Biosynthesis and regulation of GSH

GSH is the most abundant small intracellular thiol (-SH) molecule in eukaryotic cells. Its high intracellular concentration (2 – 12 mM) and low redox potential (-240 mV) enables GSH to provide reducing capacity for a number of biological reactions (24). As an antioxidant, GSH serves as an electron donor for GSH peroxidases that detoxify hydrogen peroxide by catalyzing its reduction to water (25). Furthermore, glutathione S-transferases (GSTs) are able to rid the cell of xenobiotics by forming GSH-dependent conjugates (26).

GSH is also involved in iron-sulfur (Fe-S) cluster biogenesis and maturation, redox signaling, apoptosis and metabolism of heavy metals (27,28).

GSH is synthesized in the cytosol from the amino acids glutamate, cysteine and glycine via two conserved ATP-dependent steps catalyzed by the enzymes γ-glutamylcysteine synthetase (Gsh1) and GSH synthetase (Gsh2) (29). In the first step, cysteine and glutamate are linked by Gsh1 to form γ-glutamylcysteine. The first reaction is the rate-limiting step and is regulated by cysteine availability. GSH is formed in the second reaction by Gsh2, which covalently links glycine to γ-glutamylcysteine (Figure 1.2) (30). While GSH is only made in the cytosol, its functions are required in other organelles such as the nucleus, endoplasmic reticulum, and mitochondria. In the nucleus, GSH maintains the redox state of critical protein sulfhydryls involved in DNA repair and expression, and functions as a hydrogen donor for ribonucleotide reductase (31). GSH is also found in the ER and mitochondrial intermembrane space (IMS) where thiol-containing proteins are oxidatively folded by disulfide oxidases and members of the protein disulfide isomerase (PDI) family. In these compartments, GSH is thought to function in disulfide proofreading by reducing mismatched disulfide bonds to ensure proper oxidative folding of imported proteins (32-35). Fe-S cluster biogenesis within the mitochondrial matrix also relies on distinct GSH pools within the organelle (36,37). Variations in GSH requirements for each organelle is accompanied by differences in total GSH concentration and the reduced to oxidized ratio. For instance, the GSH:GSSG ratio in the endoplasmic reticulum is less than 7:1, suggesting that the ER is relatively oxidizing (38). On the contrary, the cytosol and nucleus are very reducing with a

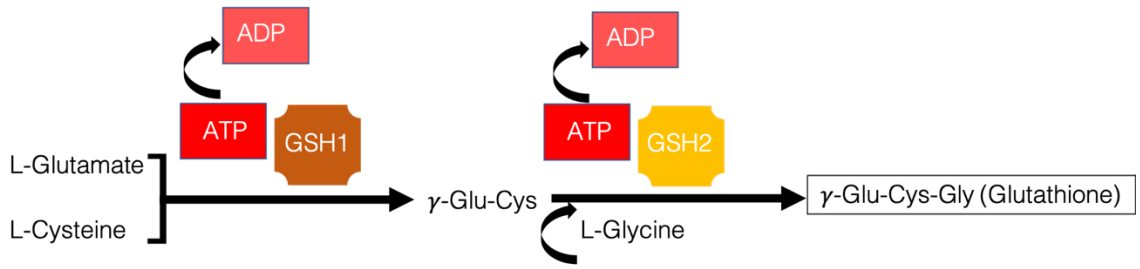

Figure 1.2: GSH biosynthesis pathway. GSH is synthesized in the cytosol via a two-step ATP-dependent enzymatic process. In the first step, γ-glutamylcysteine is formed by γ-glutamylcysteine synthetase (Gsh1). In the second step, glycine is added to the peptide via GSH synthetase (Gsh2).

GSH:GSSG ratio of 3000:1, while the mitochondrial matrix has a GSH:GSSG ratio of 900:1 (39).

Iron regulation and GSH metabolism in *Saccharomyces cerevisiae*

Tight regulation of intracellular iron levels is important for eukaryotic cells as high iron can be toxic due to its role in catalyzing the formation of hydroxyl radicals. Yet, it is indispensable for a variety of biological functions as a cofactor for several essential proteins such as Fe-S cluster proteins and hemoproteins. A few examples of important Fe-S proteins include DNA polymerases, nicotinamide adenine dinucleotide (NADH)-dehydrogenases, ferredoxins and aconitases (28). Hemoproteins contain a heme prosthetic group allowing them to carry out oxidative functions. One example of this is hemoglobin, a protein within red blood cells that is responsible for transporting oxygen to tissues. Other important hemoproteins include cytochromes, myoglobin, catalases, and peroxidases (40). Therefore, it comes as no surprise that disturbances in iron homeostasis or Fe-S cluster biogenesis are linked to many iron-related diseases such as Parkinson's diseases and anemia (17).

Fe-S clusters are a class of metal cofactors sensitive to iron oxidation and can consist of both Fe^{2+} and Fe^{3+} oxidation states. The cluster can be found in several different arrangements like [2Fe-2S], [4Fe-4S], [3Fe-3S] etc. (41) based on the type of protein the cluster is attached to, its local environment and the subcellular location of the protein. The assembly and biogenesis of the Fe-S cluster are mediated by a set of specific proteins localized in the mitochondria and cytosol, acting together in an ordered sequence of events. The initial steps of this whole process start in the mitochondrial matrix by approximately 18 proteins of the Iron-Sulfur Cluster (ISC) assembly machinery (42,43). The de novo

synthesis of the Fe-S cluster takes place with the help of a multimeric structure comprising a scaffold protein (IscU in bacteria, Isu1/Isu2 in yeast and ISCU in humans), a cysteine desulfurase complex (IscS in bacteria, Nfs1 in yeast and NFS1 in mammals), ferredoxin (electron provider) and frataxin (Fe^{2+} provider) (18,44,45). In mammals, one of the initial steps and probably the most critical one is converting cysteine to alanine by the cysteine desulfurase NFS1, a pyridoxal-5' phosphate-dependent transaminase. This reaction generates a persulfide species that delivers sulfane sulfur to the scaffold protein ISCU. The Fe-S cluster formed within the multimeric structure is tightly bound and must be transferred to the target proteins. This release from the multimeric structure is facilitated by the Hsp70 chaperone and Hsp40 co-chaperone system (Ssq1 and Jac1 in yeast), which directly binds to Isu1 and transfer its bound [2Fe-2S] cluster to one of the primary class II monothiol glutaredoxins (46).

The ISC machinery of the mitochondria generates a sulfur-containing entity, denoted as X-S (still unclear what this entity is), which must be transported to the cytosol and the nucleus for the maturation of their Fe-S protein maturation (Figure 1.3). This process requires an ATP-binding cassette (ABC) transporter Atm1 (ABCB7 in humans) located in the inner mitochondrial membrane, which exports the sulfur-containing entity to the cytosol (47). In the cytosol, approximately 11 proteins comprise the cytosolic iron-sulfur protein assembly (CIA), which generate both the cytosolic and nuclear Fe-S proteins (13,48-50), and begins with the assembly of a [4Fe-4S] cluster on the CIA multimeric scaffold protein Cfd1 (cytosolic Fe-S cluster deficient protein-1)-Nbp35 (nucleotide-binding protein 35) (51,52). The next step is transferring the [4Fe-4S] cluster from the Cfd1-Nbp35 scaffold complex to the recipient apo-proteins by the iron-

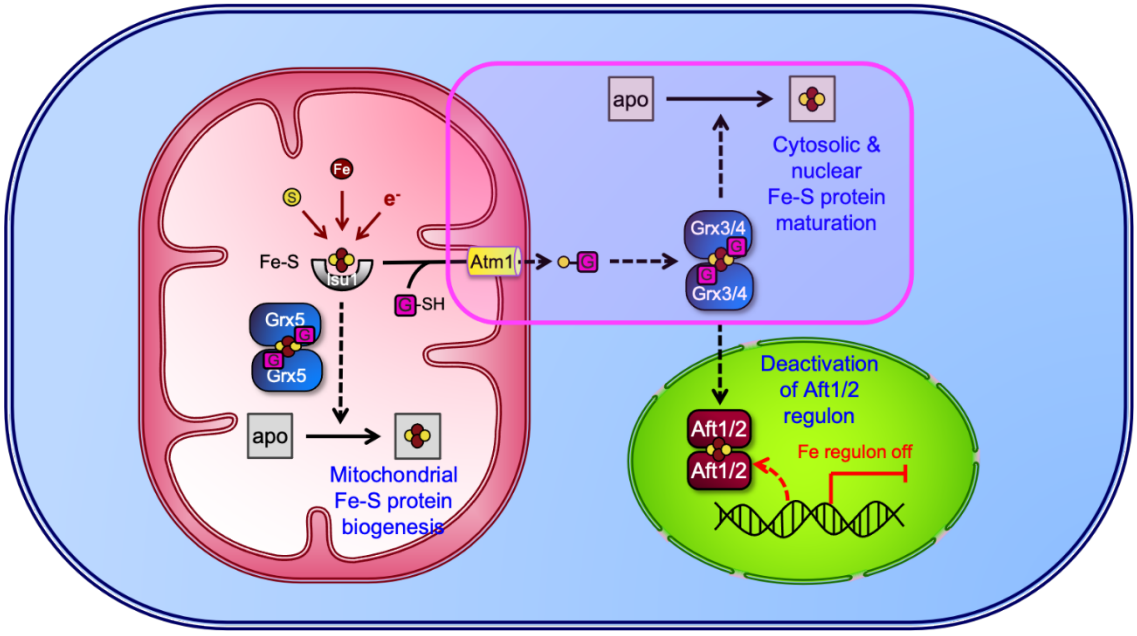

Figure 1.3: Molecular roles of Grx3/4 and GSH in iron regulation and cytosolic Fe-S cluster maturation. Fe-S clusters are synthesized in the mitochondrial matrix by proteins in the Fe-S cluster assembly pathway. Once assembled, an unknown sulfur-containing substance is transported out of the mitochondria by the Atm1 transporter. GSH is required for the export process. Grx3 and Grx4 use GSH to help coordinate Fe-S clusters. This Grx3/4- [2Fe-2S] complex is thought to form a heterodimer with Fra2 that then relays a signal to Aft1/2 and promotes its dissociation from target DNA. Aft1/2 is therefore deactivated and transported out of the mitochondria by the Msn5 exportin (not shown). Figure created by C. Outten.

only hydrogenase-like protein Nar1 and the CIA targeting complex comprising Cia1, Cia2 and Mms19 (51-56).

Role of Atm1 and GSH in Fe-S cluster biogenesis

Atm1 (an ABC transporter) connects the mitochondrial ISC and the cytosolic CIA machinery. Its homologues are also functionally conserved in other eukaryotes (57-63). It exports the sulfur containing entity X-S (produced in the mitochondria) to the cytosol (64,65). Deletion of Gsh1 (Glutathione synthetase 1; the first enzyme in the GSH biosynthetic pathway) in yeast has been shown to increase iron levels in the mitochondria (66). On the other hand, Atm1 deletion has been reported to deactivate two cytosolic Fe-S cluster proteins, nitrite reductase and xanthine dehydrogenase (62,66). Fe-S cluster insertion into the target apo-proteins requires a reduced thiol state of its cysteinyl sulfur ligand. This seems to be independent of the thiol reducing systems like GSH/Grx and thioredoxin (Trx) systems in yeast mitochondria (67), but in a mammalian system, oxidation of such cysteinyl residues represent a Parkinson's disease model as a consequence of GSH depletion (68). There is still some controversy regarding the specific type of substrate Atm1 binds. It has been reported that in an in vitro study that a GSH-ligated [2Fe-2S] cluster (GS_4) is a substrate of Atm1 (69), although it remains to be seen whether this substrate is physiologically relevant or not. The question remains as to whether [2Fe-2S] (GS_4) is an actual substrate or it is GSH that binds to Atm1 since the dissociation constant (K_m) is similar for both molecules (16,69,70). Other substrates of Atm1 that have been studied somewhat extensively are GSSG (oxidized glutathione) and GSSSG (glutathione persulfide). Schaedler *et al*., has suggested that GSSSG is the proper substrate of Atm1 and GSSG serves as a vehicle for that (37). They reasoned that GSSSG

is relatively more stable than GSSH and stimulates the ATPase activity of Atm1, which cannot be done by GSSH (37). These observations have somewhat been validated by Ida *et al*., who has shown the presence of sulfurated compounds in the cytosol, including polysulfides and GSH derivatives (11).

Recently, the laboratory of Michel Toledano has been at the forefront, suggesting a link between GSH-mediated thiol redox maintenance and iron metabolism. They have shown and suggested that GSH's primary function is to support iron metabolism, and it only plays a secondary role in maintaining the cell's thiol redox homeostasis (11). They showed that a unique genome-wide consequence of GSH depletion is an iron starvation-like response that remodeled most of the iron-dependent mitochondrial and extra-mitochondrial pathways (11). They also showed that GSH depletion did not cause any proteome-wide thiol oxidation and suggested that GSH is not indispensable for cytosolic thiol-redox maintenance. Inactivation of the thioredoxin pathway also showed that GSH alone was not capable of supporting the redox load of the cell on its own (11).

GSH transporters

The transport of GSH across many different membranes within a variety of organisms has been well studied. However, only a few GSH transporters have been identified. The first known GSH transporters were the mammalian multidrug resistance protein and yeast Ycf1 belonging to the ATP-binding cassette (ABC) transporter superfamily. The proteins were found to efflux excess GSH out of the cytoplasm at the plasma membrane of mammalian cells and vacuolar membrane in yeast, respectively (71,72). These transporters have a broad range of substrates and a relatively low affinity for GSH with K_m of approximately 15 mM (73,74). Furthermore, they were shown to

facilitate excretion from the cytosol and subsequent degradation of GSH and GSSG (72). Thus, the first identification of proteins that transport GSH, although with low affinity, were not representative of GSH uptake.

More recently, a yeast genomic search for candidate GSH transporters in *S. cerevisiae* led to the discovery of the plasma membrane localized Hgt1/Opt1 as the first high affinity GSH transporter. Hgt1 belongs to a novel and structurally uncharacterized oligopeptide transporter (OPT) family (75,76). Homologues of Hgt1 can be found in fungi, plants, bacteria, and archaea (77). The importance of GSH transport across the plasma membrane of mammalian cells have been established, yet no Hgt1 human homologues have been identified.

Many structural and mechanistic aspects of members of the OPT family are unknown. However, the dependence of the OPT members on proton-coupled transport has been established. In efforts to identify the substrate binding residues of Hgt1, an alanine scanning mutagenesis of polar or charged residues was done in the putative transmembrane domain (78,79). This study revealed four transmembrane domains (TMD1, TMD4, TMD9, TMD12) and a proline-rich intracellular loop (537-568) that are critical for GSH transport. Residues N124 of TMD1, Q222 of TMD4, Q526 of TMD9 and K562 of the intracellular loop were found to interact with the GSH directly or indirectly. A later analysis of residues important for substrate recognition revealed that both Q526 and F523 of TMD9 are required. Both residues are also conserved among OPT members known to uptake GSH. Characterization of Hgt1 has been an important step as it provides a model for how transporters bind and transport GSH across membranes.

In reference to other organelles, the endoplasmic reticulum (ER) is more oxidizing and early reports suggested that GSSG is selectively imported into the ER lumen (34). A subsequent study using rat liver microsomal vesicles found that reduced GSH is selectively imported into hepatic endoplasmic reticulum while GSSG is virtually nonpermeable. A portion of imported GSH is converted into the GSSG by the intraluminal oxidation of GSH. Interestingly, GSSG generated in the microsomal lumen scarcely exited from the vesicles. Therefore, retention of GSSG in the ER may be responsible for an oxidizing environment (80). In a recent search to identify a candidate ER GSH transporter, Ponsero *et al*., screened null and temperature-sensitive mutants of genes encoding ER transmembrane proteins. As a result, protein-conducting channel Sec61 was found to transport GSH into the ER of *S. cerevisiae* by facilitated diffusion (81). The discovery of an ER transporter has added to the list of already identified GSH-specific transporters located in various membranes in *S. cerevisiae* (Figure 1.4).

Scope of Thesis

The tripeptide glutathione (GSH) is an essential and multifaceted thiol-containing molecule found in all eukaryotic cells. Due to its role in cell signaling, detoxification, protein folding, iron homeostasis, maintenance of GSH pools and redox balance is crucial to the overall health of cells. The biosynthesis of GSH occurs exclusively in the cytosol. However, distinct GSH pools can be found in other subcellular compartments. The development of targeted GFP-based probes and intracellular measurement of GSH have contributed to our understanding of regulatory processes that affect the subcellular environment. Although, there remains many gaps in our understanding of organelle specific GSH regulation.

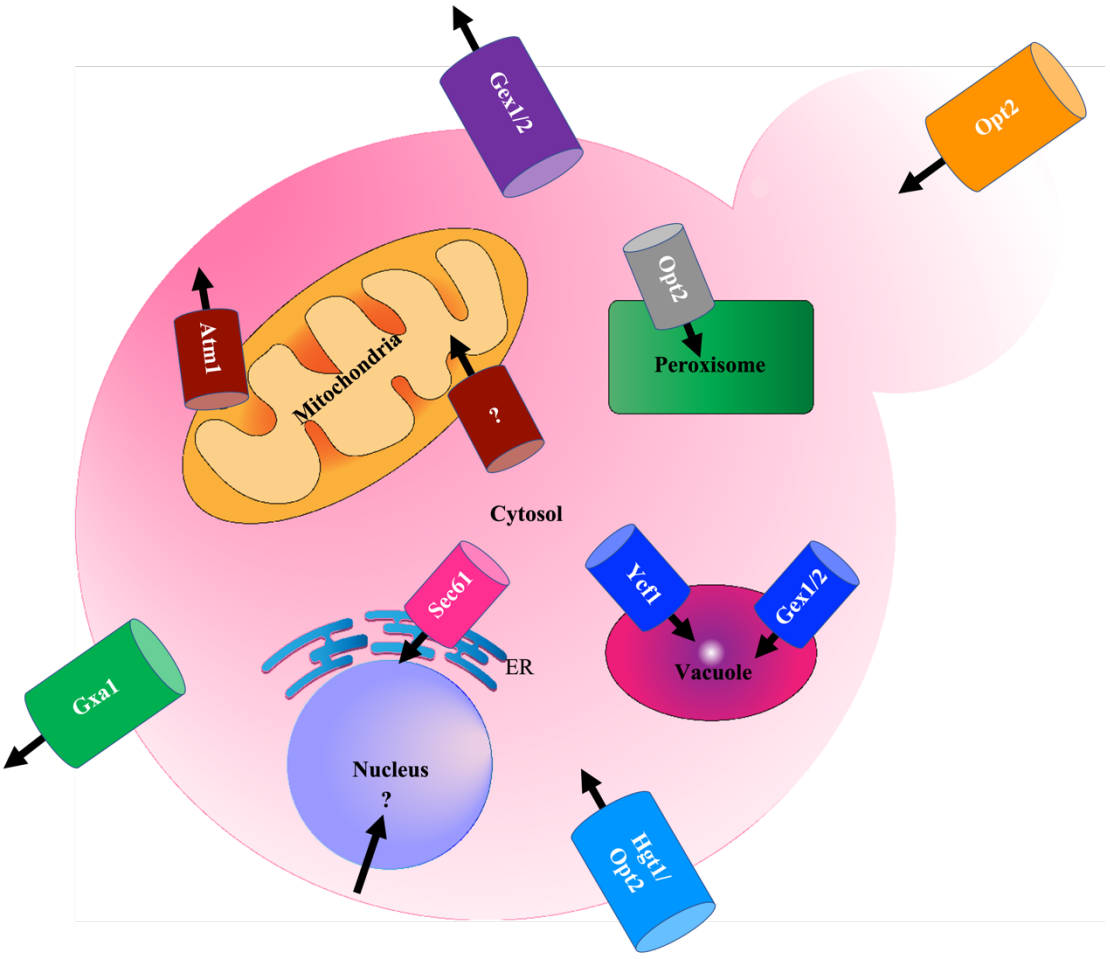

Figure 1.4: Schematic of known and predicted GSH transporters in *Saccharomyces cerevisiae.* GSH is exclusively made in the cytosol or may be imported from the extracellular environment. GSH synthesized and imported in the cytosol must be transported into subcellular compartments. The illustration shows known GSH transporters and organelles predicted to contain GSH transporters.

Chapter 2 is the study to gauge the effects of GSH overaccumulation on the subcellular redox state. We expressed a targeted GFP-based pH sensor (pHluorin) in WT and *gsh1*Δ cells, along with overexpressing a plasma membrane high affinity glutathione transporter (Hgt1) to study the impact of pH changes and subsequent changes in redox potential. GSH or GSSG was added to the media leading to GSH/GSSG overaccumulation and both the cytosol and matrix-pHluorin sensors helped in tracking the corresponding pH changes. These data helped us to better understand the impact of GSH trafficking on the GSH:GSSG thiol redox state of the cytosol and the mitochondrial matrix.

In chapter 3, we studied the impact of overexpressing Hgt1 transporter on cells depleted in GSH (*gsh1*Δ). We showed with the help of liquid growth curve assays that at lower GSH concentrations, *HGT1* overexpression helps in rescuing these cells from GSH auxotrophy, when GSH is added externally. We also showed with the help of redox westerns and with varying concentrations of GSH, that thiol redox state does not change when *HGT1* is overexpressed in *gsh1*Δ cells. With the help of site-directed mutagenesis we showed that mutated Hgt1 transporter has altered GSH uptake capability than the WT transporter. Surprisingly, we also observed less GSH uptake when *HGT1* is overexpressed, than that in the vector control cells. These results helped us in characterizing the Hgt1 transporter.

Chapter 4 showed us that cysteine can act as a substitute of GSH in *gsh1*Δ cells that overexpress *HGT1*. We demonstrated that even after growing these cells for 72 hrs, to make sure that there is absolutely no GSH, cysteine could still rescue these cells in the presence of Hgt1 transporter overexpression. Our results also confirm that *HGT1* overexpression in *gsh1*Δ cells partially rescue the iron starvation response associated with GSH depletion.

We performed enzymatic assays of both cytosolic and mitochondrial Fe-S cluster enzymes, along with a quantitative transcriptional reporter assay, to confirm these results. We also showed that the mere presence of iron in the growth media is not sufficient for the growth of *gsh1*Δ cells and additional nutrients are required for rescuing the cells from GSH auxotrophy. In our studies we showed the nutrient to be cysteine.

Techniques developed or modified for our research needs have been described in the last chapter. The procedures were emulated from published protocols to obtain the reported results. Some of these procedures have been done for the first time in our lab and needed extensive optimization. All the necessary details have been written for those procedures. Collectively, these experiments have allowed us to genetically modify intracellular GSH and assess the consequences of these changes in whole cell, cytosolic and mitochondrial compartments.

References

1. Aller, I., Rouhier, N., and Meyer, A. J. (2013) Development of roGFP2-derived redox probes for measurement of the glutathione redox potential in the cytosol of severely glutathione-deficient rml1 seedlings. *Front Plant Sci* **4**, 506
2. Mari, M., Morales, A., Colell, A., Garcia-Ruiz, C., and Fernandez-Checa, J. C. (2009) Mitochondrial glutathione, a key survival antioxidant. *Antioxid Redox Signal* **11**, 2685-2700
3. Herrero, E., Belli, G., and Casa, C. (2010) Structural and functional diversity of glutaredoxins in yeast. *Curr Protein Pept Sci* **11**, 659-668
4. Deponte, M. (2017) The Incomplete Glutathione Puzzle: Just Guessing at Numbers and Figures? *Antioxid Redox Signal* **27**, 1130-1161
5. Hanschmann, E. M., Godoy, J. R., Berndt, C., Hudemann, C., and Lillig, C. H. (2013) Thioredoxins, glutaredoxins, and peroxiredoxins--molecular mechanisms and health significance: from cofactors to antioxidants to redox signaling. *Antioxid Redox Signal* **19**, 1539-1605
6. Jacquot, J. P., and Zaffagnini, M. (2019) Thioredoxin and Glutaredoxin Systems Antioxidants Special Issue. *Antioxidants (Basel)* **8**
7. Lillig, C. H., and Berndt, C. (2013) Glutaredoxins in thiol/disulfide exchange. *Antioxid Redox Signal* **18**, 1654-1665
8. Lillig, C. H., Berndt, C., and Holmgren, A. (2008) Glutaredoxin systems. *Biochim Biophys Acta* **1780**, 1304-1317

9. Toledano, M. B., and Huang, M. E. (2017) The Unfinished Puzzle of Glutathione Physiological Functions, an Old Molecule That Still Retains Many Enigmas. *Antioxid Redox Signal* **27**, 1127-1129

10. Herrero, E., Ros, J., Belli, G., and Cabiscol, E. (2008) Redox control and oxidative stress in yeast cells. *Biochim Biophys Acta* **1780**, 1217-1235

11. Kumar, C., Igbaria, A., D'Autreaux, B., Planson, A. G., Junot, C., Godat, E., Bachhawat, A. K., Delaunay-Moisan, A., and Toledano, M. B. (2011) Glutathione revisited: a vital function in iron metabolism and ancillary role in thiol-redox control. *EMBO J* **30**, 2044-2056

12. Li, J., and Cowan, J. A. (2015) Glutathione-coordinated [2Fe-2S] cluster: a viable physiological substrate for mitochondrial ABCB7 transport. *Chem Commun (Camb)* **51**, 2253-2255

13. Lill, R., Dutkiewicz, R., Freibert, S. A., Heidenreich, T., Mascarenhas, J., Netz, D. J., Paul, V. D., Pierik, A. J., Richter, N., Stumpfig, M., Srinivasan, V., Stehling, O., and Muhlenhoff, U. (2015) The role of mitochondria and the CIA machinery in the maturation of cytosolic and nuclear iron-sulfur proteins. *Eur J Cell Biol* **94**, 280-291

14. Balk, J., and Schaedler, T. A. (2014) Iron cofactor assembly in plants. *Annu Rev Plant Biol* **65**, 125-153

15. Schaedler, T. A., Faust, B., Shintre, C. A., Carpenter, E. P., Srinivasan, V., van Veen, H. W., and Balk, J. (2015) Structures and functions of mitochondrial ABC transporters. *Biochem Soc Trans* **43**, 943-951

16. Srinivasan, V., Pierik, A. J., and Lill, R. (2014) Crystal structures of nucleotide-free and glutathione-bound mitochondrial ABC transporter Atm1. *Science* **343**, 1137-1140

17. Berndt, C., and Lillig, C. H. (2017) Glutathione, Glutaredoxins, and Iron. *Antioxid Redox Signal* **27**, 1235-1251

18. Braymer, J. J., and Lill, R. (2017) Iron-sulfur cluster biogenesis and trafficking in mitochondria. *J Biol Chem* **292**, 12754-12763

19. Jia, M., Sen, S., Wachnowsky, C., Fidai, I., Cowan, J. A., and Wysocki, V. H. (2020) Characterization of [2Fe-2S]-Cluster-Bridged Protein Complexes and Reaction Intermediates by use of Native Mass Spectrometric Methods. *Angew Chem Int Ed Engl* **59**, 6724-6728

20. Lill, R., and Freibert, S. A. (2020) Mechanisms of Mitochondrial Iron-Sulfur Protein Biogenesis. *Annu Rev Biochem* **89**, 471-499

21. Abdalla, M., Dai, Y. N., Chi, C. B., Cheng, W., Cao, D. D., Zhou, K., Ali, W., Chen, Y., and Zhou, C. Z. (2016) Crystal structure of yeast monothiol glutaredoxin Grx6 in complex with a glutathione-coordinated [2Fe-2S] cluster. *Acta Crystallogr F Struct Biol Commun* **72**, 732-737

22. Izquierdo, A., Casas, C., Muhlenhoff, U., Lillig, C. H., and Herrero, E. (2008) Saccharomyces cerevisiae Grx6 and Grx7 are monothiol glutaredoxins associated with the early secretory pathway. *Eukaryot Cell* **7**, 1415-1426

23. Mesecke, N., Mittler, S., Eckers, E., Herrmann, J. M., and Deponte, M. (2008) Two novel monothiol glutaredoxins from Saccharomyces cerevisiae provide further

insight into iron-sulfur cluster binding, oligomerization, and enzymatic activity of glutaredoxins. *Biochemistry* **47**, 1452-1463

24. Schafer, F. Q., and Buettner, G. R. (2001) Redox environment of the cell as viewed through the redox state of the glutathione disulfide/glutathione couple. *Free Radic Biol Med* **30**, 1191-1212

25. Dalvi, S. M., Patil, V. W., and Ramraje, N. N. (2012) The roles of glutathione, glutathione peroxidase, glutathione reductase and the carbonyl protein in pulmonary and extra pulmonary tuberculosis. *J Clin Diagn Res* **6**, 1462-1465

26. Couto, N., Wood, J., and Barber, J. (2016) The role of glutathione reductase and related enzymes on cellular redox homoeostasis network. *Free Radic Biol Med* **95**, 27-42

27. Aquilano, K., Baldelli, S., and Ciriolo, M. R. (2014) Glutathione: new roles in redox signaling for an old antioxidant. *Front Pharmacol* **5**, 196

28. Lill, R. (2009) Function and biogenesis of iron-sulphur proteins. *Nature* **460**, 831-838

29. Ribas, V., Garcia-Ruiz, C., and Fernandez-Checa, J. C. (2014) Glutathione and mitochondria. *Front Pharmacol* **5**, 151

30. Pompella, A., Visvikis, A., Paolicchi, A., De Tata, V., and Casini, A. F. (2003) The changing faces of glutathione, a cellular protagonist. *Biochem Pharmacol* **66**, 1499-1503

31. Valko, M., Leibfritz, D., Moncol, J., Cronin, M. T., Mazur, M., and Telser, J. (2007) Free radicals and antioxidants in normal physiological functions and human disease. *Int J Biochem Cell Biol* **39**, 44-84

32. Bien, M., Longen, S., Wagener, N., Chwalla, I., Herrmann, J. M., and Riemer, J. (2010) Mitochondrial disulfide bond formation is driven by intersubunit electron transfer in Erv1 and proofread by glutathione. *Mol Cell* **37**, 516-528

33. Chakravarthi, S., and Bulleid, N. J. (2004) Glutathione is required to regulate the formation of native disulfide bonds within proteins entering the secretory pathway. *J Biol Chem* **279**, 39872-39879

34. Hwang, C., Sinskey, A. J., and Lodish, H. F. (1992) Oxidized redox state of glutathione in the endoplasmic reticulum. *Science* **257**, 1496-1502

35. Molteni, S. N., Fassio, A., Ciriolo, M. R., Filomeni, G., Pasqualetto, E., Fagioli, C., and Sitia, R. (2004) Glutathione limits Ero1-dependent oxidation in the endoplasmic reticulum. *J Biol Chem* **279**, 32667-32673

36. Ayer, A., Tan, S. X., Grant, C. M., Meyer, A. J., Dawes, I. W., and Perrone, G. G. (2010) The critical role of glutathione in maintenance of the mitochondrial genome. *Free Radic Biol Med* **49**, 1956-1968

37. Schaedler, T. A., Thornton, J. D., Kruse, I., Schwarzlander, M., Meyer, A. J., van Veen, H. W., and Balk, J. (2014) A conserved mitochondrial ATP-binding cassette transporter exports glutathione polysulfide for cytosolic metal cofactor assembly. *J Biol Chem* **289**, 23264-23274

38. Montero, D., Tachibana, C., Rahr Winther, J., and Appenzeller-Herzog, C. (2013) Intracellular glutathione pools are heterogeneously concentrated. *Redox Biol* **1**, 508-513

39. Toledano, M. B., Delaunay-Moisan, A., Outten, C. E., and Igbaria, A. (2013) Functions and cellular compartmentation of the thioredoxin and glutathione pathways in yeast. *Antioxid Redox Signal* **18**, 1699-1711

40. Murphy, E. R., Sacco, R. E., Dickenson, A., Metzger, D. J., Hu, Y., Orndorff, P. E., and Connell, T. D. (2002) BhuR, a virulence-associated outer membrane protein of Bordetella avium, is required for the acquisition of iron from heme and hemoproteins. *Infect Immun* **70**, 5390-5403

41. Ribbe, M. W., Hu, Y., Hodgson, K. O., and Hedman, B. (2014) Biosynthesis of nitrogenase metalloclusters. *Chem Rev* **114**, 4063-4080

42. Freibert, S. A., Goldberg, A. V., Hacker, C., Molik, S., Dean, P., Williams, T. A., Nakjang, S., Long, S., Sendra, K., Bill, E., Heinz, E., Hirt, R. P., Lucocq, J. M., Embley, T. M., and Lill, R. (2017) Evolutionary conservation and in vitro reconstitution of microsporidian iron-sulfur cluster biosynthesis. *Nat Commun* **8**, 13932

43. Zheng, L., Cash, V. L., Flint, D. H., and Dean, D. R. (1998) Assembly of iron-sulfur clusters. Identification of an iscSUA-hscBA-fdx gene cluster from Azotobacter vinelandii. *J Biol Chem* **273**, 13264-13272

44. Boniecki, M. T., Freibert, S. A., Muhlenhoff, U., Lill, R., and Cygler, M. (2017) Structure and functional dynamics of the mitochondrial Fe/S cluster synthesis complex. *Nat Commun* **8**, 1287

45. Fox, N. G., Yu, X., Feng, X., Bailey, H. J., Martelli, A., Nabhan, J. F., Strain-Damerell, C., Bulawa, C., Yue, W. W., and Han, S. (2019) Structure of the human

frataxin-bound iron-sulfur cluster assembly complex provides insight into its activation mechanism. *Nat Commun* **10**, 2210

46. Uzarska, M. A., Dutkiewicz, R., Freibert, S. A., Lill, R., and Muhlenhoff, U. (2013) The mitochondrial Hsp70 chaperone Ssq1 facilitates Fe/S cluster transfer from Isu1 to Grx5 by complex formation. *Mol Biol Cell* **24**, 1830-1841

47. Kispal, G., Csere, P., Prohl, C., and Lill, R. (1999) The mitochondrial proteins Atm1p and Nfs1p are essential for biogenesis of cytosolic Fe/S proteins. *EMBO J* **18**, 3981-3989

48. Ciofi-Baffoni, S., Nasta, V., and Banci, L. (2018) Protein networks in the maturation of human iron-sulfur proteins. *Metallomics* **10**, 49-72

49. Netz, D. J., Mascarenhas, J., Stehling, O., Pierik, A. J., and Lill, R. (2014) Maturation of cytosolic and nuclear iron-sulfur proteins. *Trends Cell Biol* **24**, 303-312

50. Paul, V. D., and Lill, R. (2015) Biogenesis of cytosolic and nuclear iron-sulfur proteins and their role in genome stability. *Biochim Biophys Acta* **1853**, 1528-1539

51. Balk, J., Aguilar Netz, D. J., Tepper, K., Pierik, A. J., and Lill, R. (2005) The essential WD40 protein Cia1 is involved in a late step of cytosolic and nuclear iron-sulfur protein assembly. *Mol Cell Biol* **25**, 10833-10841

52. Balk, J., Pierik, A. J., Netz, D. J., Muhlenhoff, U., and Lill, R. (2004) The hydrogenase-like Nar1p is essential for maturation of cytosolic and nuclear iron-sulphur proteins. *EMBO J* **23**, 2105-2115

53. Gari, K., Leon Ortiz, A. M., Borel, V., Flynn, H., Skehel, J. M., and Boulton, S. J. (2012) MMS19 links cytoplasmic iron-sulfur cluster assembly to DNA metabolism. *Science* **337**, 243-245

54. Song, D., and Lee, F. S. (2008) A role for IOP1 in mammalian cytosolic iron-sulfur protein biogenesis. *J Biol Chem* **283**, 9231-9238

55. Srinivasan, V., Netz, D. J., Webert, H., Mascarenhas, J., Pierik, A. J., Michel, H., and Lill, R. (2007) Structure of the yeast WD40 domain protein Cia1, a component acting late in iron-sulfur protein biogenesis. *Structure* **15**, 1246-1257

56. Stehling, O., Mascarenhas, J., Vashisht, A. A., Sheftel, A. D., Niggemeyer, B., Rosser, R., Pierik, A. J., Wohlschlegel, J. A., and Lill, R. (2013) Human CIA2A-FAM96A and CIA2B-FAM96B integrate iron homeostasis and maturation of different subsets of cytosolic-nuclear iron-sulfur proteins. *Cell Metab* **18**, 187-198

57. Bernard, D. G., Cheng, Y., Zhao, Y., and Balk, J. (2009) An allelic mutant series of ATM3 reveals its key role in the biogenesis of cytosolic iron-sulfur proteins in Arabidopsis. *Plant Physiol* **151**, 590-602

58. Cavadini, P., Biasiotto, G., Poli, M., Levi, S., Verardi, R., Zanella, I., Derosas, M., Ingrassia, R., Corrado, M., and Arosio, P. (2007) RNA silencing of the mitochondrial ABCB7 transporter in HeLa cells causes an iron-deficient phenotype with mitochondrial iron overload. *Blood* **109**, 3552-3559

59. Garcia-Santamarina, S., Uzarska, M. A., Festa, R. A., Lill, R., and Thiele, D. J. (2017) Cryptococcus neoformans Iron-Sulfur Protein Biogenesis Machinery Is a Novel Layer of Protection against Cu Stress. *mBio* **8**

60. Kushnir, S., Babiychuk, E., Storozhenko, S., Davey, M. W., Papenbrock, J., De Rycke, R., Engler, G., Stephan, U. W., Lange, H., Kispal, G., Lill, R., and Van Montagu, M. (2001) A mutation of the mitochondrial ABC transporter Sta1 leads to dwarfism and chlorosis in the Arabidopsis mutant starik. *Plant Cell* **13**, 89-100

61. Pondarre, C., Antiochos, B. B., Campagna, D. R., Clarke, S. L., Greer, E. L., Deck, K. M., McDonald, A., Han, A. P., Medlock, A., Kutok, J. L., Anderson, S. A., Eisenstein, R. S., and Fleming, M. D. (2006) The mitochondrial ATP-binding cassette transporter Abcb7 is essential in mice and participates in cytosolic iron-sulfur cluster biogenesis. *Hum Mol Genet* **15**, 953-964

62. Wang, Z., Ma, T., Huang, Y., Wang, J., Chen, Y., Kistler, H. C., Ma, Z., and Yin, Y. (2019) A fungal ABC transporter FgAtm1 regulates iron homeostasis via the transcription factor cascade FgAreA-HapX. *PLoS Pathog* **15**, e1007791

63. Zuo, J., Wu, Z., Li, Y., Shen, Z., Feng, X., Zhang, M., and Ye, H. (2017) Mitochondrial ABC Transporter ATM3 Is Essential for Cytosolic Iron-Sulfur Cluster Assembly. *Plant Physiol* **173**, 2096-2109

64. Kispal, G., Csere, P., Guiard, B., and Lill, R. (1997) The ABC transporter Atm1p is required for mitochondrial iron homeostasis. *FEBS Lett* **418**, 346-350

65. Miao, R., Kim, H., Koppolu, U. M., Ellis, E. A., Scott, R. A., and Lindahl, P. A. (2009) Biophysical characterization of the iron in mitochondria from Atm1p-depleted Saccharomyces cerevisiae. *Biochemistry* **48**, 9556-9568

66. Sipos, K., Lange, H., Fekete, Z., Ullmann, P., Lill, R., and Kispal, G. (2002) Maturation of cytosolic iron-sulfur proteins requires glutathione. *J Biol Chem* **277**, 26944-26949

67. Braymer, J. J., Stumpfig, M., Thelen, S., Muhlenhoff, U., and Lill, R. (2019) Depletion of thiol reducing capacity impairs cytosolic but not mitochondrial iron-sulfur protein assembly machineries. *Biochim Biophys Acta Mol Cell Res* **1866**, 240-251

68. Balijepalli, S., Boyd, M. R., and Ravindranath, V. (1999) Inhibition of mitochondrial complex I by haloperidol: the role of thiol oxidation. *Neuropharmacology* **38**, 567-577

69. Qi, W., Li, J., and Cowan, J. A. (2014) A structural model for glutathione-complexed iron-sulfur cluster as a substrate for ABCB7-type transporters. *Chem Commun (Camb)* **50**, 3795-3798

70. Kuhnke, G., Neumann, K., Muhlenhoff, U., and Lill, R. (2006) Stimulation of the ATPase activity of the yeast mitochondrial ABC transporter Atm1p by thiol compounds. *Mol Membr Biol* **23**, 173-184

71. Li, L., Lee, T. K., Meier, P. J., and Ballatori, N. (1998) Identification of glutathione as a driving force and leukotriene C4 as a substrate for oatp1, the hepatic sinusoidal organic solute transporter. *J Biol Chem* **273**, 16184-16191

72. Rebbeor, J. F., Connolly, G. C., Dumont, M. E., and Ballatori, N. (1998) ATP-dependent transport of reduced glutathione on YCF1, the yeast orthologue of mammalian multidrug resistance associated proteins. *J Biol Chem* **273**, 33449-33454

73. Rebbeor, J. F., Connolly, G. C., Dumont, M. E., and Ballatori, N. (1998) ATP-dependent transport of reduced glutathione in yeast secretory vesicles. *Biochem J* **334 (Pt 3)**, 723-729

74. Rappa, G., Lorico, A., Flavell, R. A., and Sartorelli, A. C. (1997) Evidence that the multidrug resistance protein (MRP) functions as a co-transporter of glutathione and natural product toxins. *Cancer Res* **57**, 5232-5237

75. Bourbouloux, A., Shahi, P., Chakladar, A., Delrot, S., and Bachhawat, A. K. (2000) Hgt1p, a high affinity glutathione transporter from the yeast Saccharomyces cerevisiae. *J Biol Chem* **275**, 13259-13265

76. Bachhawat, A. K., Thakur, A., Kaur, J., and Zulkifli, M. (2013) Glutathione transporters. *Biochim Biophys Acta* **1830**, 3154-3164

77. Curie, C., Panaviene, Z., Loulergue, C., Dellaporta, S. L., Briat, J. F., and Walker, E. L. (2001) Maize yellow stripe1 encodes a membrane protein directly involved in Fe(III) uptake. *Nature* **409**, 346-349

78. Thakur, A., and Bachhawat, A. K. (2010) The role of transmembrane domain 9 in substrate recognition by the fungal high-affinity glutathione transporters. *Biochem J* **429**, 593-602

79. Kaur, J., and Bachhawat, A. K. (2009) Gln-222 in transmembrane domain 4 and Gln-526 in transmembrane domain 9 are critical for substrate recognition in the yeast high affinity glutathione transporter, Hgt1p. *J Biol Chem* **284**, 23872-23884

80. Banhegyi, G., Lusini, L., Puskas, F., Rossi, R., Fulceri, R., Braun, L., Mile, V., di Simplicio, P., Mandl, J., and Benedetti, A. (1999) Preferential transport of glutathione versus glutathione disulfide in rat liver microsomal vesicles. *J Biol Chem* **274**, 12213-12216

81. Ponsero, A. J., Igbaria, A., Darch, M. A., Miled, S., Outten, C. E., Winther, J. R., Palais, G., D'Autréaux, B., Delaunay-Moisan, A., and Toledano, M. B. (2017)

Endoplasmic Reticulum Transport of Glutathione by Sec61 Is Regulated by Ero1 and Bip. *Mol Cell* **67**, 962-973.e965

CHAPTER 2

SUBCELLULAR PH MEASUREMENTS SHOW A SUBSTANTIAL DECREASE OF INTRACELLULAR PH WITH HGT1 OVEREXPRESSION UPON GSH/GSSG ADDITION

Abstract

Maintenance of thiol redox balance is essential in both prokaryotes and eukaryotes. Glutathione (GSH) has been shown to be a major cellular redox buffer and is critical for mitochondrial functions such as Fe-S cluster biogenesis, oxidative phosphorylation, and mitochondrial protein import. Since thiol-disulfide exchange reactions involve the transfer of protons as well as electrons, their redox potentials vary with pH. These pH differences should be taken into consideration while calculating the cytosol, mitochondrial matrix, and the intermembrane space (IMS) redox potentials. Previous studies in our group have suggested that GSH:GSSG redox state in subcellular compartments such as the cytosol, matrix and IMS is maintained separately, but it is still unclear how perturbations of the GSH:GSSG couple influence the distribution of GSH:GSSG between these compartments. Our goal is to understand the mechanisms for maintaining thiol redox equilibrium in different compartments under severe redox stress and determine how GSH:GSSG is exchanged between the cytosol, matrix and IMS under these conditions. Using a targeted GFP-based pH sensor in yeast strains overexpressing a plasma membrane GSH:GSSG transporter, we examined the pH changes in the cytosol and mitochondrial compartments

upon addition of GSH/GSSG to the growth medium. GSH and GSSG overaccumulation were found to directly impact changes in the subcellular compartments, suggesting concomitant changes in redox potentials as well.

Introduction

The different organelles in the cell all maintain their own specific pH, which is used to define and maintain the processes associated with each organelle. Yeast vacuoles, for instance, are reported to have an acidic pH (82-84). The proton gradient across the vacuolar membrane has been shown to be essential for the transport of various compounds (85,86). The pH of the mitochondrial matrix on the other hand is reported to be alkaline, with a pH of 8.0 (87). This is the result of electron transport chain activity, which pumps protons from matrix across the inner membrane to generate a proton gradient (ΔpH) and an electrochemical gradient ($\Delta\psi$) constituting the proton motive force used for ATP synthesis. The pH of the peroxisomal lumen is reported to be 8.2; this coincides with the pH optimum for most peroxisomal enzymes, which lies between 8 and 9 (88). Lastly the secretory pathway has been shown to acidify from 7.2 in the endoplasmic reticulum to 5.2 in the secretory granules. This acidification is necessary for proper protein sorting and modification (89). Another way the internal pH impacts the cell is the protein conformation and enzyme activity. Various ionization states of acidic and basic amino acid side chains are heavily dependent on pH changes during protein synthesis. The stepwise acidification is crucial for sorting of proteins and during their post-translational modification (89,90). There are numerous examples where the pH dependence of ER to Golgi transport (91-93) and Golgi to ER retrieval of ER-resident proteins have been shown (94-97). The studies have appropriately and adequately demonstrated the importance of pH maintenance in

different compartments and shown that its alterations can contribute to the pathology of certain diseases.

These examples illustrate that organelle-specific pH is a crucial parameter in cell physiology. Therefore, an accurate organelle-specific tool to monitor changes in pH is required to fully understand cellular functioning. Current techniques used to measure the pH are ^{31}P NMR (98), probing with pH-sensitive fluorescent dyes (99,100), deploying radioactively labelled membrane-permeable weak acids or bases (101), as well as the equilibrium distribution of benzoic acid (102). However, none of these techniques are organelle specific and thus they are bound to result in measurement of an average cellular pH. In recent years, green fluorescent protein (GFP)-based sensors for detecting intracellular pH changes (pHluorin) and changes in GSH: GSSG redox couple (rxYFP and roGFP1/2) have been developed (103-105). Since then, numerous studies have used these sensors to shed light on subcellular pH changes and redox state changes inside the cell.

The GFP-based redox sensor rxYFP is engineered with two spatially adjacent cysteines (103) that forms a disulfide, leading to a 2-fold reduction in the intrinsic fluorescence. In rxYFP, the cysteines specifically equilibrate with GSH and GSSG via rapid disulfide exchange reactions catalyzed by glutaredoxins (Grxs). Although these sensors found application in GSH:GSSG redox potential measurements in the cytosol, nucleus, mitochondrial matrix and intermembrane space in *S. cerevisiae* (106,107), the quenching of the YFP fluorescence by halides and other small anions posed a problem for fluorescence measurements (108) (Figure 2.1).

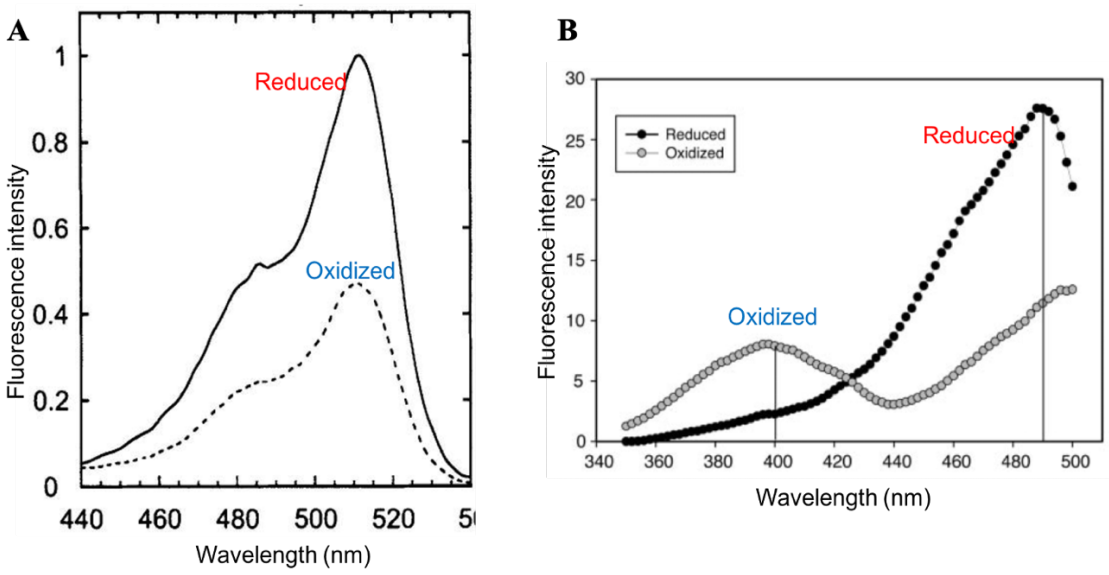

Figure 2.1: Excitation spectra of redox sensors (A) rxYFP (103) and (B) roGFP2 (104).

This demanded generation of more advanced redox-sensitive sensors for GSH:GSSG redox couple, leading to creation of roGFP2. The major advantage that the roGFP2 sensor has over rxYFP is that it is ratiometric in nature, i.e., the sensor has two excitation peaks that increase or decrease in opposite directions when the sensor is oxidized or reduced. Therefore, the ratio of peak intensities at 405 and 488 nm allows calculation of the degree of oxidation, thereby cancelling out any variations in light intensity or photobleaching of the sensor (109).

Disulfide exchange reactions with Grxs involve proton transfer thereby creating a dependence on pH changes. Fortunately, pH-sensitive GFP (pHluorin) (Figure 2.2) provides a convenient way of measuring subcellular pH, which allows determination of the redox state of subcellular compartments (105). Like roGFP2, pHluorins are ratiometric sensors. This protein displays a reversible excitation ratio change between higher and lower pH (pH 7.5 and 5.5) i.e., the intensity of the two excitation peaks either decrease or increase in opposite directions with changes in pH, thus providing a more accurate *in vivo* fluorescence pH measurement.

Experimental Procedures

Yeast strains, plasmids, media, and growth conditions: *Saccharomyces cerevisiae* strains used in this study were WT BY4741 (*MAT*a *his3*Δ1 *leu2*Δ0 *met15*Δ0 *ura3*Δ0) and *gsh1Δ* BY4741. The *gsh1Δ* strain was made by deleting the *GSH1* gene in WT BY4741 using pGSH1KO (made by former lab member Dr. Crystal Conaway McGee; see plasmid construction for more information). Yeast transformations were performed using standard lithium acetate protocol (110).

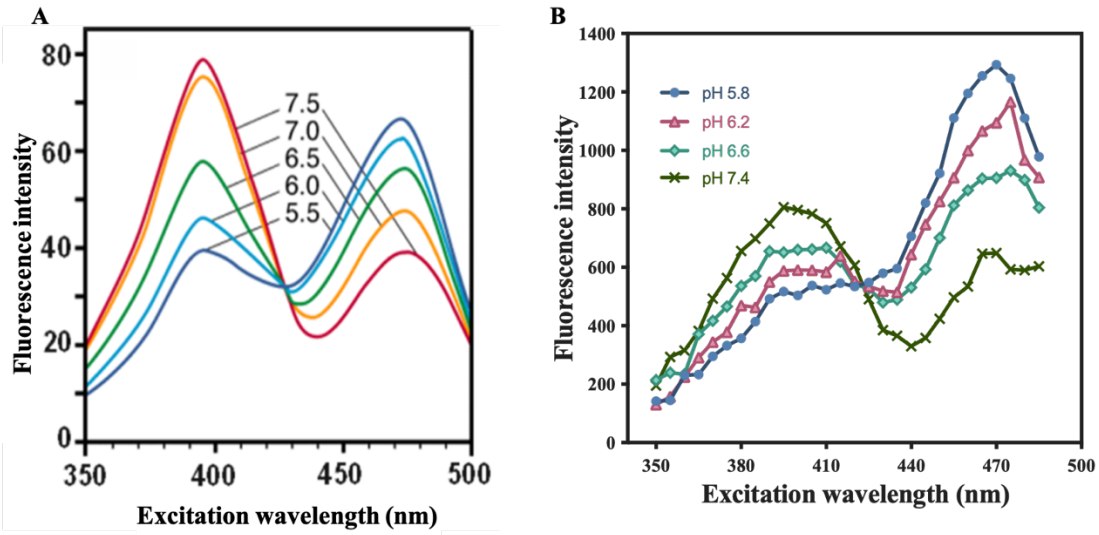

Figure 2.2: Excitation spectra of (A) pHluorin (105) and excitation spectra of pHluorin (B) as verified experimentally in the lab.

Yeast strains were cultured at 30 °C in synthetic complete (SC) media (US Biological) supplemented with 2% glucose as the carbon source with appropriate amino acids. Low fluorescent yeast nitrogen base (YNB without folic acid and riboflavin, Sunrise Science Products) was used for calibration and measurement experiments Nalgene MF75 vacuum filter units (PES membrane, sterile, Thermo Scientific) were used to sterile filter the media before use.

Plasmid construction: The *GSH1* deletion plasmid pGSH1KO (YIp, *HIS3*) was made by former lab member Dr. Crystal Conaway McGee (111). The yeast integrating plasmid was linearized with EcoRI and inserted into the genome of yeast strains via homologous recombination. The p416*TEF-HGT1* plasmid (*CEN, URA3*) which allows *HGT1* to be constitutively expressed via the *TEF1* promoter was a kind gift from Dr. Michael Toledano (CEA-Saclay, Université Paris-Saclay, Gif-sur-Yvette, France) and originally created by Dr. Anand Kumar Bachhawat (Institute of Microbial Technology, Chandigarh, India) (11,75,78). The URA3-2μ plasmids expressing cytosolic and matrix pHluorin sensors (pYES2-*URA3*-2μ) (112) were obtained from Dr. Gertien Smits (Department of Molecular Biology and Microbial Food Safety, Swammerdam Institute for Life Sciences (SILS), University of Amsterdam, The Netherlands). The *LEU2-CEN* pHluorin expression plasmids, pJH700 (cytosol-pHluorin) and pJH701 (matrix-pHluorin) were previously constructed by a former member of the lab, Dr. Jingjing Hu (113). Briefly, a SacII enzyme site was added to the original cytosolic and matrix pHluorin sensors (pYES2-*URA3*-2μ) after the *CYC1* terminator by site-directed mutagenesis. These plasmids were digested with SpeI and SacII, and the fragment containing the *ACT1*

promoter, the coding sequence of pHluorin, and the *CYC1* terminator was inserted into the *LEU2-CEN* vector pRS415, yielding pJH700 and pJH701.

Redox western blot analysis of rxYFP (performed by Dr. Max Darch) (114): Redox western blot analysis of rxYFP was adapted from previous methods (107). Briefly, cells were grown and treated with GSH or GSSG with the indicated concentrations. Cell cultures were acid-quenched with trichloroacetic acid (TCA) (Sigma) (15% (w/v) final concentration) at 4 °C for 20 min. Five OD600 U of cells were harvested by centrifugation and resuspended in 1 ml of 10% TCA. Following glass bead lysis, the lysed cells were transferred to a new tube and pelleted by centrifugation. The pellet was resuspended in 500 µl of 1X non-reducing SDS sample buffer containing 40 mM N-ethylmaleimide (NEM) (Sigma). Following a 10-min incubation at room temperature, the proteins were separated on a 16% Tris-glycine gel (Invitrogen). Reduced and oxidized forms of rxYFP were analyzed by quantitative immunoblot using an Odyssey Infrared Imaging System (LI-COR, Lincoln, NE).

In situ pHluorin calibration and pHluorin measurements: Yeast strains were grown in 50-ml centrifuge tubes to an OD_{600} of 1.0 in SC media, centrifuged for 5 minutes at 3000 rpm and resuspended in phosphate buffered saline (PBS) containing 100 µg/ml digitonin. After 10 min, cells were washed with PBS and put on ice. Cells were transferred to 96-well black plates (Thermo Scientific, Catalog # 237108) to an OD_{600} of 1.0 in McIlvain's buffer of pH values ranging from 4.8 to 8.4 (112). pHluorin fluorescence emission was measured at 512 nm using the Biotek Synergy H1 plate reader providing excitation at 390 nm and 470 nm. Background fluorescence for a WT strain not expressing pHluorin was subtracted from the measurements. The ratio of emission intensity (R_{390}/R_{470}) was calculated and

plotted against the corresponding buffer pH. The data were fit to the following sigmoidal curve function using GraphPad Prism: $R = R_{min} + \frac{(R_{max} - R_{min})}{1+10^{(pK_a - pH)}}$ where R is the ratio of fluorescence emission intensities for excitation at 390 nm and 470 nm (R_{390}/R_{470}) at a given pH, R_{min} is the ratio (R_{390}/R_{470}) measured for cells in the most acidic (pH 4.8) buffer, and R_{max} is the ratio (R_{390}/R_{470}) measured for cells in the most alkaline (pH 8.4) buffer. The constant pK_a was determined from the inflection point of the curve. Individual pH values were calculated from experimental R readings using R_{max}, R_{min}, and pK_a from the calibration curves and the following equation: $\text{pH} = \text{p}K_a + log\left[\frac{(R - R_{min})}{(R_{max} - R)}\right]$ (115). Please refer to chapter 5 for the detailed procedure.

Redox potential calculations: The rxYFP sensor equilibrates with GSH:GSSG pools according to the following reaction (Scheme 1) (107):

$\text{rxYFP}^{\text{SH}}_{\text{SH}} + \text{GSSG} \Leftrightarrow \text{rxYFP}^{\text{S}}_{\text{S}} + 2\text{GSH}$ (Scheme 1)

The ratio of oxidized to reduced rxYFP and the standard reduction potential of rxYFP and was inserted into the Nernst equation (Eq. 1) to measure the redox potential of GSH:GSSG pools in live cells.

$\Delta E = \Delta E^{\circ} - \frac{RT}{nF} \ln Q$ (Eq. 1)

In this equation, R is the gas constant (8.314 J K^{-1} mol^{-1}), T is the temperature in K, n is the number of electrons, F is Faraday's constant (96, 485 C mol^{-1}). At 30 °C, for the reaction shown in Scheme 1, Eq. 1 can be rewritten as Eq. 2.

$E_{\text{GSH}} = E^{\circ\prime}_{GSH} - \frac{60.1\ mV}{2} \log \frac{[GSH]2}{[GSSG]}$

$= E^{\circ\prime}_{rxYFP} - \frac{60.1\ mV}{2} \log \frac{\mathrm{rxYFP^{SH}_{SH}}}{\mathrm{rxYFP^{S}_{S}}} = E_{rxYFP}$ (Eq. 2)

At pH 7.0, the standard reduction potential of rxYFP ($E^{\circ\prime}_{rxYFP}$) is -265 mV (107). The reduction potential of rxYFP at different pH values was calculated using the expression shown in Eq. 3 (24).

$E_{\mathrm{pH}} = E^{\circ\prime}$ + [(pH - 7.0) x -60.1] mV (Eq. 3)

Results

Calibration of the pHluorin sensor: To verify that the pHluorin sensor is responsive to pH changes in live yeast cells, we used McIlvaine's citrate/phosphate buffer to make buffers of different pHs, starting from 4.8 to 8.4 with 0.2 units of graduation as described in the methods section. Live yeast cells permeabilized with digitonin were incubated in these different buffers to measure the responsiveness of the intracellular pH sensor. We performed an excitation scan between wavelengths 350 nm and 485 nm with the emission set at 512 nm and observed that the fluorescent response of the pHluorin sensor was ratiometric as expected (Figure 2.2B). For *in vivo* calibration of the pH sensor, the data were fit with the Henderson-Hasselbalch equation to yield calibration curves yielding pK_a values close to the expected pHluorin pK_a of 6.9 (Figure 2.3 and 2.4) (116). It can be clearly observed that the calibration curve of both the cytosol- and the matrix-pHluorin sensors follow the sigmoidal pattern that is typical for pH-dependent measurements.

Measurement of pH changes upon GSH/GSSG overaccumulation: Previous studies have shown and suggested that glutathione transport in leaf tissues was mediated with proton co-transport (117), and later it was shown that in yeast, Hgt1 acts as a symporter, i.e., it imports GSH or GSSH along with protons into the cell (75).

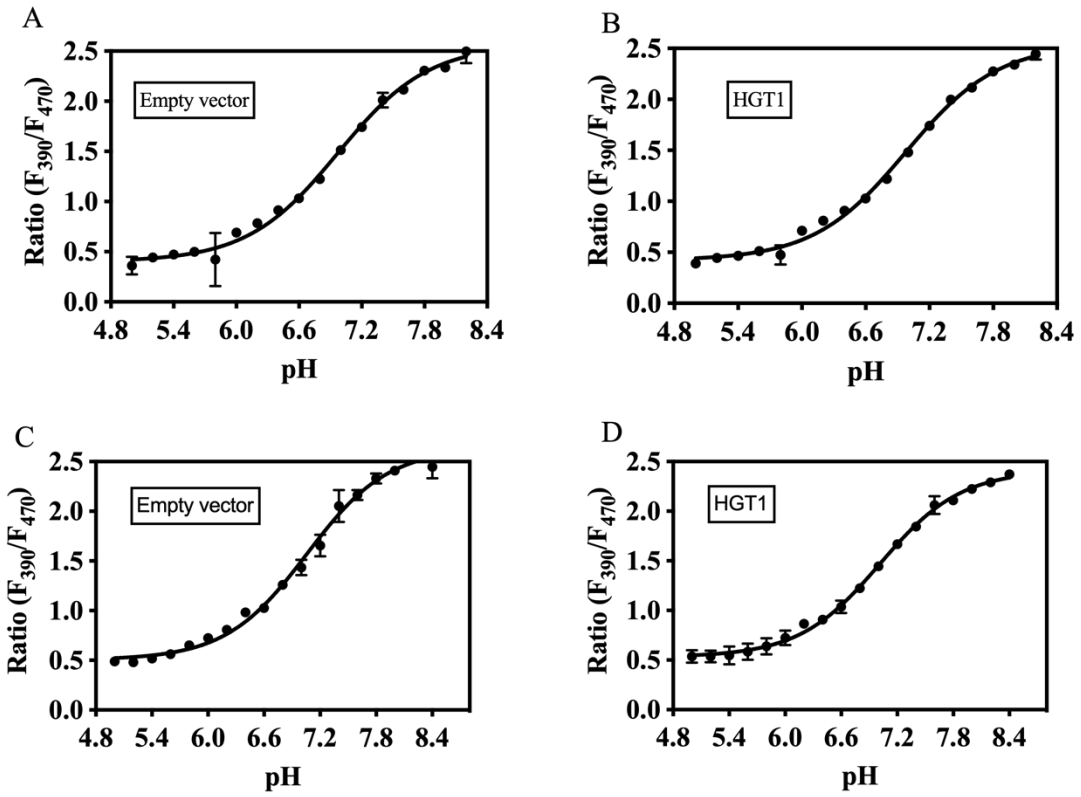

Figure 2.3: Calibration curve of matrix-pHluorin with empty vector and *HGT1* overexpression (A and B) and cytosol-pHluorin with empty vector and *HGT1* overexpression (C and D) in WT BY4741 cells. Calibration curves were fit using the Henderson-Hasselbalch equation [pK_a; (A) 6.97 ± 0.07, (B) 6.98 ± 0.05, (C) 7.06 ± 0.08, (D) 7.02 ± 0.05].

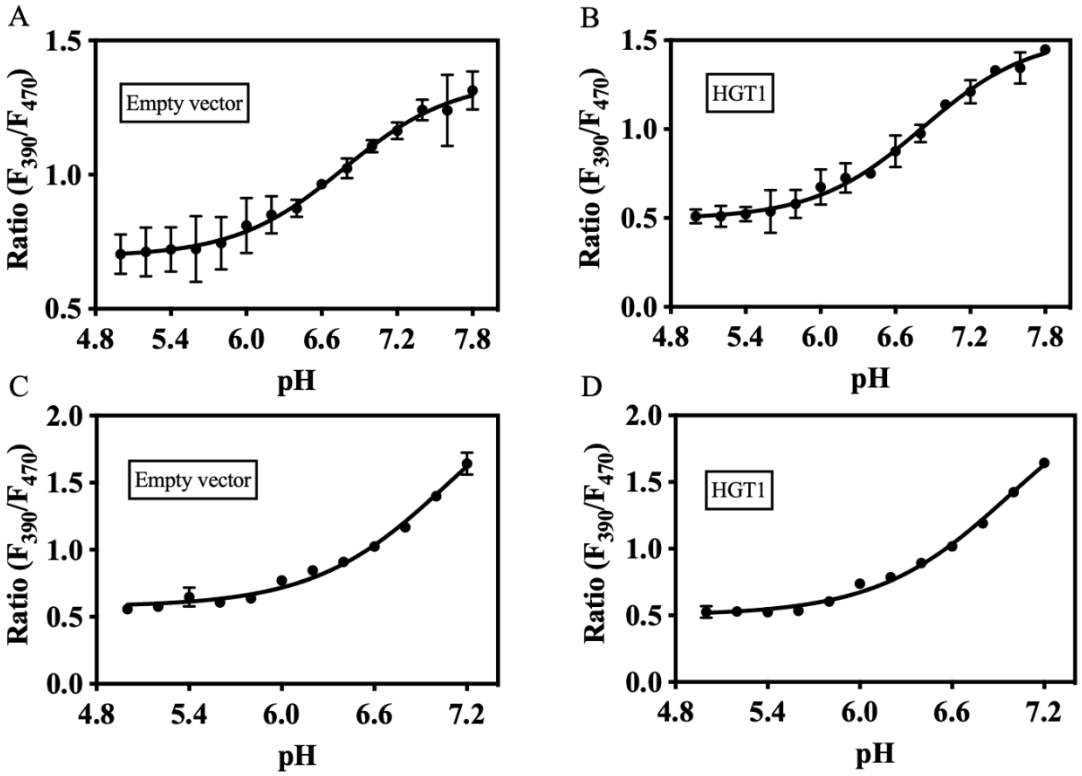

Figure 2.4: Calibration curve of matrix-pHluorin with empty vector and *HGT1* overexpression (A and B) and cytosol-pHluorin with empty vector and *HGT1* overexpression (C and D) in *gsh1Δ* cells. Calibration curves were fit using the Henderson-Hasselbalch equation [p*K*a; (A) 6.78 ± 0.21, (B) 6.82 ± 0.13, (C) 7.08 ± 0.18, (D) 6.98 ± 0.11].

As a result, it is imperative to measure the changes in pH, and subsequently, changes in the redox potential *in vivo*, since the redox state is strongly affected by intracellular pH. Since Hgt1 is the primary GSH:GSSG transporter on the plasma membrane of yeast, we wanted to see if Hgt1-mediated GSH:GSSG transport alters the intracellular pH value. We expressed the cytosol sensor in WT and *gsh1Δ* cells, with the Hgt1 transporter and the vector control overexpression and performed pH measurements at different time points after GSH or GSSG addition. As expected, we did not observe any change in pH both in the WT as well as the *gsh1*Δ cells transformed with the vector control plasmid, even after the addition of lower as well as higher concentrations of GSH or GSSG (Figure 2.5). The initial pH values (at zero time point, before adding GSH/GSSG) of the cytosol in the WT cells are comparable to the previously published results (7.2 - 7.4) (112). The *gsh1Δ* cells showed very similar pH values to WT cells in the absence of *HGT1* overexpression, indicating that GSH levels do not strongly impact pH balance in the cell. After the addition of GSH or GSSG into the growth media, the cytosol pH of the Hgt1 cells (in both WT and *gsh1Δ*) significantly decreases by 0.4 pH units within 5 to 30 minutes (Figure 2.6). After approximately 1 hour, the cytosol pH values stop decreasing, becomes stable but stays at the lower pH, at least until the 2-hr time point. This data suggests that Hgt1 overexpressed cells import GSH/GSSG as well as protons, as expected and that ultimately would lead to a rapid and persistent decrease in intracellular pH. It was also interesting to observe that around the GSH concentration of 20 – 30 μM, especially in WT + *HGT1* overexpression cells, the visible change in pH started to show up. It seemed that the impact of GSSG addition to the media is a bit more pronounced than that of GSH addition, both in WT as well as *gsh1*Δ cells. It might be because one GSSG molecule can be reduced to two GSH

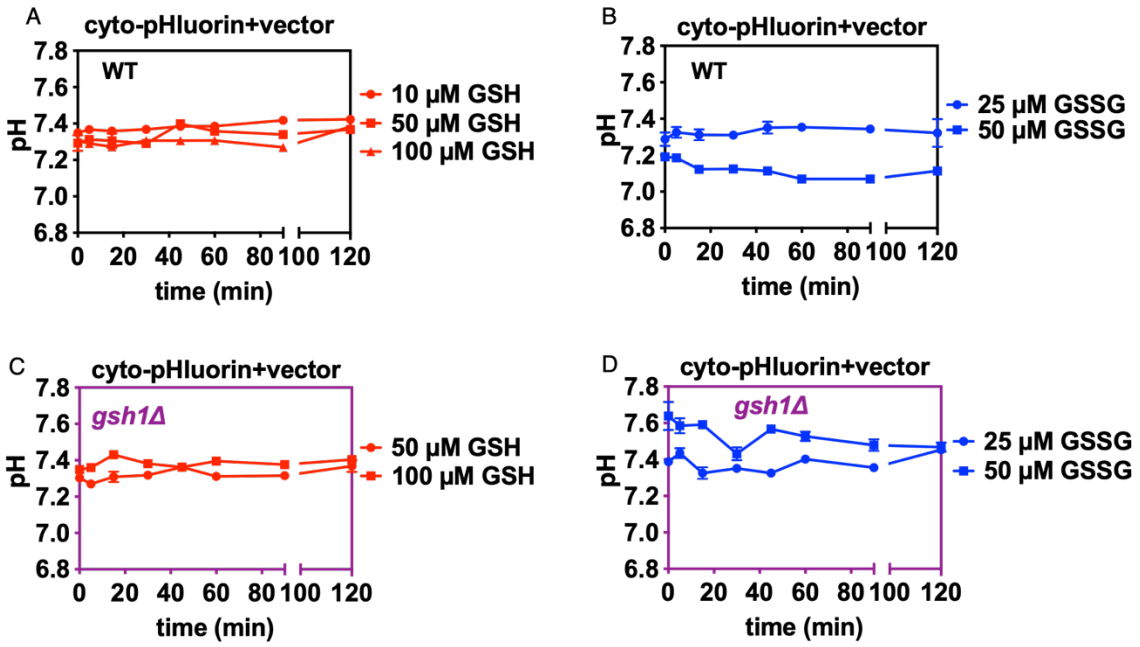

Figure 2.5: Negligible changes in intracellular pH after treatment with GSH or GSSG. Both WT and *gsh1Δ* cells, transformed with the vector control plasmid, show almost no change in the cytosolic pH. The cells have been treated with the indicated concentration of GSH or GSSG.

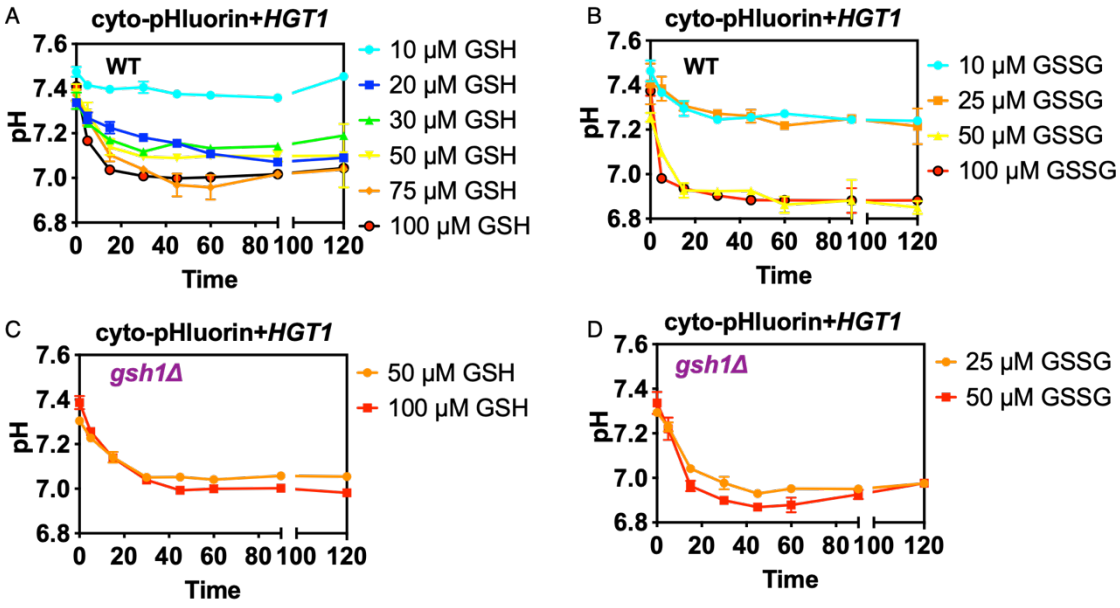

Figure 2.6: Measurable changes in intracellular pH after treatment with GSH (A, C) or GSSG (B, D). Both WT (A, B) and *gsh1Δ* cells (C, D) overexpressing the Hgt1 transporter show substantial changes in the cytosolic pH. The cells have been treated with the indicated concentration of GSH or GSSG.

molecules and subsequently the change in pH probably would be more impactful. We could also observe that at 75 and 100 µM GSH concentration, the decrease in pH seemed to be saturated and there is almost no difference in the pH change between these two GSH concentrations. Similarly, 50 and 100 µM GSSG concentration showed very similar trend of pH changes. These trends seem to be similar in both WT and *gsh1*Δ cells.

Both WT and *gsh1*Δ cells with the vector control plasmid do not show any change in pH, even after the addition of GSH or GSSG (Figure 2.7). Unexpectedly, while observing the changes in the mitochondrial matrix pH, we noticed that after the addition of GSH/GSSG, instead of a decrease in pH, the pH goes up immediately and then returns to steady state levels at approximately the 20th minute (Figure 2.8). This phenomenon can be observed in both the WT and the *gsh1Δ* cells with *HGT1* overexpression (more so in the WT cells). The upward increase in pH is quite significant and goes up towards the alkaline side of the pH scale, approximately 0.5 units in the WT cells and 0.3 units in the *gsh1Δ* cells. Here again, just like with the cytosol-pHluorin, around or above 20 µM concentration of GSH, the visible change in pH begins to show up. We also see that there is no change in the pH spike, starting from 50 µM GSH and it stays the same with 100 µM GSH concentration, in both WT and *gsh1*Δ cells. A similar trend could be seen with GSSG treatment with WT cells but in *gsh1*Δ cells, we could see a much bigger pH spike with 50 µM GSSG treatment. We might need higher concentrations than 50 µM GSSG to reach a saturation point in *gsh1*Δ cells. That would probably show us a complete picture of difference between treatment with GSH and/or GSSG. Unfortunately, the fluorescence from the IMS-pHluorin (intermembrane space sensor) is too low to get a good signal-to-noise ratio, although studies have shown that IMS pH is typically 0 – 0.7 pH units lower

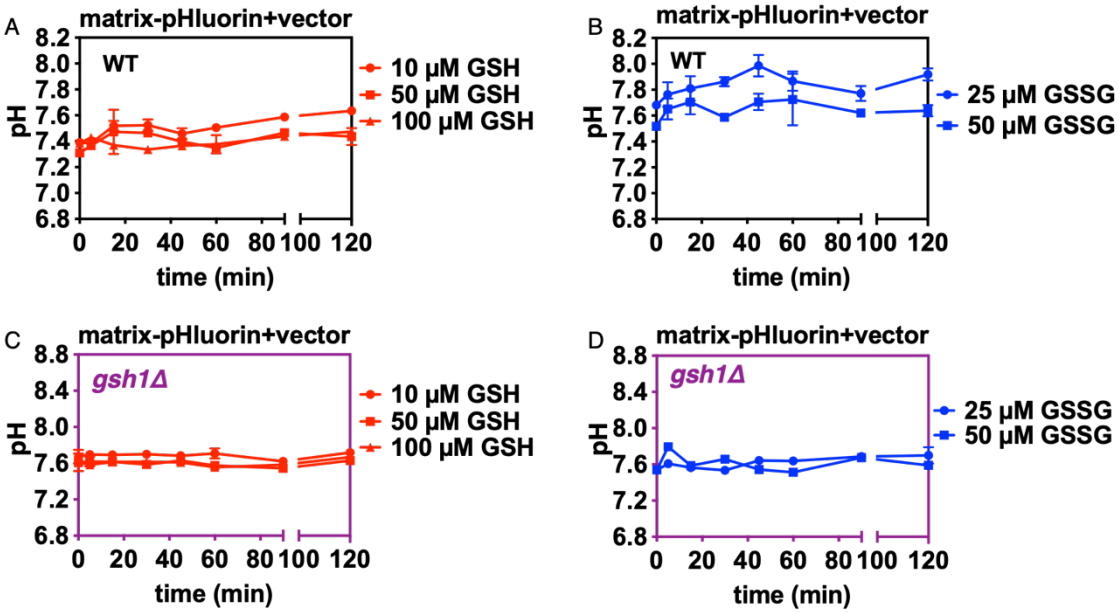

Figure 2.7: Negligible changes in intracellular pH after treatment with GSH or GSSG. Both WT (A, B) and *gsh1*Δ cells (C, D) transformed with the vector control plasmid show almost no change in the mitochondrial pH. The cells have been treated with the indicated concentration of GSH (A, C) or GSSG (B, D).

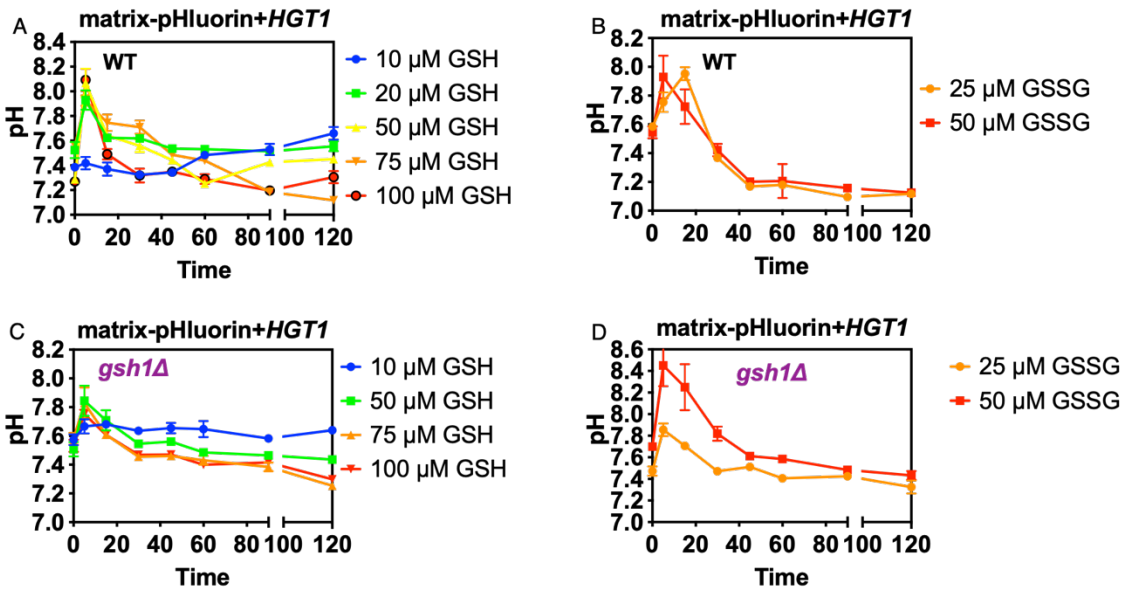

Figure 2.8: Substantial changes in intracellular pH after treatment with GSH or GSSG. Both WT (A, B) and *gsh1Δ* cells (C, D) overexpressing the Hgt1 transporter show substantial changes in the mitochondrial matrix pH. The cells have been treated with the indicated concentration of GSH (A, C) or GSSG (B, D).

than the cytosolic pH (118). So unfortunately, the same experiments with the IMS-pHluorin to detect the changes in pH in the intermembrane space of the mitochondria could not be performed.

Measurement of redox potential upon GSH/GSSG overaccumulation: Redox potential is strongly affected by the change in pH values since thiol-disulfide exchange reactions involve the transfer of protons as well as electrons. Therefore, in order to measure the actual redox potential of the rxYFP redox sensors, incorporating the pH changes, we combined the rxYFP redox western measurements and the pHluorin measurements (for the pH values). The rxYFP redox westerns were performed by a previous C. Outten group member, Dr. Max Darch (114), but his calculations were done under the assumption that the pH was 7.0 and was constant at every time point. We took his calculated values of the oxidized rxYFP sensor for both cytosol and mitochondria and combined them with our measurements of change in pH at every time point, under the same conditions, for the WT cells. The pH values from the pHluorin measurements at every time point were used to calculate the redox potential of rxYFP. The values were inserted into the Nernst equation together with the ratio of oxidized and reduced rxYFP to calculate the redox potential in the *HGT1* overexpression strain upon GSH/GSSG overaccumulation. Max found that rxYFP redox state in the cytosol increases in approximately 5 to 30 minutes upon GSH/GSSG overaccumulation, and then slightly diminishes in one hour (Figure 2.9) (114). In the case of the matrix-rxYFP redox potential, it decreases in approximately 5 to 20 minutes after treatment with GSH/GSSG and then goes back up in one hour (Figure 2.10). The difference between these redox potential calculations is mainly due to changes in

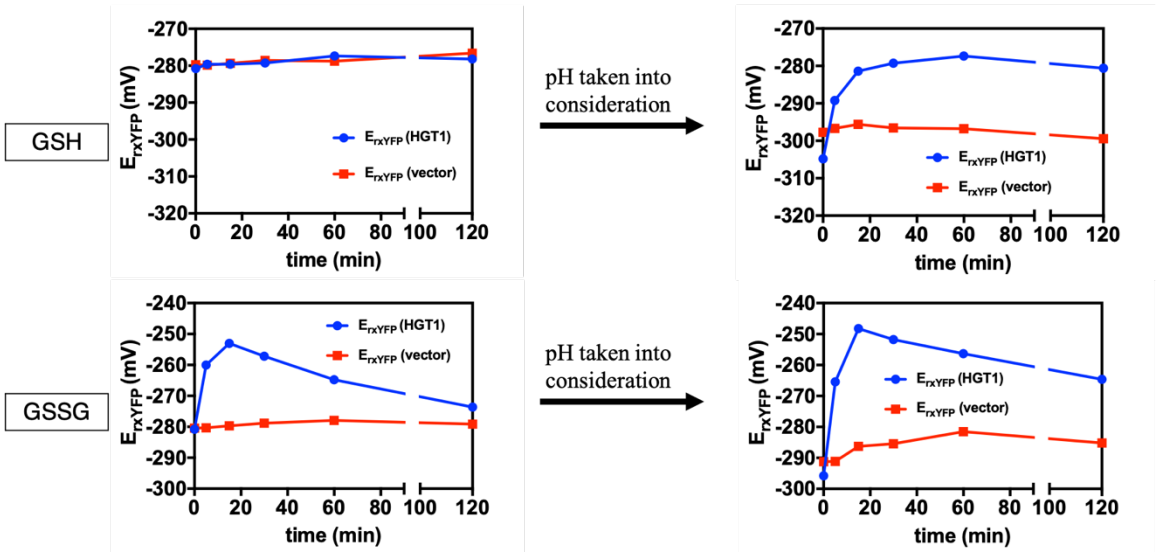

Figure 2.9: Changes in pH lead to substantial changes in the redox potential of the cytosol. pH measurements after GSH (100 µM) or GSSG (50 µM) treatment of the WT BY4741 cells transformed with the vector control or *HGT1* overexpression plasmid were used to calculate rxYFP redox potentials at specific time points (right panel). The original uncorrected E_{rxYFP} values (left panel) were obtained by our previous lab member Dr. Max Darch (114).

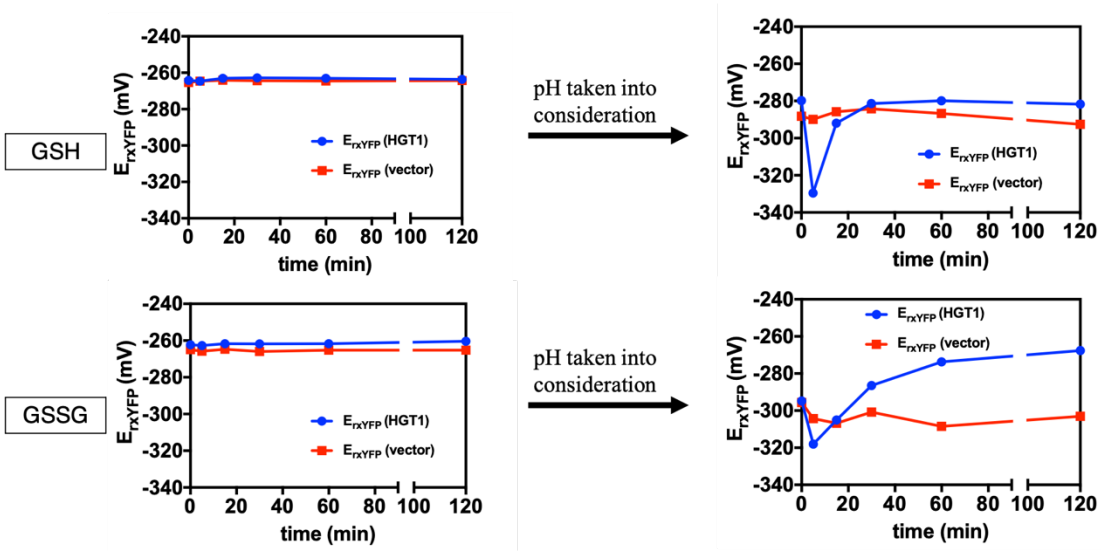

Figure 2.10: Changes in pH lead to substantial changes in the redox potential of the mitochondrial matrix. pH measurement after GSH (100 µM) or GSSG (50 µM) treatment of WT BY4741 cells transformed the vector control or *HGT1* overexpression plasmid used to calculate rxYFP redox potentials at specific time points (right panel). The original uncorrected E_{rxYFP} values (left panel) were obtained by our previous lab member Dr. Max Darch (114).

intracellular pH. In summation, these data suggest that the redox potential of subcellular compartments is differently perturbed by the subcellular pH changes.

Discussion

The concentration of GSH in cells and tissues is affected by the equilibrium between biosynthesis, degradation, storage, and transport of GSH and GSSG to other organelles. The concentration and redox state of GSH:GSSG pools in different compartments are precisely controlled to maintain the cell's normal function. Import and transport of GSH in and around the cell play a key role in the control and regulation of GSH homeostasis. A high affinity GSH:GSSG transporter (Hgt1) has been identified and characterized in yeast (75,76). An *hgt1*Δ deletion strain is inviable in a GSH biosynthetic mutant (*gsh1Δ*) background and does not show any detectable plasma membrane GSH transport (75).The intracellular GSH and GSSG level increased about 10-fold in the *HGT1* overexpression strain compared to the WT control strain upon addition with 50 μM GSH to the growth media. Using the *HGT1* overexpression strain, we wanted to observe the changes in subcellular pH and subsequently test their effects on the subcellular redox potential. Since the redox state is largely affected by the intracellular pH and Hgt1 is also a proton co-transporter, pH measurements are required for the accurate calculation of redox potential changes due to GSH/GSSG overaccumulation. We then expressed these targeted pH sensors in the *HGT1* overexpression strain and measured the subcellular pH at different time points after adding GSH/GSSG to the growth media. Our data demonstrate that cytosol pH values of the *HGT1* strain are significantly decreased in 5 minutes upon GSH/GSSG addition and stabilizes after 1 hour, while the matrix pH immediately sees an increase after GSH/GSSG addition. Incorporating the pH values into the Nernst equation

for redox calculations revealed that the cytosolic redox potentials are significantly increased, and the matrix redox potential decreased upon GSH/GSSG addition. When comparing the redox change peak of GSH overaccumulation with the GSSG overaccumulation in the cytosol, we found there is an approximately 30 mV difference, while the redox potential change in the matrix is not that dramatic (in the opposite direction). This phenomenon that GSSG overaccumulation has more effect on the cytosol than the mitochondria suggests that GSSG is reduced by the cytosolic glutathione reductase enzyme (Glr1) and then transported into the mitochondria.

The unexpectedly consistent observation using the matrix-pHluorin sensor demonstrating that the matrix pH immediately increases significantly after GSH/GSSG addition to the growth media requires more experiments and explanation. We presume that it is related to the electron transport chain and oxidative phosphorylation and there is a probable connection between these pathways and redox stress. We already know that the matrix pH is more alkaline in nature than the cytosol and the IMS. This is due to the presence of higher concentration of protons outside the matrix, which then flow into the matrix (down its concentration gradient) to drive ATP synthesis. We hypothesize that the increased proton import by *HGT1* may drive increase proton flow into the matrix, subsequently leading to higher rate of formation of ATP and higher rate of oxygen consumption. Our future work will focus more on exploring these ideas.

References

11. Kumar, C., Igbaria, A., D'Autreaux, B., Planson, A. G., Junot, C., Godat, E., Bachhawat, A. K., Delaunay-Moisan, A., and Toledano, M. B. (2011) Glutathione revisited: a vital function in iron metabolism and ancillary role in thiol-redox control. *EMBO J* **30**, 2044-2056

24. Schafer, F. Q., and Buettner, G. R. (2001) Redox environment of the cell as viewed through the redox state of the glutathione disulfide/glutathione couple. *Free Radic Biol Med* **30**, 1191-1212

75. Bourbouloux, A., Shahi, P., Chakladar, A., Delrot, S., and Bachhawat, A. K. (2000) Hgt1p, a high affinity glutathione transporter from the yeast Saccharomyces cerevisiae. *J Biol Chem* **275**, 13259-13265

76. Bachhawat, A. K., Thakur, A., Kaur, J., and Zulkifli, M. (2013) Glutathione transporters. *Biochim Biophys Acta* **1830**, 3154-3164

78. Thakur, A., and Bachhawat, A. K. (2010) The role of transmembrane domain 9 in substrate recognition by the fungal high-affinity glutathione transporters. *Biochem J* **429**, 593-602

82. Preston, R. A., Murphy, R. F., and Jones, E. W. (1989) Assay of vacuolar pH in yeast and identification of acidification-defective mutants. *Proc Natl Acad Sci U S A* **86**, 7027-7031

83. Brett, C. L., Tukaye, D. N., Mukherjee, S., and Rao, R. (2005) The yeast endosomal Na+K+/H+ exchanger Nhx1 regulates cellular pH to control vesicle trafficking. *Mol Biol Cell* **16**, 1396-1405

84. Martinez-Munoz, G. A., and Kane, P. (2008) Vacuolar and plasma membrane proton pumps collaborate to achieve cytosolic pH homeostasis in yeast. *J Biol Chem* **283**, 20309-20319

85. Nishimura, K., Igarashi, K., and Kakinuma, Y. (1998) Proton gradient-driven nickel uptake by vacuolar membrane vesicles of Saccharomyces cerevisiae. *J Bacteriol* **180**, 1962-1964

86. Ohsumi, Y., and Anraku, Y. (1981) Active transport of basic amino acids driven by a proton motive force in vacuolar membrane vesicles of Saccharomyces cerevisiae. *J Biol Chem* **256**, 2079-2082

87. Llopis, J., McCaffery, J. M., Miyawaki, A., Farquhar, M. G., and Tsien, R. Y. (1998) Measurement of cytosolic, mitochondrial, and Golgi pH in single living cells with green fluorescent proteins. *Proc Natl Acad Sci U S A* **95**, 6803-6808

88. van Roermund, C. W., de Jong, M., L, I. J., van Marle, J., Dansen, T. B., Wanders, R. J., and Waterham, H. R. (2004) The peroxisomal lumen in Saccharomyces cerevisiae is alkaline. *J Cell Sci* **117**, 4231-4237

89. Paroutis, P., Touret, N., and Grinstein, S. (2004) The pH of the secretory pathway: measurement, determinants, and regulation. *Physiology (Bethesda)* **19**, 207-215

90. Dancourt, J., and Barlowe, C. (2010) Protein sorting receptors in the early secretory pathway. *Annu Rev Biochem* **79**, 777-802

91. Appenzeller-Herzog, C., Roche, A. C., Nufer, O., and Hauri, H. P. (2004) pH-induced conversion of the transport lectin ERGIC-53 triggers glycoprotein release. *J Biol Chem* **279**, 12943-12950

92. Scheel, A. A., and Pelham, H. R. (1996) Purification and characterization of the human KDEL receptor. *Biochemistry* **35**, 10203-10209

93. Wilson, D. W., Lewis, M. J., and Pelham, H. R. (1993) pH-dependent binding of KDEL to its receptor in vitro. *J Biol Chem* **268**, 7465-7468

94. Vavassori, S., Cortini, M., Masui, S., Sannino, S., Anelli, T., Caserta, I. R., Fagioli, C., Mossuto, M. F., Fornili, A., van Anken, E., Degano, M., Inaba, K., and Sitia, R. (2013) A pH-regulated quality control cycle for surveillance of secretory protein assembly. *Mol Cell* **50**, 783-792

95. Sannino, S., Anelli, T., Cortini, M., Masui, S., Degano, M., Fagioli, C., Inaba, K., and Sitia, R. (2014) Progressive quality control of secretory proteins in the early secretory compartment by ERp44. *J Cell Sci* **127**, 4260-4269

96. Watanabe, S., Harayama, M., Kanemura, S., Sitia, R., and Inaba, K. (2017) Structural basis of pH-dependent client binding by ERp44, a key regulator of protein secretion at the ER-Golgi interface. *Proc Natl Acad Sci U S A* **114**, E3224-E3232

97. Shibuya, A., Margulis, N., Christiano, R., Walther, T. C., and Barlowe, C. (2015) The Erv41-Erv46 complex serves as a retrograde receptor to retrieve escaped ER proteins. *J Cell Biol* **208**, 197-209

98. Gillies, R. J., Ugurbil, K., den Hollander, J. A., and Shulman, R. G. (1981) 31P NMR studies of intracellular pH and phosphate metabolism during cell division cycle of Saccharomyces cerevisiae. *Proc Natl Acad Sci U S A* **78**, 2125-2129

99. Bracey, D., Holyoak, C. D., and Coote, P. J. (1998) Comparison of the inhibitory effect of sorbic acid and amphotericin B on Saccharomyces cerevisiae: is growth inhibition dependent on reduced intracellular pH? *J Appl Microbiol* **85**, 1056-1066

100. Lanz, E., Slavik, J., and Kotyk, A. (1999) 2',7'-bis-(2-carboxyethyl)-5(6)-carboxyfluorescein as a dual-emission fluorescent indicator of intracellular pH suitable for argon laser confocal microscopy. *Folia Microbiol (Praha)* **44**, 429-434

101. Krebs, H. A., Wiggins, D., Stubbs, M., Sols, A., and Bedoya, F. (1983) Studies on the mechanism of the antifungal action of benzoate. *Biochem J* **214**, 657-663

102. Kresnowati, M. T., Suarez-Mendez, C., Groothuizen, M. K., van Winden, W. A., and Heijnen, J. J. (2007) Measurement of fast dynamic intracellular pH in Saccharomyces cerevisiae using benzoic acid pulse. *Biotechnol Bioeng* **97**, 86-98

103. Ostergaard, H., Henriksen, A., Hansen, F. G., and Winther, J. R. (2001) Shedding light on disulfide bond formation: engineering a redox switch in green fluorescent protein. *EMBO J* **20**, 5853-5862

104. Dooley, C. T., Dore, T. M., Hanson, G. T., Jackson, W. C., Remington, S. J., and Tsien, R. Y. (2004) Imaging dynamic redox changes in mammalian cells with green fluorescent protein indicators. *J Biol Chem* **279**, 22284-22293

105. Miesenbock, G., De Angelis, D. A., and Rothman, J. E. (1998) Visualizing secretion and synaptic transmission with pH-sensitive green fluorescent proteins. *Nature* **394**, 192-195

106. Hu, J., Dong, L., and Outten, C. E. (2008) The redox environment in the mitochondrial intermembrane space is maintained separately from the cytosol and matrix. *J Biol Chem* **283**, 29126-29134

107. Ostergaard, H., Tachibana, C., and Winther, J. R. (2004) Monitoring disulfide bond formation in the eukaryotic cytosol. *J Cell Biol* **166**, 337-345

108. Wachter, R. M., Yarbrough, D., Kallio, K., and Remington, S. J. (2000) Crystallographic and energetic analysis of binding of selected anions to the yellow variants of green fluorescent protein. *J Mol Biol* **301**, 157-171

109. Hanson, G. T., Aggeler, R., Oglesbee, D., Cannon, M., Capaldi, R. A., Tsien, R. Y., and Remington, S. J. (2004) Investigating mitochondrial redox potential with redox-sensitive green fluorescent protein indicators. *J Biol Chem* **279**, 13044-13053

110. Gietz, R. D., and Schiestl, R. H. (1991) Applications of high efficiency lithium acetate transformation of intact yeast cells using single-stranded nucleic acids as carrier. *Yeast* **7**, 253-263

111. McGee, C. C. (2019) *Impact of Glutathione Transporters on Subcellular Glutathione Pools and Cell Survival in Saccharomyces Cerevisiae.* PhD Doctoral dissertation, University of South Carolina

112. Orij, R., Postmus, J., Ter Beek, A., Brul, S., and Smits, G. J. (2009) In vivo measurement of cytosolic and mitochondrial pH using a pH-sensitive GFP derivative in Saccharomyces cerevisiae reveals a relation between intracellular pH and growth. *Microbiology* **155**, 268-278

113. Hu, J. (2010) Investigating Subcellular Thiol Redox Chemistry with GFP-based Sensors. *Doctoral dissertation*

114. Darch, A. M. (2015) Subcellular glutathione distribution during severe redox stress and characterizing thiol redox control of human Cu, Zn superoxide dismutase. *Doctoral dissertation*

115. Bagar, T., Altenbach, K., Read, N. D., and Bencina, M. (2009) Live-Cell imaging and measurement of intracellular pH in filamentous fungi using a genetically encoded ratiometric probe. *Eukaryot Cell* **8**, 703-712

116. Martinière, A., Desbrosses, G., Sentenac, H., and Paris, N. (2013) Development and properties of genetically encoded pH sensors in plants. *Frontiers in Plant Science* **4**

117. Jamai, A., Tommasini, R., Martinoia, E., and Delrot, S. (1996) Characterization of Glutathione Uptake in Broad Bean Leaf Protoplasts. *Plant Physiol* **111**, 1145-1152

118. Cortese, J. D., Voglino, A. L., and Hackenbrock, C. R. (1992) The ionic strength of the intermembrane space of intact mitochondria is not affected by the pH or volume of the intermembrane space. *Biochim Biophys Acta* **1100**, 189-197

CHAPTER 3

HGT1 OVEREXPRESSION RESCUES THE GROWTH DEFECT OF GSH1Δ CELLS BUT DOES NOT ALTER THE INTRACELLULAR GSH:GSSG REDOX STATE

Abstract

Hgt1 is a plasma membrane high affinity glutathione transporter that first came into the limelight in the last decade. This transporter is known for its ability to acts as a symporter, as it can simultaneously import both glutathione (GSH) and protons. It has been previously reported that Hgt1 overexpression in yeast leads to overaccumulation of GSH inside the cell, when GSH is supplied from an external source. Interestingly, in the presence of the same transporter, too high of a concentration of GSH leads to cell death. We wanted to examine this phenotype in yeast and compare to the opposite extremes in which the levels of GSH inside the cell are depleted. We did this by deleting the first enzyme of the glutathione biosynthetic pathway, gamma-glutamylcysteine synthase or Gsh1 (*gsh1Δ*). Since glutathione is an essential factor in yeast, *gsh1Δ* cells are inviable in the absence of added GSH or GSSG in the media. We also overexpressed the Hgt1 transporter in these cells to create a model system that allows us to control GSH levels inside the cell by adding different concentration of GSH to the medium. Surprisingly, we found that *gsh1Δ* cells overexpressing *HGT1* have a lower concentration of GSH in whole cell extracts as well as fractionated extracts, compared to the *gsh1Δ* control cells.

We also used an *in vivo* rxYFP redox sensor and redox western blots to reveal that Hgt1 overexpression mediated oxidative changes inside the cell. Finally, we used site-directed mutagenesis to demonstrate that the active form of the Hgt1 transporter is necessary for rescue of the GSH auxotrophy of the *gsh1Δ* strains.

Introduction

The electrochemical proton gradient acts as the driving force for the uptake and efflux of many metabolites and ions across the plasma membrane of fungi and plants (119,120). A large number of transporters in these organisms are, therefore, proton coupled (121). However, the mechanisms by which proton coupling to substrate transport occurs differs in different transporters. The *Saccharomyces cerevisiae* plasma membrane high affinity glutathione (GSH) transporter Hgt1 is one such proton-coupled transporter (75,76). It uses the inwardly directed proton electrochemical gradient to drive the uphill transport of GSH against a concentration gradient (75,120). Hgt1 belongs to the oligopeptide transporter (OPT) family. Members of this family fall into two broad clades that mediate the uptake the GSH, peptides, modified peptides, and metal-binding secondary amino acid derivatives (122-124). Hgt1 remains the best-studied member of this OPT family. Extensive mapping of the residues in the transmembrane domains (TMDs) has led to significant insights into the TMDs and their residues important for GSH binding and translocation (78,79,125,126). Kinetic studies have indicated that the affinity of Hgt1 for GSH is high (K_m = 54 μM) and the uptake of GSH by this transporter is not sensitive to competition by amino acids or other tripeptides (75). However, significant inhibition has been observed with oxidized glutathione (GSSG) and GSH conjugates (GS-NEM) suggesting that these are also possible substrates of the transporter (75).

It has been reported that overexpression of the Hgt1 transporter in budding yeast leads to overaccumulation of both reduced and oxidized glutathione (GSH and GSSG) when excess GSH or GSSG is added in the media (11). This overaccumulation of GSH is toxic and lethal for the cells. We overexpressed the Hgt1 transporter in *gsh1Δ* cells to study how the cells respond to dramatic changes in GSH levels from deplete to replete conditions. We then grew these cells with different concentrations of GSH in the media to track the impact on intracellular GSH levels over time. Surprisingly, a previous lab member (Dr. Crystal Conaway McGee) discovered that overexpression of *HGT1* in *gsh1Δ* cells bypasses the GSH auxotrophy of this strain (111). Here we demonstrate that after overnight growth in low levels of GSH, we found that GSH levels are generally two times higher in *gsh1Δ* cells transformed with empty vector control compared to *gsh1Δ* cells transformed with an *HGT1* overexpression plasmid. After some careful consideration, we chose and replaced six different amino acids of the Hgt1 transporter with alanine using site directed mutagenesis to determine if the active form of Hgt1 transporter is specifically needed for GSH import and accumulation. We noticed varying levels of GSH getting accumulated inside the cell. More experiments are warranted to show the difference between the wild type and mutated Hgt1 transporter's ability to bring in GSH.

An *in vivo* method for measuring the subcellular redox state of GSH:GSSG is an effective approach to address redox control in individual compartments. Ostergaard and co-workers developed a genetically encoded, cytosolic redox sensor based on the yellow variant of green fluorescent protein (GFP) called redox-sensitive YFP (rxYFP) (107). GFP and its derivatives provide ideal scaffolds for creating *in vivo* sensors due to their protease resistance and high stability in a broad range of pH and buffer conditions (127). The rxYFP

protein can be used to measure the redox potential in live cells via the formation of an engineered disulfide bond that perturbs the local chromophore environment without significantly altering the overall β-fold (103). The relative ratio of oxidized to reduced rxYFP can also be assessed via non-reducing SDS-PAGE in which the two forms have different electrophoretic mobilities. Ostergaard and co-workers have shown both *in vivo* and *in vitro* that the cysteines in rxYFP specifically equilibrate with GSH and GSSG via rapid disulfide exchange reactions with the cytosolic glutaredoxins (GRXs) (107). The ratio of oxidized to reduced rxYFP measured in the cell can be used to generate an *in vivo* readout of the GSH:GSSG redox state. In this study, we have measured the dynamic response of the changes in the cytosolic redox potential after treating the cells with glutathione.

Experimental Procedures

Yeast strains, media, and growth conditions: *S. cerevisiae* strains used in this study were BY4741 (*MAT*a *his3*Δ1 *leu2*Δ0 *met15*Δ0 *ura3*Δ0). The *gsh1Δ* strain was made in BY4741 by deleting the *GSH1* gene using pGSH1KO (made by former lab member Dr. Crystal Conaway McGee; see plasmid info in chapter 2). Yeast transformations were performed using the standard lithium acetate protocol (110). Yeast strains were cultured at 30 °C in synthetic complete (SC) media (US Biological) supplemented with 2% glucose as the carbon source with appropriate amino acids or supplemented minimal media, termed 6AA/B media (0.671% yeast nitrogen base without amino acids and with ammonium sulfate 2% glucose, supplemented with six essential amino acids and bases at the following concentrations: 20 mg/L adenine, 60 mg/L leucine, 30 mg/L lysine, 20 mg/L histidine, 20

mg/L tryptophan and 20 mg/L methionine). Where required, media was solidified using 2% bacteriological agar (US Biological).

Plasmid construction and site directed mutagenesis: The plasmid pJH208 (originally made by former lab member Dr. Jingjing Hu) expressing cytosol-rxYFP was constructed by digesting the rxYFP yeast expression plasmid pHOJ150 (107) with NotI and SacII. The NotI-SacII digested fragment containing the *PGK1* promoter, the coding sequence of rxYFP, and the *TDH3* terminator was then inserted into the *URA3-CEN* vector pRS316 (128). The single amino acid mutated Hgt1 transporters were made using the QuikChange II Site Directed Mutagenesis protocol (Agilent Technologies). The steps of the protocol with detail description are provided in Chapter 5 (Supplementary Methods). The forward and reverse primers are listed in Table 3.1.

Growth curves in liquid media: To determine the growth pattern of yeast strains, cells were plated on SC (-Ura) 2% glucose plates containing 0.05 µM GSH for 2-3 days. Each strain was later inoculated into fresh SC selection media at an OD_{600} of 0.05. Growth phenotypes of yeast strains were determined in sterile 96-plates using a Synergy H1 plate-reader and Gen5 software 2.09. All the strains were grown in the liquid media for a total duration of 40 hours, with readings taken at OD_{600}, every 30 minutes.

GSH assay: Glutathione level was measured in whole cell extracts using the 5, 5-dithiobis (2-nitrobenzoic acid) GSSG reductase cycling assay as previously mentioned (129). For whole cell measurements, 2 X 10^7 cells (or 2 X 10^9 cells for GSH depleted cells) were harvested via centrifugation at 12000 rpm for 30 seconds. Cell pellets were washed twice with water. Lysis was performed by vigorous vortexing using 1% 5-sulfosalicylic

Table 3.1: Primers used for making Hgt1 transporter mutants, by site-directed mutagenesis. Mutated residues are shown in bold.

Primer name	Primer sequence (5' – 3')
E177A_forward	GGCCCATTTACCAAAAAGG**CT**CACGCCGTGGTCAC
E177A_reverse	GTGACCACGGCGTG**AG**CCTTTTTGGTAAATGGGCC
Y193A_forward	GGCGCTTACTTCCTCTACTGCA**GC**CGCTATGTACATTTTGA
Y193A_reverse	TCAAAATGTACATAGCG**GC**TGCAGTAGAGGAAGTAAGCGCC
Y226A_forward	GGTTTGGACATCTCAAATGATTGGT**GC**TGGTGCTGCAGGT
Y226A_reverse	ACCTGCAGCACCA**GC**ACCAATCATTTGAGATGTCCAAACC
D335A_forward	GGTGCGTTGCCAATTACATTTG**C**CTACACCCAGGTTTC
D335A_reverse	GAAACCTGGGTGTAG**G**CAAATGTAATTGGCAACGCACC
Y374A_forward	GTCATAGTGCTGCCATGTCTT**GC**TTTTACGAATACCTGGTATGC
Y374A_reverse	GCATACCAGGTATTCGTAAAA**GC**AAGACATGGCAGCACTATGAC
H445A_forward	TGTTATCGCCGTTTTTGTC**GC**CTGCATCTTATACCACGGT
H445A_reverse	ACCGTGGTATAAGATGCAG**GC**GACAAAAACGGCGATAACA

acid (wt/vol) and glass beads. The resulting supernatant containing GSH was incubated on ice for 30 minutes and cleared via centrifugation.

Redox Western Blots: Redox western blot analysis of rxYFP was adapted from previous methods (107). Briefly, cells were grown in selecting SC medium to mid-log phase. Cells were treated with different concentrations of GSH overnight or treated with a short pulse of GSH and cells taken out at different time points. Cell cultures were acid quenched with trichloroacetic acid (TCA) (15% w/v final concentration) at 4 °C for 20 minutes. OD_{600} = 5 cells were harvested by centrifugation and resuspended in 1 ml of 10% TCA. Following glass bead lysis, the lysed cells were transferred to a new tube and pelleted by centrifugation. The pellet was resuspended in 500 µl of 1x non-reducing SDS sample buffer containing 40 mM N-ethylmaleimide (NEM). Following a 10-minute incubation at room temperature, the proteins were separated on a 12% Bis-Tris gel (Invitrogen). Reduced and oxidized forms of rxYFP were analyzed by quantitative immunoblot using an Odyssey Infrared Imaging System (LI-COR, Lincoln, NE) as previously described (106).

Redox potential calculations from redox western blots: The calculations have been described in detail in Chapter 2. At pH 7.0, the standard reduction potential of rxYFP ($E^{\circ\prime}_{rxYFP}$) is -265 mV (107). The reduction potential of cytosolic rxYFP has been calculated at pH 7.4.

Results

HGT1 overexpression rescues the growth defect of gsh1Δ cells and causes increased sensitivity to GSH: Constitutive expression of the high affinity glutathione transporter Hgt1 is known to cause overaccumulation of GSH, as has been shown by Kumar et al. (11). We wanted to see if *HGT1* overexpression has any effect on the cells

where GSH is depleted. This way we could monitor the growth pattern of the cells when they shifted from GSH deplete to GSH replete condition. Kumar *et al*., suggested that GSH concentrations higher than 20 μM impeded growth of *HGT1* expressing cells (11). We mostly confirmed this phenotype in WT + *HGT1* cells. Surprisingly, we also observed that concentration as low as 5 μM was toxic for *gsh1Δ* + *HGT1* cells. This specific phenotype has been shown and confirmed by my previous lab mate Dr. Crystal Conaway McGee, by spot test experiments (111). During liquid growth curve experiments, we observed a sharp and significant decline in growth of the *gsh1Δ* + *HGT1* cells, going from 5 μM to 25 μM GSH concentration (Figure 3.1). WT + *HGT1* cells at 25 μM GSH concentration also showed a significant decline in growth, but it was not as sharp as *gsh1Δ* + *HGT1* cells. These results suggest that overexpression of *HGT1* rescues the growth defect of *gsh1Δ* strains and there are clear distinctions between WT + *HGT1* and *gsh1Δ* + *HGT1* cells in the sensitivity towards lower and higher concentrations of glutathione.

Increasing GSH concentrations lead to differential uptake of GSH in gsh1Δ cells: My previous lab mate Dr. Crystal Conaway McGee first showed that the *gsh1Δ* + *HGT1* cells unexpectedly grew in the absence of GSH in the media (111). Due to this unexpected growth pattern, intracellular GSH was assessed in *gsh1Δ* cells grown overnight with various GSH concentrations. In this study, the minimum amount of GSH necessary for growth of both *gsh1Δ* + vector and *gsh1Δ* + *HGT1* cells cultured from SC + 0.05 μM GSH plates was 0.1 μM GSH. Dr. Conaway showed that, when grown with increasing but relatively low GSH concentrations, *HGT1* overexpression had no effect on intracellular GSH in WT strains (111). While GSH levels were very low but still detectable in *gsh1Δ* cells cultured in concentrations less than 1 μM GSH, these measurements show that *gsh1Δ*

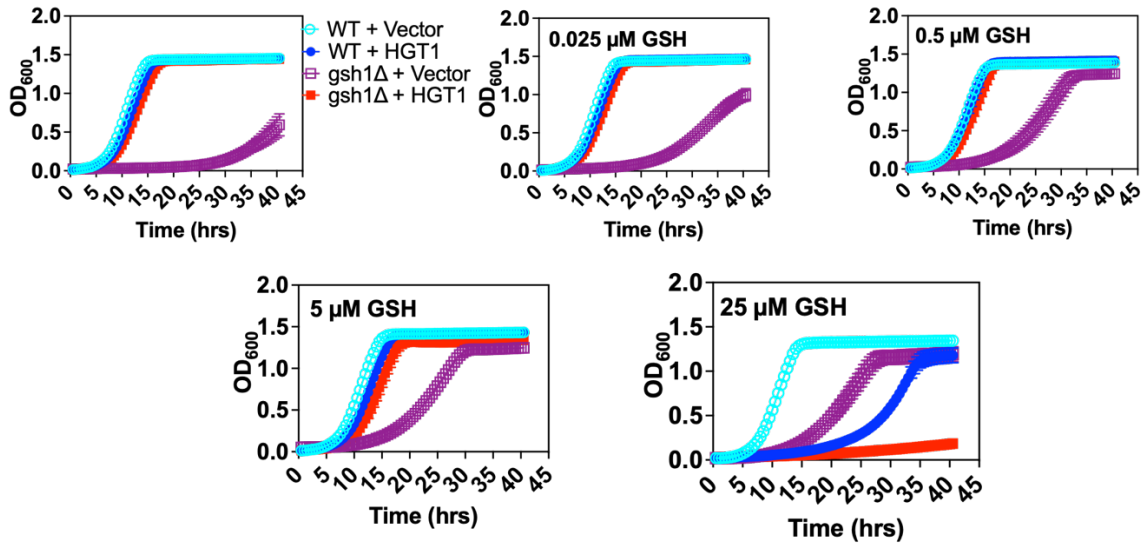

Figure 3.1: *HGT1* overexpression rescues the growth defect of *gsh1Δ* cells and causes increased sensitivity to GSH. WT and *gsh1Δ* strains were pre-grown on SC + 0.05 µM GSH selection plates. Growth and sensitivity to GSH was analyzed by using a Synergy H1 plate-reader. The growth curves are reported as means of 3 independent experiments with error bars representing the standard deviation (SD).

+ *HGT1* cells accumulate less GSH in overnight growth than the vector control (Figure 3.2). As shown by Kumar *et al*., *HGT1* cells treated with GSH increase shortly after adding GSH to the growth media and decrease over time. The authors suggested that the decrease in the GSH levels was due to its degradation by the γ – glutamyl transpeptidase (γ – GT) independent Dug1-Dug2-Dug3 pathway (11). Therefore, our data for the *gsh1Δ* cells coincided with the published literature. It is possible that the low level of GSH rapidly imported by the *HGT1* overexpression is degraded quickly by the Dug pathway, while slower controlled import with native *HGT1* expression avoids this rapid degradation.

Intracellular GSH: GSSG redox state is similar in gsh1Δ strains: There is an ongoing controversy regarding the main role of GSH in redox vs. iron homeostasis. The current point of view directs us towards its primary role as a mediator of Fe-S cluster biogenesis and iron homeostasis. This dichotomy in GSH's functionality has been explored by our collaborator, Dr. Michael Toledano (9,11). Therefore, to test the impact of *HGT1* overexpression on the intracellular redox state of *gsh1Δ* cells, we performed a modified western blot technique known as a redox western that preserves disulfide bonds. We transformed cells with a cytosolic GFP-based redox sensor, rxYFP, which equilibrates with the local GSH:GSSG pools via thiol-disulfide exchange reactions catalyzed by glutaredoxins. The detail of this technique is mentioned in the dissertation and the published article of our previous lab mate Dr. Jingjing Hu (106,113). We measured the changes in the cytosolic thiol redox balance of both *gsh1Δ* + vector and *gsh1Δ* + *HGT1* cells and observed that there is virtually no change in their subsequent redox potential

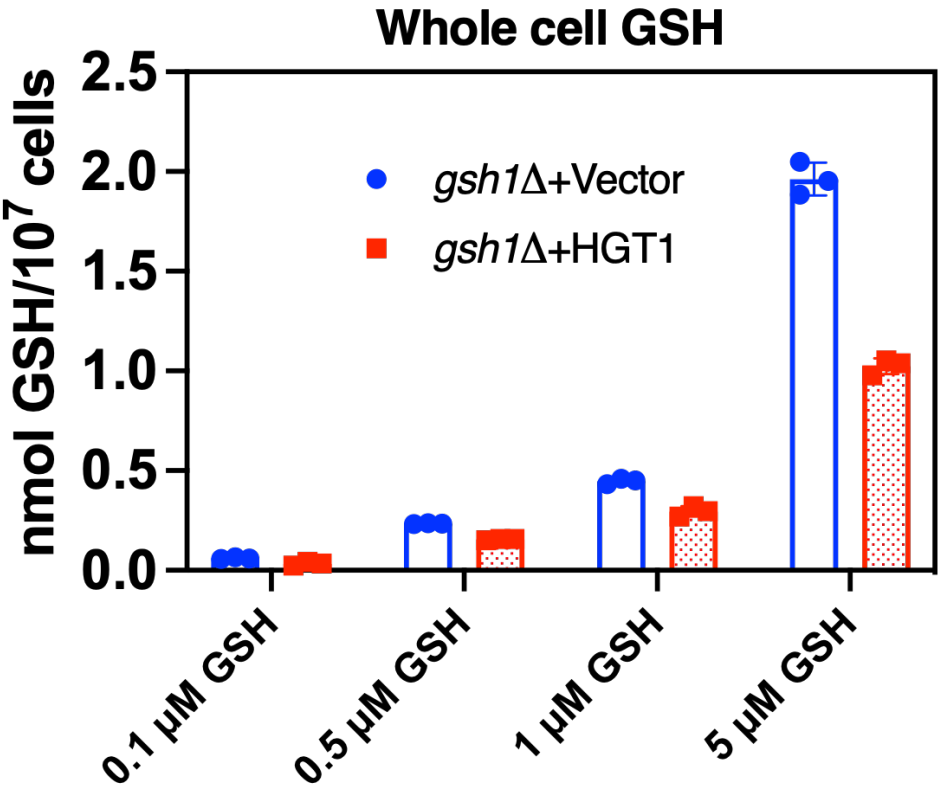

Figure 3.2: Overnight incubation of *gsh1Δ* strains with increasing GSH concentrations led to less GSH accumulation in *gsh1Δ* + *HGT1* cells. Yeast strains were pre-grown on SC + 0.05 µM GSH selection plates and inoculated in SC media with various concentrations of GSH. Cells were acidified with 1% SSA and whole cell GSH in *gsh1Δ* strains containing vector and *HGT1* plasmids was measured using the DTNB recycling assay. Data shown are means of three independent experiments with error bars representing standard deviation (SD).

(Figure 3.3). This observation led us to believe that varying levels of GSH in the *gsh1Δ + HGT1* cells do not necessarily translate to varying redox potential with different GSH concentration.

A functional Hgt1 transporter is important for the rescue of gsh1Δ + HGT1 overexpression cells: The peculiar observations regarding the overexpression of Hgt1 transporter in *gsh1Δ* cells prodded us to ask whether, the active or the functional form of Hgt1 is required to rescue the *gsh1Δ* auxotrophy. It is possible that the rescue is not directly related to the functionality of Hgt1 but could be an indirect effect of *HGT1* overexpression. There have not been any structural studies of Hgt1 transporter showing the interaction between the transporter and GSH or GSSG. Hgt1 is a 12-pass plasma membrane transporter and like so many other plasma membrane proteins, it is very difficult to isolate and purify. Zulkifli *et al*., first showed the necessary residues of the transporter for the effective import of GSH/GSSG into the cell (130). They observed that six of these residues, if mutated to alanine, demonstrated very weak cytosolic acidification in response to GSH transport. However, these mutations did not cause a significant defect on either protein expression or its cell surface localization. We chose these six residues and mutated them to alanine to test and compare the levels of GSH uptake in the cells after overnight incubation with different concentrations of GSH. The WT Hgt1 and the empty vector plasmid behaved as before but the alanine mutants showed varying levels of GSH uptake (Figure 3.4). Although, we could observe a general trend of varying levels of GSH uptake, we could not conclude what specific amino acid residue would be affecting the uptake of GSH the most. More time-dependent experiments with a short GSH pulse are warranted to figure this out.

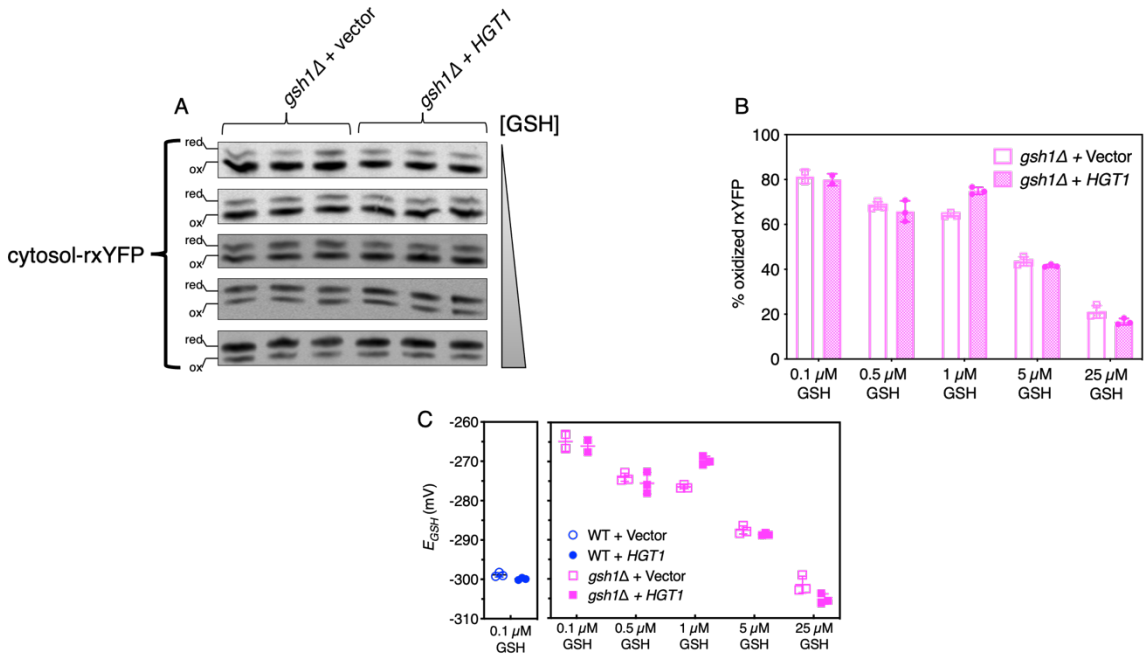

Figure 3.3: Intracellular GSH:GSSG redox state is similar in *gsh1*Δ strains ± HGT1.Yeast strains were pre-grown on SC + 0.05 μM GSH selection plates and inoculated in SC media with indicated concentrations of GSH. (A) redox western blot of the samples (in triplicate) separated by non-reducing SDS-PAGE and immunoblotted with anti-GFP. (B) reduced (red) and oxidized (ox) forms of rxYFP were quantified using an Odyssey Infrared Imaging System. (C) redox potential of cytosolic rxYFP were calculated with pH 7.4. Data shown are means of three independent experiments with error bars representing standard deviation (SD).

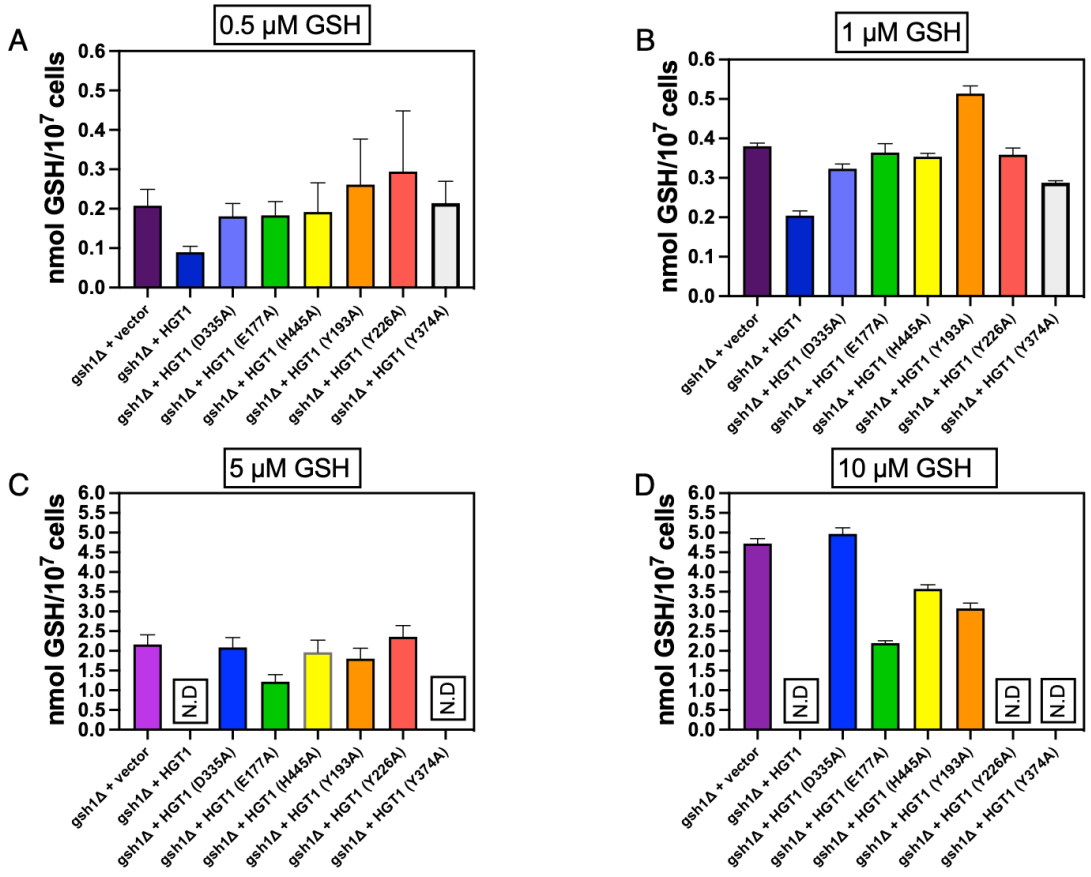

Figure 3.4: Comparative uptake of GSH by alanine mutants of Hgt1p transporter.Yeast strains were pre-grown on SC + 0.05 µM GSH selection plates and inoculated in SC media with various concentrations of GSH and grown overnight to mid-log phase. Cells were acidified with 1% SSA and whole cell GSH in the *gsh1*Δ strains containing vector and *HGT1* plasmids was measured using the DTNB recycling assay. Data shown are means of three independent experiments with error bars representing the standard deviation (SD).

We also performed spot test experiments to see the changes in growth phenotype of *gsh1*Δ cells overexpressed with WT Hgt1 and the mutated ones, along with the empty vector control. The experiments were done both anaerobically and aerobically (Figure 3.5 and 3.6). The GSH concentrations were similar to the concentrations used for detecting varying GSH levels with Hgt1 mutants (Figure 3.4). Interestingly, we saw the difference in growth between the WT and mutated *HGT1* overexpression cells more in the aerobically performed spot tests than the anaerobic one. This is probably because Hgt1 transporter already needs very little amount of GSH to rescue the *gsh1*Δ cells to begin with. So, the difference between WT and mutant Hgt1 is more visible in aerobic condition since the presence of oxygen already makes the *gsh1*Δ cells very stressed. For this reason, we presume however little GSH is getting inside the cells, it is enough for the cells to get rescued. But the growth differences are more accentuated by the presence of added oxidative stress. We could observe that the cells with residues E177A, Y193A, Y226A and Y374A were behaving like the empty vector control and had difficulty in growing at the lowest GSH concentration (0.5 μM), while residues D335A and H445A were growing like the cells with WT Hgt1 overexpression cells. We tried to correlate these results with the GSH uptake assay and observed that at the highest GSH concentration (10 μM), the pattern is somewhat similar to the spot tests with the lowest GSH concentration (0.5 μM), except for the D335A residue, which showed GSH levels similar to the empty vector control. We could not observe similar patterns between the two assays with the other remaining GSH concentrations.

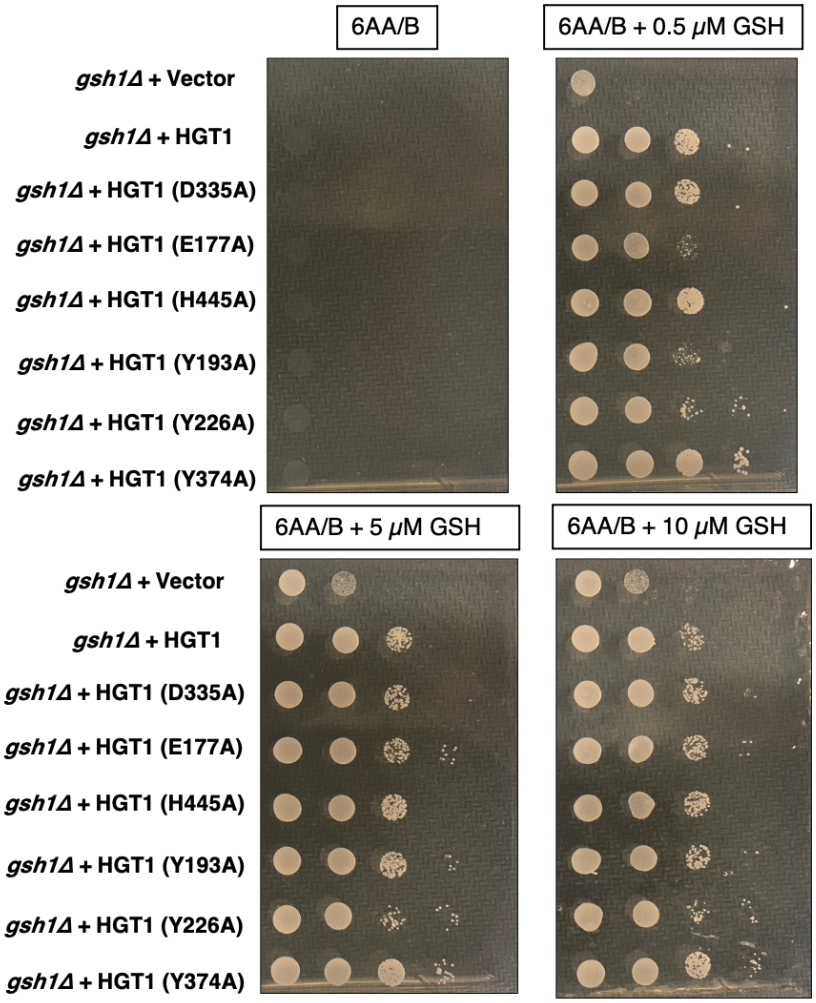

Figure 3.5: Growth difference between *gsh1*Δ cells overexpressed with WT and mutant Hgt1 transporter. *gsh1Δ* strains transformed with p416TEF-*HGT1* (WT), p416TEF-*HGT1* (mutant) or vector control (p416TEF) were pre-grown on SC media selection plates with 0.05 μM GSH added. Yeast strains were serially diluted and spotted on 6AA/B minimal media with indicated concentrations of GSH, and grown anaerobically for 2-3 days at 30 °C.

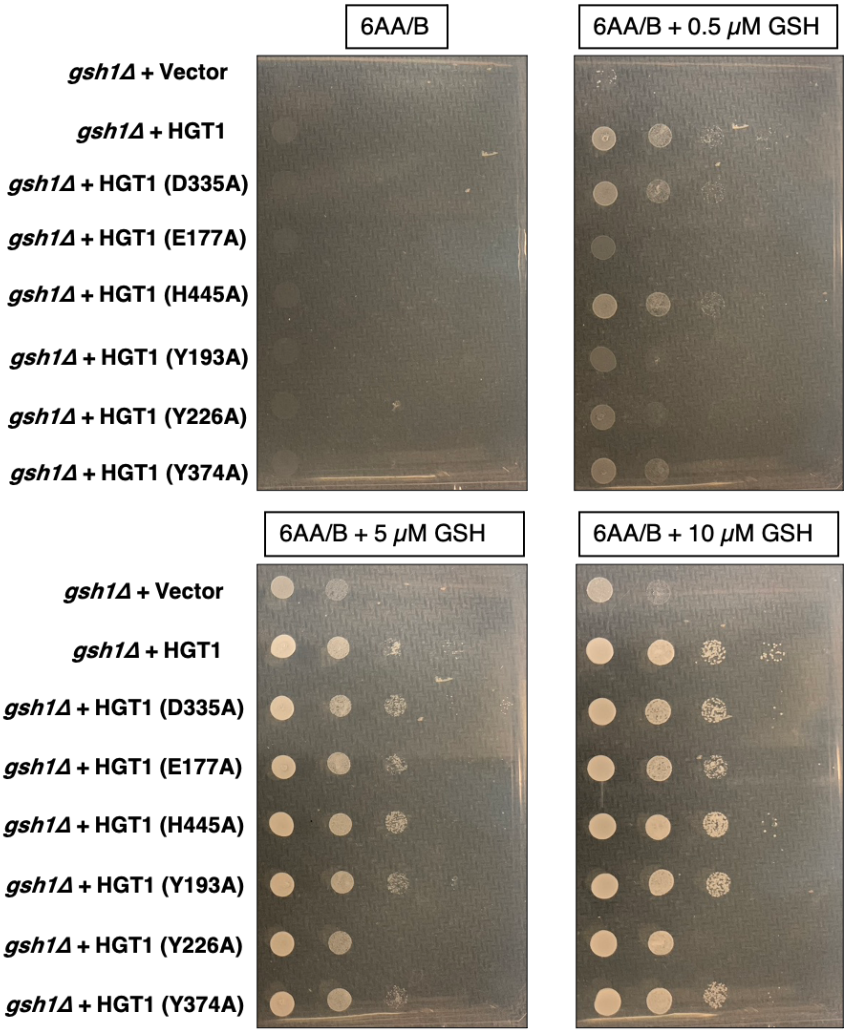

Figure 3.6: Growth differences between *gsh1*Δ cells overexpressed with WT and mutant Hgt1 transporter. *gsh1Δ* strains transformed with p416TEF-*HGT1* (WT), p416TEF-*HGT1* (mutant) or vector control (p416TEF) were pre-grown on SC media selection plates with 0.05 μM GSH added. Yeast strains were serially diluted and spotted on 6AA/B minimal media with indicated concentrations of GSH, and grown aerobically for 2-3 days at 30 °C.

Discussion

The discovery and characterization of the glutathione transporter Hgt1 started in early 2000, when Bourbouloux *et al*., first reported it as a high affinity glutathione transporter as well as a proton symporter (75). Unfortunately, no structural studies regarding its mechanism of interaction with GSH and protons or its mode of regulation have been reported. This is partly because Hgt1 is a large plasma membrane protein, and these specific proteins are notoriously difficult to solubilize and purify. Only a handful of studies regarding the characterization of Hgt1 has been reported but those studies have focused primarily on the specific amino acid residues important for the functionality of the transporter (78,79,125,126,130) and not on the transporter's mode of action and its subsequent downstream effects inside the cell. In our lab, we decided to utilize the Hgt1 transporter to study GSH trafficking and its effect on GSH:GSSG thiol redox balance inside the cell. We also devised a new model where overexpressed the Hgt1 transporter in both WT as well as *gsh1Δ* cells to observe the downstream effects of large GSH fluctuations inside the cell. Our model is based on a study by Kumar *et al*., demonstrating that overexpression of the Hgt1 transporter leads to GSH overaccumulation inside the cells (11).

The difference between lower concentration and higher concentration of GSH with respect to the growth pattern of *gsh1Δ* + *HGT1* cells, was clearly observed in the liquid growth curve assay. At lower concentration, WT + *HGT1* and *gsh1Δ* + *HGT1* cells grew very similarly but at the higher GSH concentrations, the effect of Hgt1 overexpression in both WT and *gsh1Δ* cells was drastic, as the cells were growing poorly. A complete opposite effect of lower and higher GSH concentration was observed in vector control

cells. The reason for the lethality of Hgt1 overexpression at higher GSH concentrations has been reported to be initiation of the iron-starvation response and unfolded protein response of the cell as explained by Kumar *et al*. and Ponsero *et al*. (11,81). Apart from the liquid growth curve assay, my previous lab mate Dr. Crystal Conaway McGee also performed the spot test experiment with the same conditions and showed the same results and conclusion (111).

To understand how the Hgt1 transporter impacts the GSH uptake and homeostasis in the cells, we overexpressed the transporter in both WT and *gsh1Δ* cells and compared these with isogenic strains transformed with a vector control. Dr. Crystal Conaway McGee performed the experiments with relatively low GSH concentrations in the media (0.1 – 5 μM GSH) using WT cells and showed that there is no significant difference in total intracellular GSH levels between the vector control and the strains with Hgt1 transporter overexpression. When the experiment was done in the *gsh1Δ* cells under the same conditions, while GSH levels were difficult to detect in *gsh1Δ* cells cultured in concentrations less than 1 μM, detectable GSH measurements showed that *gsh1Δ + HGT1* retain less GSH in overnight growth than the vector control. These results imply that probably the already stressed *gsh1Δ* cells may accumulate GSH faster with Hgt1 overexpression and the resulting accumulated GSH is then metabolized or degraded quicker. This degradation is presumably mediated by the Dug1-Dug2-Dug3 pathway, which is an alternative GSH degradation pathway (131). The evidence of this purported phenomenon has been provided by Kumar *et al*., in their study (11).

Next, we wanted to see if this peculiar behavior of Hgt1 transporter regarding GSH uptake translates into a variation of the GSH:GSSG thiol redox balance. Surprisingly, we

did not observe any change in the intracellular GSH:GSSG redox state due to Hgt1 overexpression and the resulting redox potential values were the same for both the strains (*HGT1* and empty vector). This data suggested that even though the *gsh1Δ* cells are stressed and have an altered redox state, overexpression of a high affinity GSH transporter does not substantially alter the steady state GSH:GSSG thiol redox state in comparison to *gsh1*Δ strains without *HGT1* overexpression. Only at higher GSH concentration (25 μM), the redox potential of the *gsh1Δ* and WT strains are matched. This data also alludes to a very recent theory that the primary role of GSH is the mediation of Fe-S cluster biogenesis and iron homeostasis, and not the widely believed maintenance of thiol redox balance. We focused more on this direction in the next chapter.

We wanted to confirm whether an active form of the Hgt1 transporter is responsible for the aberrant GSH uptake pattern observed before. Alternatively, the GSH auxotrophy rescue of *gsh1Δ* strains could be an indirect effect of *HGT1* overexpression. Therefore, we generated six variant forms of the transporter using site-directed mutagenesis. This was based on a study reported by Zulkifli *et al*., where they mutated several amino acids to alanine, in an attempt to characterize the important residues necessary for the functionality of the Hgt1 transporter (130). We measured GSH uptake in the *gsh1Δ* cells upon overexpression of WT and mutant Hgt1 transporter, in comparison to the vector control. Although, we could see that there are variations in the GSH uptake due to the mutated transporter, we could not conclude and specify it to a pattern, but this data confirmed that the mutant Hgt1 transporters have altered GSH transport activity. The Bachhawat lab used ^{35}S-GSH with GSH transport assay for measuring GSH levels in WT cells. We used *gsh1*Δ strains with DTNB recycling assay to measure the GSH levels inside the cells. We also

used varying concentrations of GSH to determine the difference of GSH uptake between WT Hgt1 and its mutants. The Bachhawat lab also did the experiments at pH 5.5. So, there were substantial differences about the methods of GSH uptake measurement between Bachhawat lab and our lab. Although we cannot really compare the results between the two studies, we observed that GSH uptake with the mutated residues Y226A and Y374A followed similar pattern in both the studies. The empty vector and WT Hgt1 transporter overexpression strains behaved as expected. Perhaps a short pulse of GSH (may be 30 minutes), instead of the overnight growth with GSH, is required for the GSH uptake assay to come to a specific conclusion.

We also wanted to see if a functional Hgt1 transporter is needed for rescue of *gsh1*Δ strains in the absence of GSH or if the mere presence of the transporter is enough for the rescue. Therefore, we tested if the variant Hgt1 transporters rescue the growth of *gsh1*Δ cells on media with low GSH levels. We observed that the mutant Hgt1 transporters were helping the cells to grow in minimal media in the presence of GSH, but the growth is less robust than with overexpression of the WT Hgt1 transporter, especially with the residues E177A, Y193A and Y226A. D335A and H445A residues behaved like the WT Hgt1. Surprisingly, these observations were more visible in aerobically grown cells. It is probably because WT *HGT1* overexpression (in *gsh1*Δ cells) need very little GSH to get rescued from GSH auxotrophy and mutant Hgt1 transporters already import less GSH inside the cells. So, presumably the presence of oxygen or oxidative stress helps in differentiating between the growth of WT and mutant *HGT1* overexpressed *gsh1*Δ cells. Also, it was interesting to see that the lowest concentration of GSH added in the minimal media, shows the most visible difference in growth, aerobically. Probably similar kind of experiments

should be done with concentrations lower than 0.5 μM GSH, to show the difference between WT and mutated Hgt1 transporters in *gsh1*Δ cells in anaerobic conditions. We would also need to do the experiments with the mutated Hgt1 transporters and varying cysteine concentrations to show whether the overexpression of the Hgt1 transporter is responsible for the rescue of *gsh1*Δ cells from GSH auxotrophy.

References

9. Toledano, M. B., and Huang, M. E. (2017) The Unfinished Puzzle of Glutathione Physiological Functions, an Old Molecule That Still Retains Many Enigmas. *Antioxid Redox Signal* **27**, 1127-1129

11. Kumar, C., Igbaria, A., D'Autreaux, B., Planson, A. G., Junot, C., Godat, E., Bachhawat, A. K., Delaunay-Moisan, A., and Toledano, M. B. (2011) Glutathione revisited: a vital function in iron metabolism and ancillary role in thiol-redox control. *EMBO J* **30**, 2044-2056

75. Bourbouloux, A., Shahi, P., Chakladar, A., Delrot, S., and Bachhawat, A. K. (2000) Hgt1p, a high affinity glutathione transporter from the yeast Saccharomyces cerevisiae. *J Biol Chem* **275**, 13259-13265

76. Bachhawat, A. K., Thakur, A., Kaur, J., and Zulkifli, M. (2013) Glutathione transporters. *Biochim Biophys Acta* **1830**, 3154-3164

78. Thakur, A., and Bachhawat, A. K. (2010) The role of transmembrane domain 9 in substrate recognition by the fungal high-affinity glutathione transporters. *Biochem J* **429**, 593-602

79. Kaur, J., and Bachhawat, A. K. (2009) Gln-222 in transmembrane domain 4 and Gln-526 in transmembrane domain 9 are critical for substrate recognition in the yeast high affinity glutathione transporter, Hgt1p. *J Biol Chem* **284**, 23872-23884

81. Ponsero, A. J., Igbaria, A., Darch, M. A., Miled, S., Outten, C. E., Winther, J. R., Palais, G., D'Autréaux, B., Delaunay-Moisan, A., and Toledano, M. B. (2017) Endoplasmic Reticulum Transport of Glutathione by Sec61 Is Regulated by Ero1 and Bip. *Mol Cell* **67**, 962-973.e965

103. Ostergaard, H., Henriksen, A., Hansen, F. G., and Winther, J. R. (2001) Shedding light on disulfide bond formation: engineering a redox switch in green fluorescent protein. *EMBO J* **20**, 5853-5862

106. Hu, J., Dong, L., and Outten, C. E. (2008) The redox environment in the mitochondrial intermembrane space is maintained separately from the cytosol and matrix. *J Biol Chem* **283**, 29126-29134

107. Ostergaard, H., Tachibana, C., and Winther, J. R. (2004) Monitoring disulfide bond formation in the eukaryotic cytosol. *J Cell Biol* **166**, 337-345

110. Gietz, R. D., and Schiestl, R. H. (1991) Applications of high efficiency lithium acetate transformation of intact yeast cells using single-stranded nucleic acids as carrier. *Yeast* **7**, 253-263

111. McGee, C. C. (2019) *Impact of Glutathione Transporters on Subcellular Glutathione Pools and Cell Survival in Saccharomyces Cerevisiae.* PhD Doctoral dissertation, University of South Carolina

113. Hu, J. (2010) Investigating Subcellular Thiol Redox Chemistry with GFP-based Sensors. *Doctoral dissertation*

119. Morth, J. P., Pedersen, B. P., Buch-Pedersen, M. J., Andersen, J. P., Vilsen, B., Palmgren, M. G., and Nissen, P. (2011) A structural overview of the plasma membrane Na+,K+-ATPase and H+-ATPase ion pumps. *Nat Rev Mol Cell Biol* **12**, 60-70

120. Osawa, H., Stacey, G., and Gassmann, W. (2006) ScOPT1 and AtOPT4 function as proton-coupled oligopeptide transporters with broad but distinct substrate specificities. *Biochem J* **393**, 267-275

121. Sze, H., Li, X., and Palmgren, M. G. (1999) Energization of plant cell membranes by H+-pumping ATPases. Regulation and biosynthesis. *Plant Cell* **11**, 677-690

122. Bogs, J., Bourbouloux, A., Cagnac, O., Wachter, A., Rausch, T., and Delrot, S. (2003) Functional characterization and expression analysis of a glutathione transporter, BjGT1, from Brassica juncea: evidence for regulation by heavy metal exposure. *Plant, Cell & Environment* **26**, 1703-1711

123. Koh, S., Wiles, A. M., Sharp, J. S., Naider, F. R., Becker, J. M., and Stacey, G. (2002) An oligopeptide transporter gene family in Arabidopsis. *Plant Physiol* **128**, 21-29

124. Vasconcelos, M. W., Li, G. W., Lubkowitz, M. A., and Grusak, M. A. (2008) Characterization of the PT Clade of Oligopeptide Transporters in Rice. *The Plant Genome* **1**

125. Zulkifli, M., Yadav, S., Thakur, A., Singla, S., Sharma, M., and Bachhawat, A. K. (2016) Substrate specificity and mapping of residues critical for transport in the high-affinity glutathione transporter Hgt1p. *Biochem J* **473**, 2369-2382

126. Kaur, J., Srikanth, C. V., and Bachhawat, A. K. (2009) Differential roles played by the native cysteine residues of the yeast glutathione transporter, Hgt1p. *FEMS Yeast Res* **9**, 849-866

127. Cubitt, A. B., Heim, R., Adams, S. R., Boyd, A. E., Gross, L. A., and Tsien, R. Y. (1995) Understanding, improving and using green fluorescent proteins. *Trends Biochem Sci* **20**, 448-455

128. Sikorski, R. S., and Hieter, P. (1989) A system of shuttle vectors and yeast host strains designed for efficient manipulation of DNA in Saccharomyces cerevisiae. *Genetics* **122**, 19-27

129. Anderson, M. E. (1985) Determination of glutathione and glutathione disulfide in biological samples. *Methods Enzymol* **113**, 548-555

130. Zulkifli, M., and Bachhawat, A. K. (2017) Identification of residues critical for proton-coupled glutathione translocation in the yeast glutathione transporter, Hgt1p. *Biochemical Journal* **474**, 1807-1821

131. Kaur, H., Ganguli, D., and Bachhawat, A. K. (2012) Glutathione degradation by the alternative pathway (DUG pathway) in Saccharomyces cerevisiae is initiated by (Dug2p-Dug3p)2 complex, a novel glutamine amidotransferase (GATase) enzyme acting on glutathione. *J Biol Chem* **287**, 8920-8931

CHAPTER 4

OVEREXPRESSION OF THE GLUTATHIONE TRANSPORTER HGT1 RESCUES GROWTH IN GSH-DEPLETED CELLS BY IMPORTING CYSTEINE FOR FE-S CLUSTER BIOGENESIS

Abstract

Depletion of glutathione (GSH) in yeast leads to oxidative stress and disruption of Fe-S cluster biogenesis. Consequently, in the absence of GSH in the growth media, deletion of *GSH1*, encoding the first enzyme in the GSH biosynthetic pathway, is lethal. Recently, overexpression of the high affinity GSH transporter in yeast cells has opened up new ways to track the movement of GSH inside the cell. Constitutive expression of this plasma membrane transporter promotes overaccumulation of GSH inside the cell when it is supplied from an extracellular source. We engineered a model yeast strain that combines deletion of GSH1 (*gsh1Δ*) with overexpression of *HGT1* to study the cellular effects of oscillating between GSH deplete and replete conditions, and to track the movement of GSH inside the cell. Surprisingly, we found that constitutive expression of *HGT1* in *gsh1Δ* cells rescued the GSH auxotrophy of this strain. We also show that addition of cysteine to the growth media is required for this rescue. The iron levels in the *gsh1Δ* cells are also partially rescued in the presence of Hgt1 overexpression and the data suggests that the Fe-S cluster biogenesis and maturation is partially restored in both mitochondrial and cytosol

compartments. These data suggest that cysteine may substitute for GSH in Fe-S cluster biogenesis pathways thus sustaining life in the absence of GSH.

Introduction

Glutathione (GSH) is one of the most abundant non-protein thiol compounds, present in almost all prokaryotic and eukaryotic cells. It plays numerous roles including control of redox potential, protection against oxidative stress, detoxification of endogenous and exogenously derived toxins, protein folding, storage, and transport of organic sulfur (132-134). In humans, several diseases have been strongly correlated with altered intracellular GSH levels (36,135,136). In most eukaryotes including the model yeast *Saccharomyces cerevisiae*, the biosynthesis of GSH is mediated by two ATP-dependent cytoplasmic enzymes, γ-glutamylcysteine synthase, encoded by *GSH1* in yeast, and glutathione synthetase, encoded by *GSH2*. GSH may be either utilized in the cytosol or transported by specific transporters to the endoplasmic reticulum (34,80,81,134,137), the mitochondria (138) and/or the extracellular milieu (139). Additionally, GSH serves as an iron ligand for some Fe-S binding proteins involved in iron regulation and the biogenesis and maturation of Fe-S cluster proteins (66,140-142). The importance of GSH is highlighted by the fact that depletion of GSH pools is detrimental to the health and viability of eukaryotes. In yeast, low GSH levels result in oxidant sensitivity, mitochondrial dysfunction, disruption of iron regulation and limited cell growth (36). Similarly, elevated GSH triggers the unfolded protein response (UPR) in the ER and disrupts iron homeostasis, leading to cell death (11). Hence, the homeostatic maintenance of GSH is critical.

The primary cellular functions of GSH have been a subject of controversy in recent years. In the past, GSH's major cellular function has been linked to its redox buffering

properties, although recent studies have emphasized the importance of enzyme kinetics, rather than the thermodynamic redox state of reduced (GSH) and oxidized (GSSG) glutathione pools, in regulating the redox equilibrium for thiol-disulfide pairs. GSH also serves as a major antioxidant cofactor, providing reducing equivalents for enzymes that neutralize reactive oxygen species and repair oxidative damage (4,9). However, emerging studies in yeast have pinpointed GSH's role in iron metabolism and iron-sulfur (Fe-S) cluster biogenesis as the key to its essentiality (11). Depletion of GSH in yeast results in impaired maturation of essential cytosolic Fe-S proteins, iron accumulation and constitutive activation of the iron regulon controlled by the iron-responsive transcription factor Aft1 and its paralog Aft2 (11,36,66).

Biochemical evidence for GSH transport from the extracellular environment has been demonstrated in a variety of organisms ranging from bacteria to yeast and mammalian cells. However, the only high affinity GSH transporter identified is the plasma membrane-localized protein Hgt1/Opt1 of *S. cerevisiae* (75). Reports have shown that overexpression of *HGT1* transporter along with 100 μM GSH supplementation in the media leads to overaccumulation of both reduced (GSH) and oxidized glutathione (GSSG) (11). Studies using either *gsh1Δ* or *HGT1* overexpression strains have characterized the effects of low and high levels of intracellular GSH separately. However, no studies have reported how fluctuation from GSH depletion to GSH overaccumulation affects subcellular redox homeostasis as well as cellular health and viability.

To understand how yeast respond to GSH depleted and replete conditions, we overexpressed the Hgt1 transporter in a *gsh1Δ* strain. Unexpectedly, we find that GSH depleted cells overexpressing *HGT1* are viable when grown in synthetic complete media

without any GSH supplementation. We also show that cysteine is able to partially rescue and sustain the growth of *gsh1Δ + HGT1* strains. This is in accordance to the study where cysteine was shown to partially inhibit the uptake of GSH from the extracellular environment by Hgt1, suggesting that cysteine can also be imported via Hgt1, albeit with lower specificity (75). To investigate whether the partial rescue of *gsh1Δ* cells by *HGT1* overexpression impact Fe-S cluster biogenesis and iron regulation, we measured subcellular iron levels, activity of mitochondrial and cytosolic Fe-S cluster enzymes (qualitatively and quantitatively) and measured changes in expression of *FIT2*, a Aft1-regulated gene that encodes a cell wall protein involved in iron uptake. Interestingly, our data suggests that there is a clear correlation between the partial rescue of *gsh1Δ* cells by Hgt1 overexpression and regulation of iron metabolism.

Experimental Procedures

Yeast strains, media, and growth conditions: *Saccharomyces cerevisiae* cells used in this study were derived from the wild type (WT) strains BY4741 (*MAT*a *his3*Δ1 *leu2*Δ0 *met15*Δ0 *ura3*Δ0) and BY4742 (*MAT*α *his3*Δ1 *leu2*Δ0 *lys2*Δ0 *ura3*Δ0). The BY4741 *gsh1Δ* strain was made by a former member of our lab, Dr. Crystal Conaway McGee (111) and the BY4742 *gsh1Δ* strain was generated using the *gsh1*Δ*::HIS3* plasmid pGSH1KO (111). BY4741 *FIT2pr*-GFP Aft1 reporter strains were generously donated by the lab of Dr. Adam Hughes, University of Utah (143) and its *gsh1Δ* version was also created with pGSH1KO. All *gsh1*Δ strains were selected on SC (-His) plates anaerobically with 25 μM GSH added and verified by PCR and/or phenotypic analysis. All strains utilized in this study are listed in Table 4.1. Strains were grown in synthetic complete (SC) selection media

Table 4.1: Strains used in this study.

Strain	**Genotype**	**Source**
BY4741	*MAT*a *his3*Δ1 *leu2*Δ0 *met15*Δ0 *ura3*Δ0	Research Genetics
BY4741 *gsh1*Δ	BY4741 *gsh1Δ*::*HIS3*	This study
BY4741 Aft1 reporter	BY4741 chrI(199456-199457)::P_{FIT2}-yeGFP-$Term_{ADH1}$:KanMX	(143)
BY4741 *aft1*Δ Aft1 reporter	BY4741 chrI(199456-199457)::P_{FIT2}-yeGFP-$Term_{ADH1}$:HphMX *aft1*Δ::KanMX	(143)
BY4741 *gsh1*Δ Aft1 reporter	BY4741 Aft1 reporter *gsh1Δ*::*HIS3*	This study
BY4741 *gsh1*Δ *aft1*Δ Aft1 reporter	BY4741 *aft1*Δ Aft1 reporter *gsh1Δ*::*HIS3*	This study
BY4742	*MAT*α *his3*Δ1 *leu2*Δ0 *lys2*Δ0 *ura3*Δ0	Research Genetics
BY4742 *gsh1*Δ	BY4742 *gsh1Δ*::*HIS3*	This study

(0.671% yeast nitrogen base without amino acids and with ammonium sulfate, 2% glucose and with appropriate amino acid dropout mix; US Biological) or in supplemented minimal media, termed 6AA/B media (0.671% yeast nitrogen base without amino acids and with ammonium sulfate, 2% glucose, supplemented with six essential amino acids and bases at the following concentrations: 20 mg/L adenine, 60 mg/L leucine, 30 mg/L lysine, 20 mg/L histidine, 20 mg/L tryptophan and 20 mg/L methionine). Versions of this media with five essential amino acids and bases (5AA/B) were also made by leaving out methionine or leucine, depending on the plasmid maintenance or strain requirements. Where required, media was solidified using 2% bacteriological agar (US Biological). Strains used for Aft1 reporter assays were grown in low fluorescent SC drop-out media (Sunrise Pharmaceuticals). Anaerobic cultures were maintained in O_2-depleted culture jars (BD GasPak EZ Container Systems). The BiG (bismuth-glucose) plates for visualizing sulfite reductase activity were made as previously described (144,145). Briefly, the plates contained (w/v) 0.67% yeast nitrogen base (YNB), 0.2% SC dropout mix, 1% β-alanine, 0.1% bismuth ammonium citrate, 0.3% sodium sulfite and 2% glucose (see Chapter 5 for a detailed description). The sulfide (S^{2-}) produced by sulfite reductase reacts with bismuth (Bi^{3+}) to produce the brown precipitate bismuth (III) sulfide (Bi_2S_3).

Plasmid construction and transformation: The p416TEF-*HGT1* plasmid described previously (*CEN URA3*, constitutive *TEF1* promoter driving *HGT1* expression) was used for *HGT1* overexpression (75). The *YCT1* overexpression plasmid p416TEF-*YCT1* (*CEN URA3*) obtained from Anand Bachhawat (India Institute of Science and Education Research) was previously described (146). The *CYS3* overexpression plasmid pAG426GPD-*CYS3* (2μ *URA*3, constitutive *GPD* promoter driving *CYS3* expression) was

obtained from Adam Hughes (University of Utah) (143). Yeast transformations were performed by the standard lithium acetate protocol. GSH deletion (*gsh1Δ*) strains transformed with p416TEF or p416TEF-*HGT1* were grown anaerobically on SC (-Ura) plates with 0.05-0.1 μM GSH added. The creation of p315TEF and p315TEF-*HGT1* plasmids have been described in detail in chapter 5.

Small scale mitochondrial isolation for succinate dehydrogenase assay: Subcellular fractionation of yeast cell extracts was performed as previously described by converting cells to spheroplasts, performing gentle lysis by Dounce homogenization and followed by differential centrifugation (147). In brief, yeast strains were plated on 2% glucose SC media for 2-3 days. Cells were then cultured in SC media with 0.6% glucose at 30 °C, until OD 3-4. Cells were washed with deionized water followed by SOR buffer (1.2 M sorbitol, 20 mM HEPES, pH 7.5). Pelleted cells were resuspended in SOR buffer and lysed with zymolyase for 45 minutes to 1 hour. To prevent protein degradation, spheroplasts were placed on ice and resuspended in ice-cold SM buffer (250 mM sucrose, 10 mM MOPS, pH 7.2) containing protease inhibitors. Organelle release was obtained via Dounce homogenization to disrupt the plasma membrane. The homogenate containing cytosol and crude mitochondria was separated from unbroken cells and nuclei by centrifugation at 3000 rpm for 5 min at 4 °C. The supernatant was then centrifuged at 12000 rpm for 10 min at 4 °C to separate the mitochondria from the post-mitochondrial supernatant (PMS) (147). The crude mitochondrial pellet was carefully washed with SM buffer and diluted to the desired volume. The concentration of the mitochondrial protein extract was determined by the Bradford assay.

Iron-sulfur (Fe-S) cluster enzyme assays: The succinate dehydrogenase (SDH) enzyme assay was performed essentially as previously described (148). The following reagents were mixed in a 1-ml cuvette; 50 mM HEPES (pH 7.4), 0.1 mM EDTA, 1 mM KCN, 100 µM phenazine methosulfate, 50 µM dichloroindophenol (DCIP) and 20 mM sodium succinate. Succinate and 10 µg of mitochondrial protein extract were added just before starting the reaction. The decrease in absorbance at 600 nm upon reduction of DCIP (extinction coefficient = 19.3 mM^{-1} cm^{-1}) was monitored for each sample. Activities reported reflect linear initial rates and are directly proportional to the amounts of added protein. For the aconitase enzyme assay, cells were grown in SC media with 2% glucose to stationary phase, harvested by centrifugation and broken by glass bead homogenization in phosphate buffer (pH 7.4). Cell lysates containing 75 µg of protein were assayed in a total of 750 µl of aconitase reaction buffer containing 20 mM Tris-HCl (pH 7.4), 100 mM NaCl and 0.5 mM cis-aconitate. The decrease in cis-aconitate absorbance at 240 nm was measured in a quartz cuvette as a function of time as previously described (148). An extinction coefficient of 4.88 $mM^{-1}cm^{-1}$ was utilized to calculate the enzyme activity, with 1 unit of aconitase activity is defined as 1 nmol of cis-aconitate converted/min/mg of protein. For the Leu1 (isopropylmalate isomerase) enzyme assay, cells were grown in SC (-Leu) media with 2% glucose to mid-log phase, harvested by centrifugation and broken by glass bead homogenization in TNETG buffer [10 mM Tris/Cl pH 7.4, 2.5 mM EDTA, 150 mM NaCl, 10% (v/v) glycerol, 0.5% (v/v) Triton X-100]. Cell lysates containing 75 µg of protein were assayed in a total of 1-ml of reaction mixture containing 970 µl Leu1 buffer (20 mM Tris-Cl pH 7.4, 50 mM NaCl) and 20 µl of 10 mM 3-isopropylmalic acid. The increase in absorbance at 235 nm due to the formation of 2-isopropylmalic acid was

measured in a quartz cuvette as a function of time as previously described (149). For the qualitative analysis of sulfite reductase activity, BiG plates were made as described earlier (144,145) and yeast strains were serially diluted and spotted as described below.

Growth curves in liquid media and solid media spot assays: To measure the growth of yeast strains in liquid media, cells were plated on SC (-Ura) with 2% glucose plates containing 0.05 μM GSH and grown anaerobically for 2-3 days, anaerobically. Each strain was later inoculated into fresh SC or 6AA/B selection media at an OD_{600} of 0.05. Growth phenotypes of yeast strains were determined in sterile 96-well plates using a Synergy H1 plate-reader and Gen5 software 2.09. For growth on plates, strains were harvested from SC (-Ura) with 2% glucose plates containing 0.05 μM GSH and resuspended in sterile water to OD_{600} of 1. The cells were serially diluted to 0.1, 0.01, 0.001 and 0.0001 OD_{600}. The resuspended cells were spotted on SC or 6AA/B selection plates and incubated at 30 °C aerobically or anaerobically for 2 days.

FIT2pr-GFP Aft1 reporter assay: This protocol has been described previously (143). Aft1 reporter yeast strains containing the *FIT2pr*-GFP transgene and p315TEF empty vector or p315TEF-*HGT1* overexpression plasmids were grown in SC (-Leu) with 2% glucose plates containing 0.05 μM GSH for 2-3 days. Prior to the experiment, yeast cells were grown in low fluorescent SC (-Leu) media overnight to mid-log phase (OD_{600} ~ 1) and harvested for experiments. GFP fluorescence was measured with the Biotek Synergy H1 plate reader with 485 nm excitation and 528 nm emission wavelengths (see Chapter 5 for a detailed description).

Results

To study the effects of GSH fluctuations, our lab created a *gsh1Δ* strain that constitutively uptakes GSH from the extracellular environment via overexpression of the Hgt1 transporter. Due to the essential nature of GSH in yeast, *gsh1Δ* strains were pre-grown on SC plates supplemented with 0.1 μM GSH and cultured in SC liquid media with 0.1 μM GSH until the mid-log phase was reached. Western blot analysis confirmed that *GSH1* was knocked out of both the strains that were transformed with the p416TEF empty vector and the p416TEF-*HGT1* overexpression plasmid (data not shown). The creation of this strain and its confirmation by immunoblot was done by Dr. Crystal Conaway McGee, a former member of our lab. She also confirmed and showed that *HGT1* overexpressing strains would overaccumulate GSH when supplemented with GSH in the media, both in the WT and the *gsh1Δ* strains (9,111).

HGT1 overexpression partially rescues the growth defect of gsh1Δ strains in the presence of cysteine: Due to its cellular abundance ranging from 2 mM to 12 mM and its ability to serve as a co-factor in many redox reactions, GSH is thought to be an important redox factor in the cell. Therefore, we wanted to investigate the effects of dynamic GSH fluctuations by overexpressing *HGT1* in *gsh1Δ* cells. Previously, we made the surprising observation that *gsh1Δ + HGT1* strains can grow almost as well as WT strains in both aerobic and anaerobic conditions (unpublished data of Dr. Crystal Conaway) (111). Next, we wanted to see if the availability of any specific amino acid played a role in the viability of *gsh1Δ + HGT1* strains. We therefore monitored the growth of these strains on 6AA/B media, defined as minimal media with only six amino acids and nucleobases that are essential for yeast growth, added at relatively low concentrations. In comparison, SC media

only lacks a single or a few amino acids that allows maintenance of transformed plasmids. In this minimal media, *gsh1Δ* strains are inviable with or without *HGT1* overexpression (Figure 4.1). Surprisingly, we observed that in the presence of cysteine, the *gsh1Δ + HGT1* strain showed improved growth on 6AA/B minimal media, under anaerobic conditions on solid plates (Figure 4.1) as well as under aerobic conditions (Figure 4.2). This partial rescue was visibly less pronounced under aerobic conditions, suggesting that the presence of oxygen is also detrimental for viability of the *gsh1Δ* strain, and cysteine alone cannot replace the function of GSH in the minimal media under mild oxidative stress conditions. We also noticed that cysteine was able to rescue the cells over a specific range of concentration (0.25 mM to 1 mM) and was toxic for the cells at higher concentration (2 mM). This might be due to the inability of the cells to counter the impact due to formation of reactive oxygen species (ROS) at higher cysteine concentrations (143). We confirmed partial rescue of the *gsh1Δ + HGT1* strain with added cysteine in liquid media as well (Figure 4.3). We also did experiments with addition of other amino acids to the minimal media, including the thioether-containing amino acid methionine. However, only the presence of cysteine showed partial rescue of the *gsh1Δ + HGT1* strain. *gsh1Δ + HGT1* cells also grew better on SC media, compared to 6AA/B + Cys media, suggesting that all the other amino acids, nucleobases and other nutrients in SC media collectively improve the viability of *gsh1Δ + HGT1* cells independently of cysteine (Dr. Crystal Conaway's unpublished data) (111). These results confirm that nutrient availability is important for the growth of *gsh1Δ* cells overexpressing *HGT1*, with cysteine playing a key role.

Cysteine rescues gsh1Δ + HGT1 strains following prolonged growth without GSH: To test the efficiency of rescue following prolonged growth without GSH, viability was

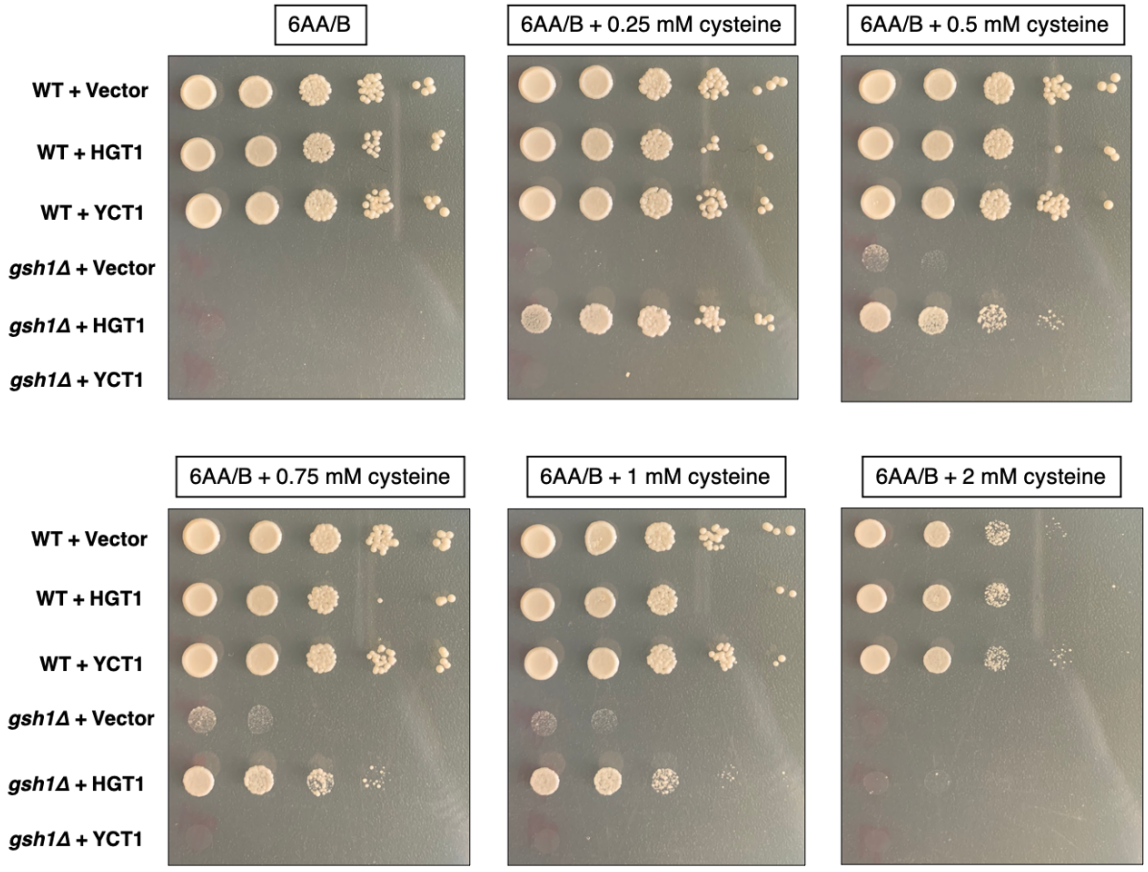

Figure 4.1: *HGT1* overexpression partially rescues the growth defect of *gsh1Δ* cells in the presence of cysteine on solid media.WT and *gsh1Δ* strains transformed with p416TEF-*HGT1*, p416TEF-*YCT1* or vector control (p416TEF) were pre-grown on SC media selection plates with 0.05 µM GSH added. Yeast strains were serially diluted and spotted on 6AA/B minimal media with increasing concentrations of cysteine, and grown anaerobically for 2-3 days at 30 °C.

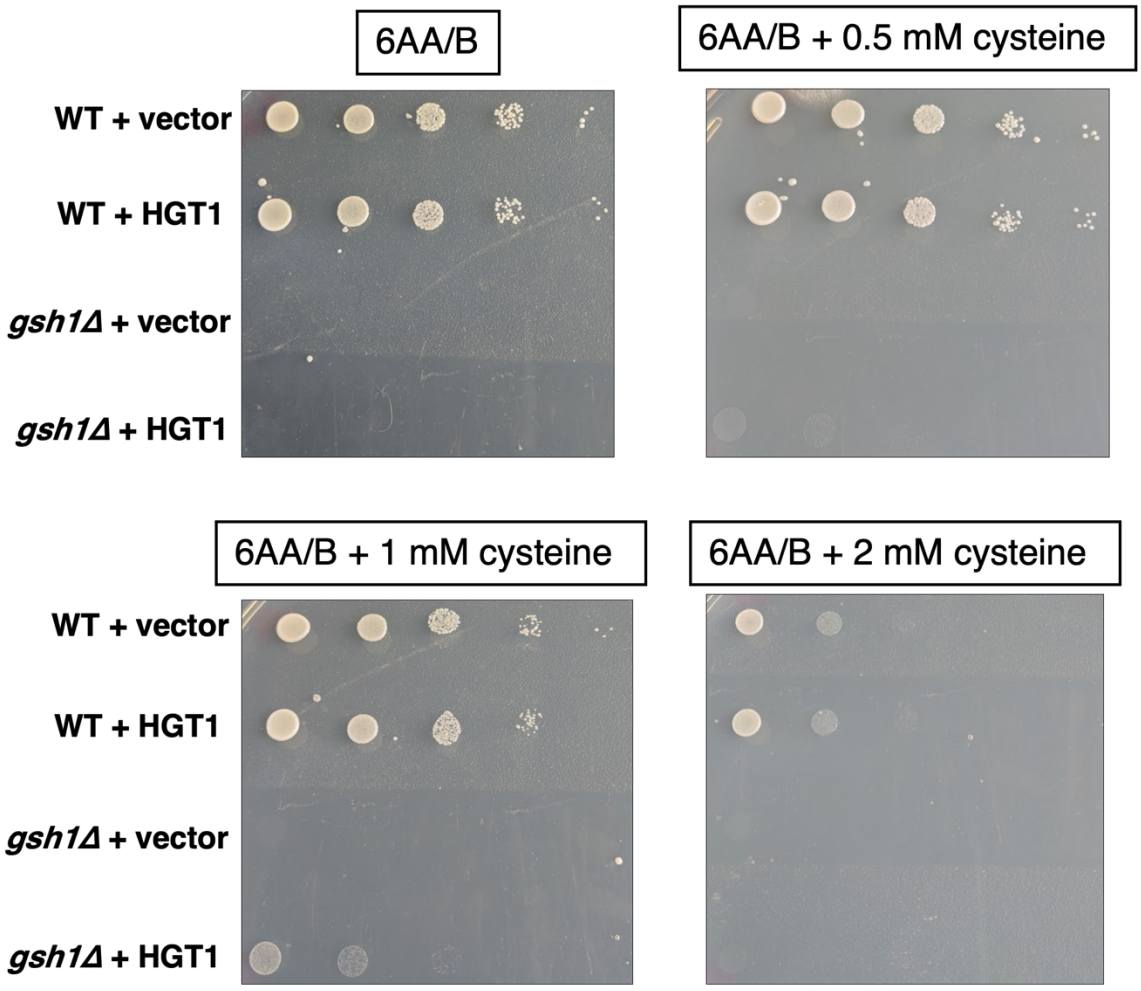

Figure 4.2: *HGT1* overexpression partially rescues the growth defect of *gsh1*Δ cells in the presence of cysteine on solid media. WT and *gsh1Δ* strains transformed with p416TEF-*HGT1*, or vector control (p416TEF) were pre-grown on SC media selection plates with 0.05 µM GSH added. Yeast strains were serially diluted and spotted on 6AA/B minimal media with increasing concentrations of cysteine, and grown aerobically for 2-3 days at 30 °C.

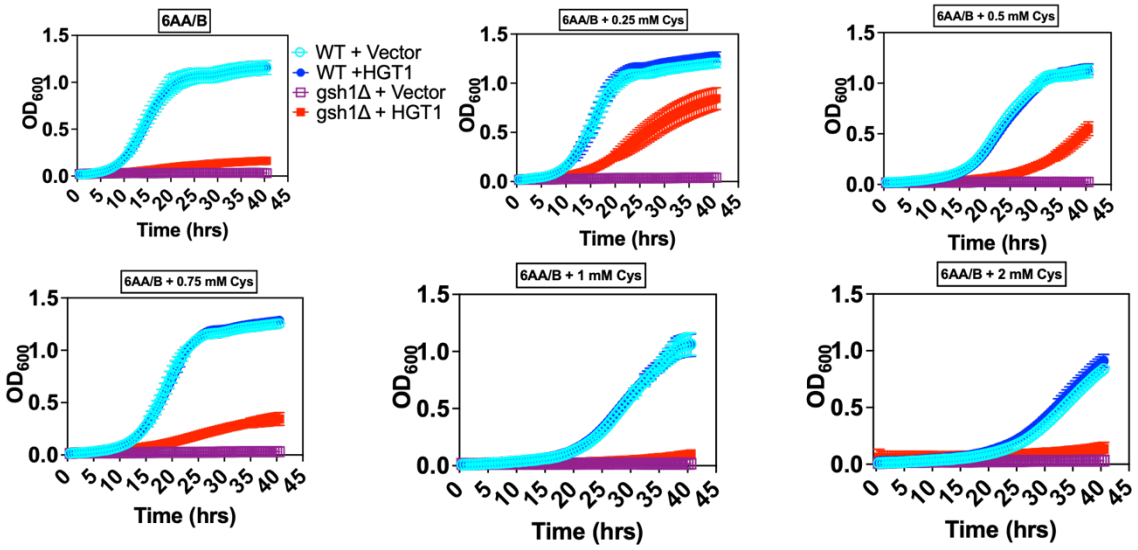

Figure 4.3: *HGT1* overexpression partially rescues the growth defect of *gsh1Δ* cells in the presence of cysteine in liquid media. *gsh1Δ* cells with *HGT1* overexpression are viable in the presence of cysteine up to a concentration of 1 mM. Strains used are the same as in Figure 4.1. Growth and sensitivity to cysteine was analyzed at 30 minutes intervals over 40 hours using a Synergy H1 plate reader. Data shown are the means of 3 independent experiments with error bars representing standard deviation (SD).

monitored after 72 hours growth in GSH-deficient media. Ayer *et al*., reported that *gsh1Δ* cells switched to GSH-deficient media undergo 8-10 cell divisions before GSH pools are too diluted to support further growth (36). Therefore, we tested whether *gsh1Δ* + *HGT1* cells would continuously grow for longer than 24 hours with >10 divisions without GSH addition. After growth in SC media for 72 hours, *gsh1Δ* + *HGT1* cells and the WT control cells were plated on 6AA/B minimal media plates without and/or without cysteine. We clearly observed that cysteine could still rescue *gsh1Δ* + *HGT1* cells without any assistance from extracellular GSH (Figure 4.4). Interestingly, the level of cysteine required in the media for maximal growth rescue of these *gsh1Δ* + *HGT1* cells (1.0 mM) was appreciably higher than the amount observed for maximal growth in Figure 4.1 (0.25 mM) in which the cells were pre-grown on SC plates with 0.05 μM GSH before spotting on the 6AA/B minimal media plates. We presume that this shift towards higher concentration of cysteine in Figure 4.4 is due to the absence of any basal level of GSH (in *gsh1Δ* + *HGT1* cells), which might have been carried over from SC plates with 0.05 μM GSH.

We also tried to confirm the importance of cysteine in another way. We theorized that if cysteine could be broken down inside the cells, rescue of GSH auxotrophy by cysteine might be hampered. We utilized a *CYS3* overexpression plasmid from Dr. Adam Hughes's lab from the University of Utah (143). The *CYS3* gene encodes for cystathionine gamma-lyase, an enzyme which breaks down cysteine to pyruvate, ammonia, and hydrogen sulfide. We overexpressed *CYS3* along with *HGT1* as well as vector controls in *gsh1*Δ cells and tested their phenotypes by spot test growth assay (Figure 4.5). We observed reduced viability of *gsh1*Δ cells on solid media with added Cys with *HGT1* and *CYS3* overexpression which suggested that the enzyme is reducing cysteine availability, which

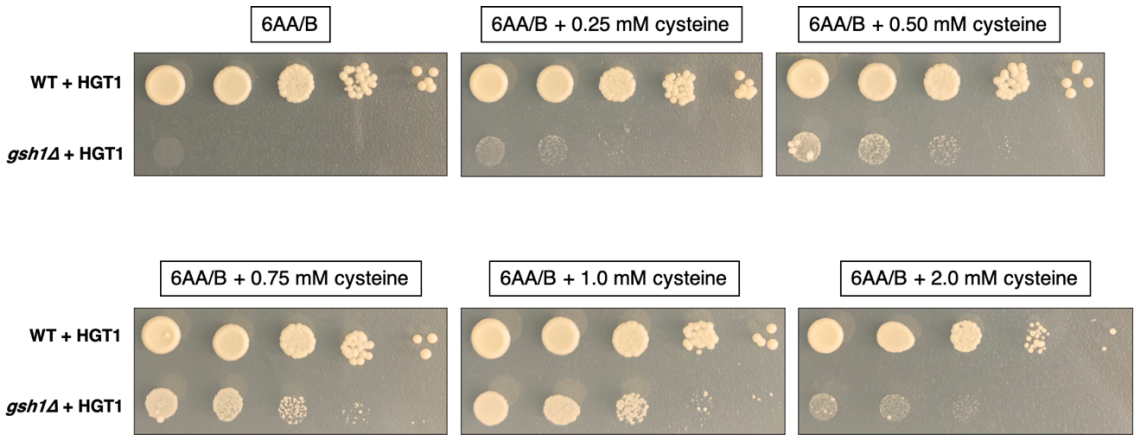

Figure 4.4: Cysteine is solely responsible for the partial rescue of *gsh1Δ* cells grown without GSH. The indicated strains (described in Figure 4.1) were grown in liquid media for 72 hours in the appropriate media (SC -Ura, with no GSH added), with dilution every 24 hours, to make sure that there was absolutely no GSH in the media. Yeast strains were then serially diluted to 1, 0.1, 0.01, 0.001 and 0.0001 OD_{600} and spotted on 6AA/B minimal media with increasing cysteine concentrations and grown anaerobically for 2-3 days at 30 °C.

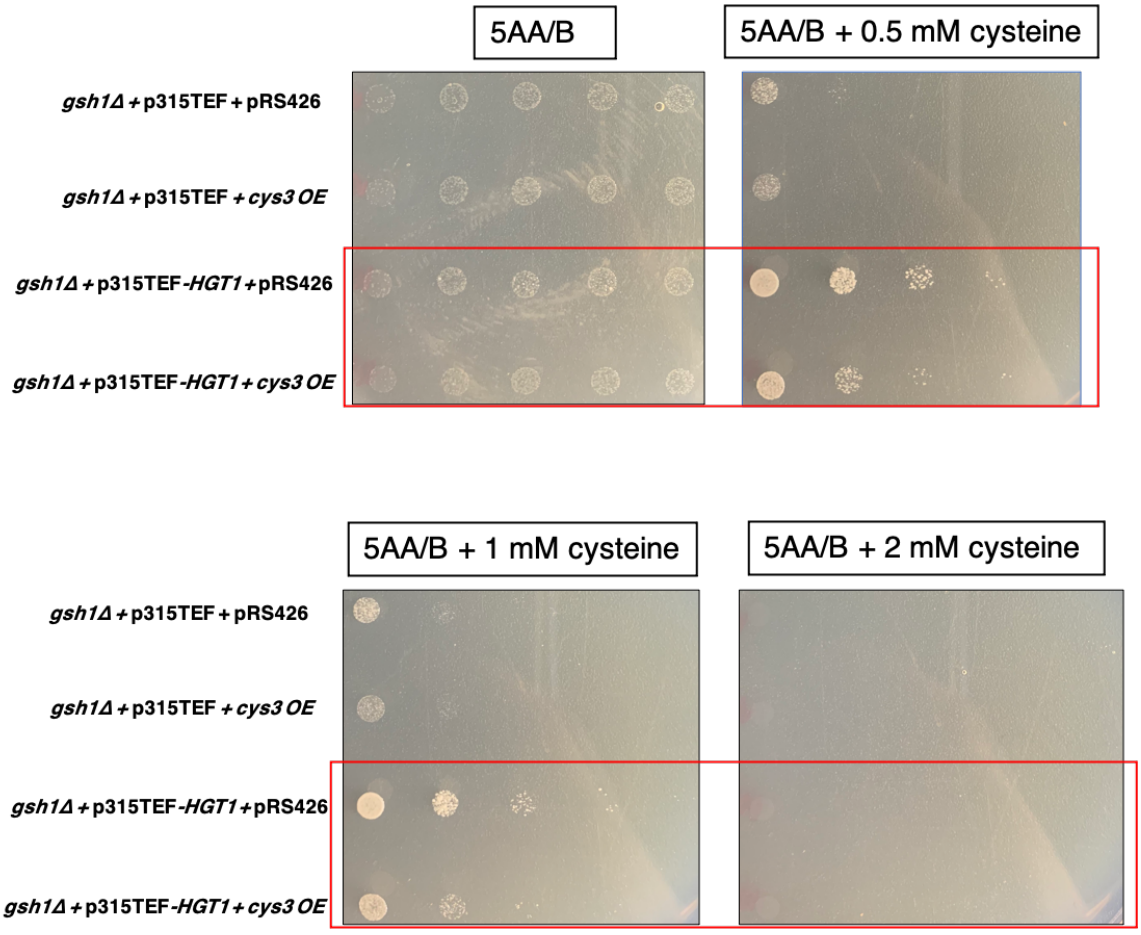

Figure 4.5: Cysteine could be degraded to reveal its importance for the recovery from GSH auxotrophy. *gsh1Δ* strains transformed with p315TEF-*HGT1*, pAG426GDP-*CYS3* or vector control (p315TEF or pRS426) were pre-grown on SC media selection plates with 0.05 µM GSH added. Yeast strains were serially diluted and spotted on 5AA/B minimal media (Ade, Lys, His, Met, Trp) with increasing concentrations of cysteine, and grown anaerobically for 2-3 days at 30 °C.

likewise counteracted the effect of *HGT1* overexpression.

To further confirm whether cysteine (which contains a thiol group) and not methionine (which has a thioether group) is the sole amino acid responsible for the partial rescue of the *gsh1Δ + HGT1* cells, a similar experiment was performed with BY4742 (*MATα his3Δ1 leu2Δ0 lys2Δ0 ura3Δ0*) yeast strains. This specific strain is not an organic sulfur auxotroph like BY4741 and does not need extracellular methionine to survive. Like BY4741, the *GSH1* gene was deleted in BY4742 and transformed with the p416TEF-*HGT1* plasmid or vector control. Therefore, the minimal media in this case was 5AA/B (without methionine) ± cysteine. We again observed that the presence of cysteine could still rescue *gsh1Δ + HGT1* without any assistance from extracellular GSH (Figure 4.6).

N-acetylcysteine (NAC) is a precursor of cysteine, but it is not found naturally. Several studies have shown that NAC is effective as an antioxidant (150-153) and it is widely used in the context of clinical studies. We wanted to see whether this thiol-containing cysteine derivative rescues *gsh1Δ + HGT1* cells as well as cysteine. Surprisingly, we observed that not only could NAC rescue growth in these cells, but it also did not impart the toxicity of cysteine at higher concentration (Figure 4.7). Even at 5 mM concentration, *gsh1Δ + HGT1* cells grew almost as well as the WT cells. Structurally, the difference between NAC and cysteine is the presence of a bulky acetyl (-CH_3CO) group in NAC, which usually is cleaved off intracellularly by deacetylase enzymes. The exact mechanism as to why NAC is not toxic to *gsh1Δ + HGT1* cells even at higher concentrations, remains unclear and warrants further experiments, such as tracking the sulfur entity using ^{35}S-labeled NAC after it enters the cell.

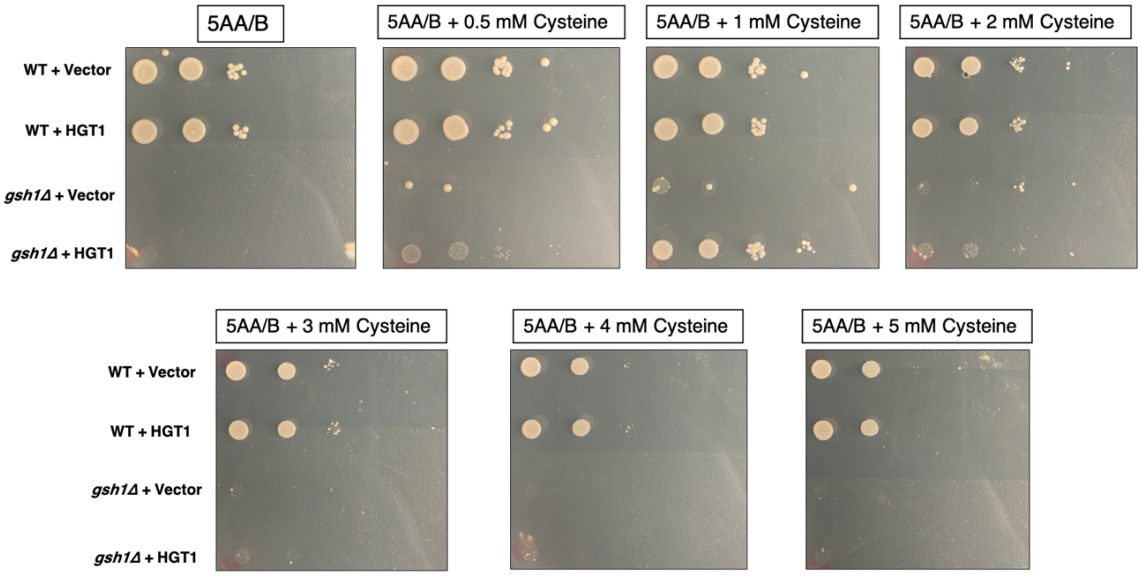

Figure 4.6: BY4742 Met+ strains also show partial rescue by *HGT1* overexpression in the presence of cysteine. BY4742 WT and *gsh1Δ* strains were pre-grown on SC media selection plates with 0.05 µM GSH (as described in Figure 4.1). Yeast strains were serially diluted and spotted on 5AA/B minimal media plates (Ade, Lys, His, Trp, Leu) without methionine and with increasing concentrations of cysteine, and grown anaerobically for 2-3 days at 30 °C.

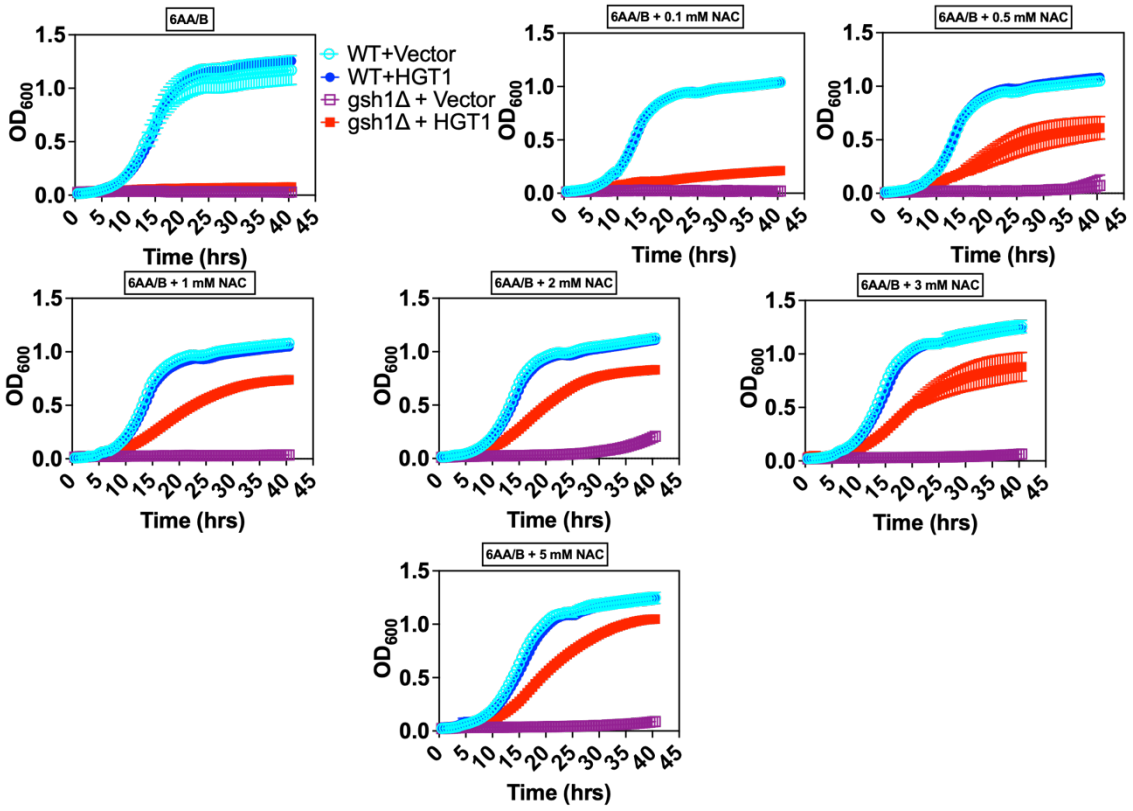

Figure 4.7: N-acetyl-cysteine (NAC) supports the growth of *gsh1Δ* + *HGT1* strains but does not impart the toxicity of cysteine at higher concentration. *gsh1Δ* cells with Hgt1 transporter overexpression are fully viable in the presence of NAC even at higher concentration. Strains are the same as in Figure 4.1. Growth and sensitivity to NAC was analyzed by using a Synergy H1 plate-reader as described in Figure 4.2. Data shown here are the means of 3 independent experiments with error bars representing standard deviation (SD).

Iron regulation defects in gsh1Δ are partially rescued by the Hgt1 transporter overexpression: Iron regulation in *Saccharomyces cerevisiae* is controlled by the paralogous transcriptional activators, Aft1 and Aft2. Iron deficiency activates Aft1 and Aft2 causing the proteins to move from the cytosol to the nucleus, where they bind to the DNA and promote the expression of iron regulon genes involved in iron uptake (154-156). GSH depletion in cells causes Aft1 activation and thus upregulation of iron uptake genes and iron overaccumulation, which also subsequently leads to decreased activity of Fe-S cluster enzymes. Therefore, we wanted to determine the impact of *HGT1* overexpression on iron metabolism in GSH-depleted cells. The following experiments were performed by my former lab mate Dr. Crystal Conaway McGee (111). It was found that the cytosolic iron levels had increased two-fold in *gsh1Δ* + vector cells while *gsh1Δ* + *HGT1* cells had similar iron levels as the WT strain (Figure 4.8). It has been previously reported that mitochondrial iron increases significantly with GSH depletion (144). We observed an approximately 16-fold increase in mitochondrial iron levels in *gsh1Δ* + vector cells compared to the WT cells. While the *gsh1Δ* + *HGT1* cells also accumulate iron, the levels are significantly lower than the *gsh1Δ* + vector cells. These results suggest that *HGT1* overexpression helps *gsh1Δ* cells regulate iron more efficiently.

Fe-S cluster defects are partially rescued by overexpression of the Hgt1 transporter: Since defects in the biosynthesis of cellular iron-sulfur (Fe-S) proteins are associated with depletion of GSH (9,11,140), we sought to investigate the Fe-S enzyme activities in the cytosol as well as the mitochondria. To monitor cytosolic Fe-S enzyme activity, we chose to investigate the activity of sulfite reductase, a [4Fe-4S] enzyme responsible for reducing sulfite (SO_3^{2-}) to sulfide (S^{2-}). This reduction reaction is monitored

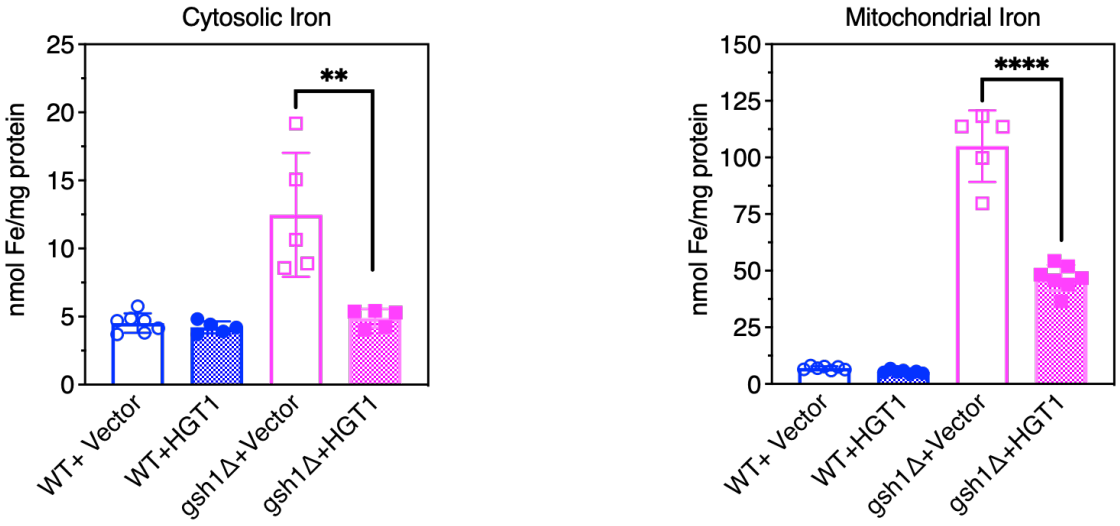

Figure 4.8: Defects in iron regulation are partially rescued by *HGT1* overexpression. The indicated BY4741 yeast strains were pre-grown on SC -Ura plates with 0.05 µM GSH for 2 days and cultured overnight in SC -Ura media. Cytosolic and mitochondrial iron was measured by atomic absorption spectroscopy. Data shown represents 3-8 independent experiments with error bars representing standard deviation (SD). For both the organelles, difference between iron levels of *gsh1Δ* + Vector and *gsh1Δ* + *HGT1* are statistically significant (as determined by an unpaired t-test), with $P < 0.01$ (cytosol) and $P < 0.0001$ (mitochondria). Iron measurements were performed by Dr. Crystal Conaway McGee (111).

in vivo on a growth plate in the presence of bismuth ammonium citrate and sodium sulfite (Na_2SO_3), which results in the formation of bismuth sulfide (Bi_2S_3) as a brown precipitate. We also included the strain *met10Δ* strain as a negative control in this specific experiment to demonstrate and differentiate between the active and inactive enzyme. *MET10* is one of the five genes (others are *MET5*, *MET8*, *MET18* and *MET20*) that encodes components of the sulfite reductase enzyme complex and is essential for its activity (145). We observed that the *gsh1Δ* + *HGT1* cells gave rise to brown colonies, although not as robust as the WT cells, suggesting partial rescue and activity of the sulfite reductase enzyme (Figure 4.9A). No colonies (white or brown) can be observed with *gsh1Δ* + vector cells, reflecting the inviability of the *gsh1Δ* cells under these growth conditions. Expectedly, the *met10Δ* + vector cells gave rise to white colonies, confirming that the enzyme is inactive and is not essential for growth under these conditions. Interestingly, we observed that the *gsh1Δ* + *HGT1* cells are unable to grow on SC plates in the presence of bismuth ammonium citrate and sodium sulfite under aerobic conditions (Figure 4.9B). It is possible that the presence of oxygen and excess sulfite together results in increased oxidative stress in this GSH-deficient strain that leads to inviability even in the presence of cysteine. We also tested the activity of a cytosolic Fe-S enzyme using a quantitative assay. Leu1 (isopropylmalate isomerase) is a [4Fe-4S] enzyme involved in leucine biosynthesis. We observed a slight but statistically significant increase in the enzyme activity of *gsh1Δ* + *HGT1* cells compared to the *gsh1Δ* + vector cells. This implies that *HGT1* overexpression in *gsh1Δ* cells may allow minimal activity of the cytosolic Fe-S cluster enzymes (Figure 4.10), in order to bypass their GSH auxotrophy. We also note that the *gsh1*Δ + vector cells were inoculated at a higher OD than the *gsh1*Δ + *HGT1* cells in order to generate enough cell

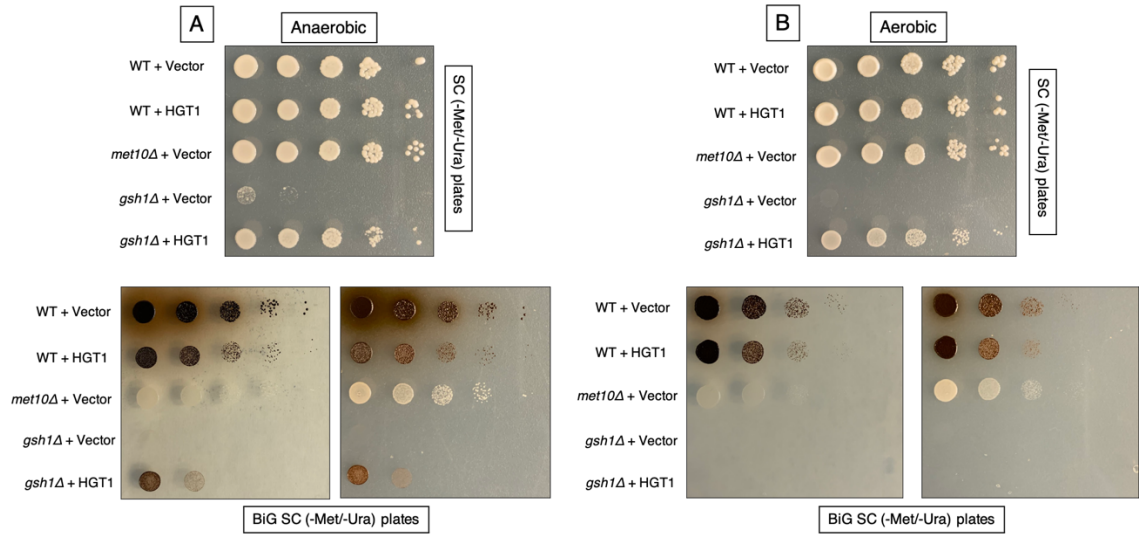

Figure 4.9: Cytosolic iron homeostasis defects are partially rescued by the Hgt1 transporter overexpression: indirect assay for sulfite reductase activity. Serial dilutions of BY4741 WT and *gsh1Δ* cells (with empty vector and *HGT1* overexpression) were spotted on SC bismuth-sulfite plates. Cells grown on SC plates without bismuth are shown at the top (A and B). BY4741 *met10Δ* + empty vector cells were used as a negative control, to have a clear distinction between the enzyme's presence and/or absence. Cells were grown anaerobically in (A) and aerobically in (B).

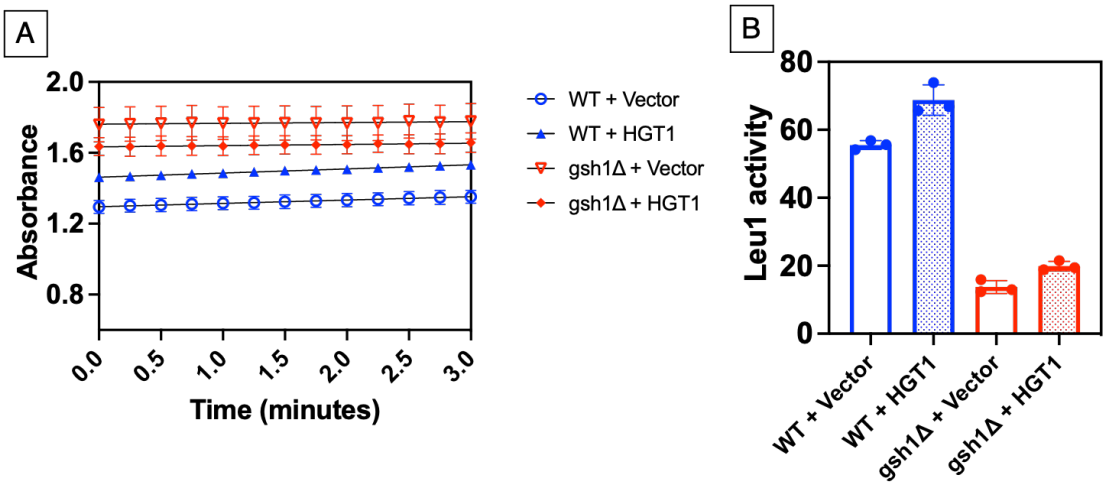

Figure 4.10: Cytosolic Fe-S protein defects in *gsh1Δ* cells is slightly rescued by the Hgt1 transporter overexpression: Leu1 activity assays. Cell lysates were prepared for the indicated yeast strains and tested for Leu1 (isopropylmalate isomerase) activity. One unit of enzyme activity is equivalent to 1.0 nmol of 3-isopropylmalate converted/min/mg protein. (A) Assay results showing the increase in absorbance at 235 nm; (B) data from (A) converted to enzymatic activity. Reported values are the means of three independent experiments and the error bars are standard deviations (SD).

mass for the assays before they reach the point of growth stasis. Crystal's analysis of GSH levels in *gsh1*Δ + vector cells grown to the point of stasis demonstrate that they have some residual, measurable GSH (111), which may facilitate a minimal level of Fe-S cluster biogenesis.

For testing the activity of the mitochondrial Fe-S enzymes, we decided to look into two specific enzymes, aconitase (converts citrate to isocitrate via cis-aconitate intermediate) and succinate dehydrogenase (SDH; converts succinate to fumarate). We could not observe any significant increase in aconitase enzyme activity in the *gsh1Δ* + *HGT1* cells compared to the *gsh1Δ* + vector cells, suggesting that the Hgt1 transporter overexpression in *gsh1Δ* cells does not strongly impact the activity of this mitochondrial Fe-S enzyme (Figure 4.11). In contrast, the WT cells exhibited robust aconitase enzyme activity comparable to previously published results (148,157). We isolated the mitochondria of these strains to test the activity of the TCA cycle enzyme and respiratory chain component, succinate dehydrogenase (SDH). Here too, we could not observe any significant increase in enzymatic activity for the *gsh1Δ + HGT1* cells (Figure 4.12) relative to *gsh1Δ* + vector control cells. The WT cells showed normal enzymatic activity comparable to previously published data (148,157). These results imply that the *HGT1* overexpression in *gsh1*Δ cells do not strongly impact the activity of the mitochondrial Fe-S enzymes It is possible that the enzymatic activities (in *gsh1Δ* cells) of all the enzymes studied are low in both the cytosolic and mitochondrial compartments and as such, the difference in their activity may not be measured in a statistically significant manner.

Our results prompted us to investigate if the presence of iron (in the form of ferrous ammonium sulfate; FAS) can rescue the cells from GSH auxotrophy, since we have

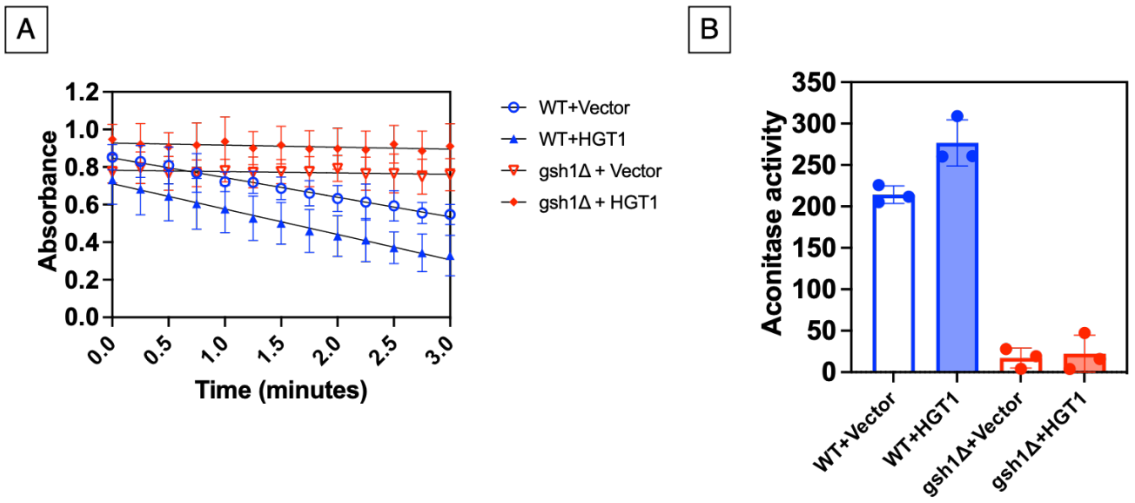

Figure 4.11: Mitochondrial Fe-S protein defects in *gsh1Δ* cells are not rescued by the Hgt1 transporter overexpression: Aconitase activity assays. Cell lysates were prepared for the indicated yeast strains and tested for aconitase activity. One unit of enzyme activity is equivalent to 1.0 nmol substrate converted/min/mg protein. (A) Assays results showing the decrease in absorbance at 240 nm; (B) data from (A) converted to enzymatic activity. Reported values are the means of three independent experiments and the error bars are standard deviation (SD).

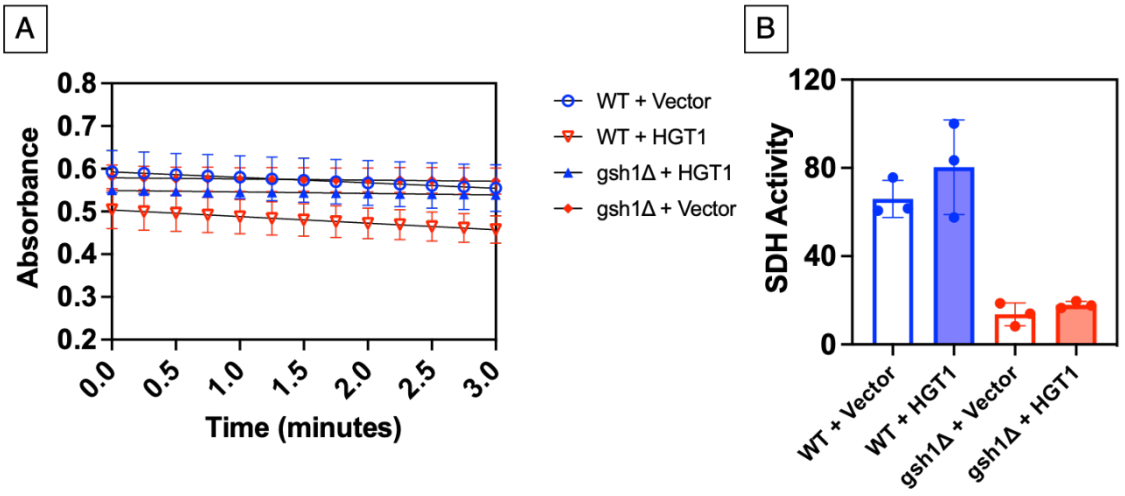

Figure 4.12: Mitochondrial Fe-S protein defects in *gsh1Δ* cells are not rescued by the Hgt1 transporter overexpression: Succinate dehydrogenase activity assays. Crude mitochondrial extracts were prepared for the indicated yeast strains and tested for succinate dehydrogenase activity. One unit of enzyme activity is equivalent to 1.0 nmol of substrate converted/min/mg protein. (A) Assays results showing the decrease in absorbance at 600 nm; (B) data from (A) converted to enzymatic activity. Reported values are the means of three independent experiments and the error bars are standard deviation (SD).

observed evidence of the Hgt1 transporter impacting Fe-S cluster biogenesis and maturation in the absence of GSH. It is possible that cysteine may chelate iron in the media and allow increased iron import through Hgt1 to help rescue Fe-S cluster biogenesis. We tried adding different concentrations of FAS in the SC media and did a liquid growth curve assay, but it remained inconclusive because the *gsh1Δ + HGT1* cells also grew robustly along with the WT cells (Figure 4.13). So, we switched to minimal media and performed the same experiment. We did not observe any rescue of the *gsh1Δ + HGT1* cells, even at higher concentrations of FAS, while the WT cells grew normally at all conditions (Figure 4.14). This implies that the mere presence of iron in the minimal media, even with the overexpression of Hgt1 transporter, is unlikely to be sufficient for rescuing the Fe-S cluster defects caused by GSH deficiency.

To further investigate the connection between Hgt1 overexpression and the rescue of GSH auxotrophy through Fe-S cluster biogenesis and maturation, we received two quantitative Aft1 transcriptional reporter strains from Dr. Adam Hughes's lab from the University of Utah. These strains house an Aft1 transcriptional reporter composed of the Aft1-responsive *FIT2* promoter (*FIT2pr*) driving expression of GFP (Figure 4.15A) (143). One of these strains also has the *AFT1* gene deleted. We deleted the *GSH1* gene encoding the Gsh1 enzyme and overexpressed the empty vector and the Hgt1 transporter in these strains. The idea is that both Fe-S cluster and GSH are required to inhibit Aft1 activity when iron is sufficient because GSH is an Fe-S cluster ligand for the Grx3-Fra2 complex which transfers an Fe-S cluster to Aft1/2. Fe-S cluster binding to Aft1/2, in turn, decreases its DNA binding affinity, leading to deactivation of the iron regulon. As a control

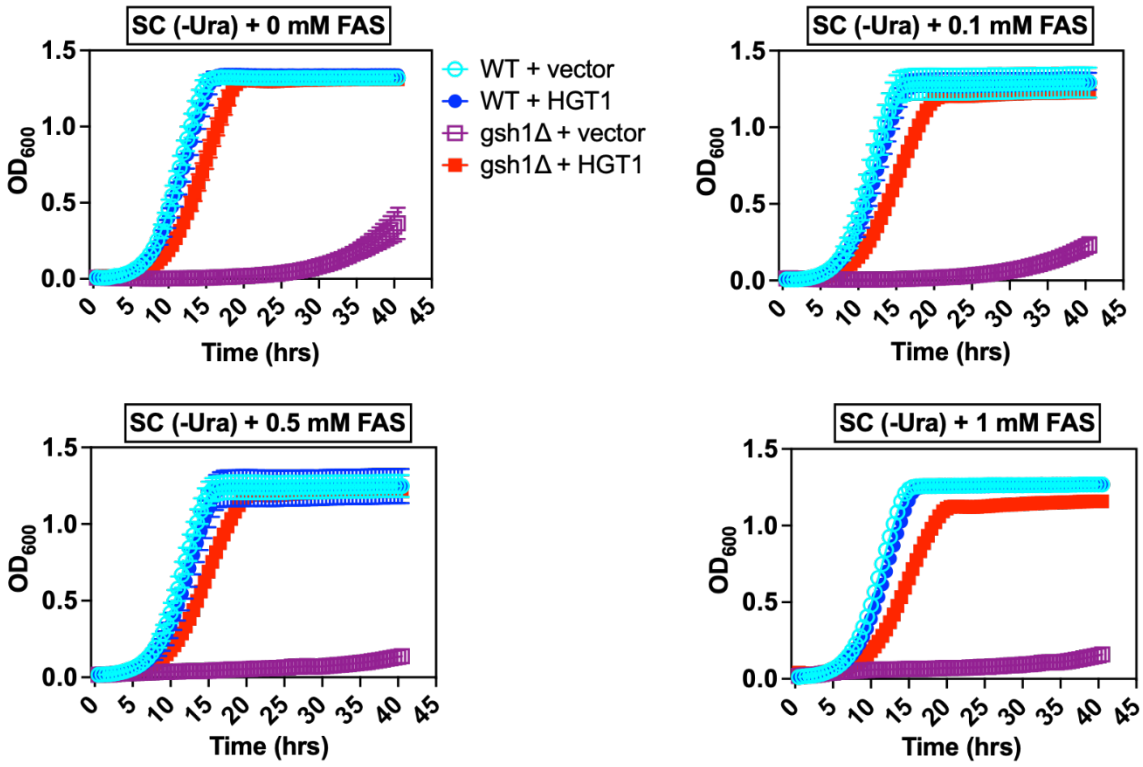

Figure 4.13: No difference between the WT/*gsh1*Δ + *HGT1* cells in SC media with iron.Yeast strains (same as in Figure 4.1) were pre-grown on SC plates with 0.05 µM GSH for 2 days. *gsh1Δ* and WT cells overexpressing *HGT1* grow in the same way in SC media and in the presence of iron. Growth was analyzed by using a Synergy H1 plate-reader. Data shown here are the means of 3 independent experiments with error bars representing standard deviation (SD).

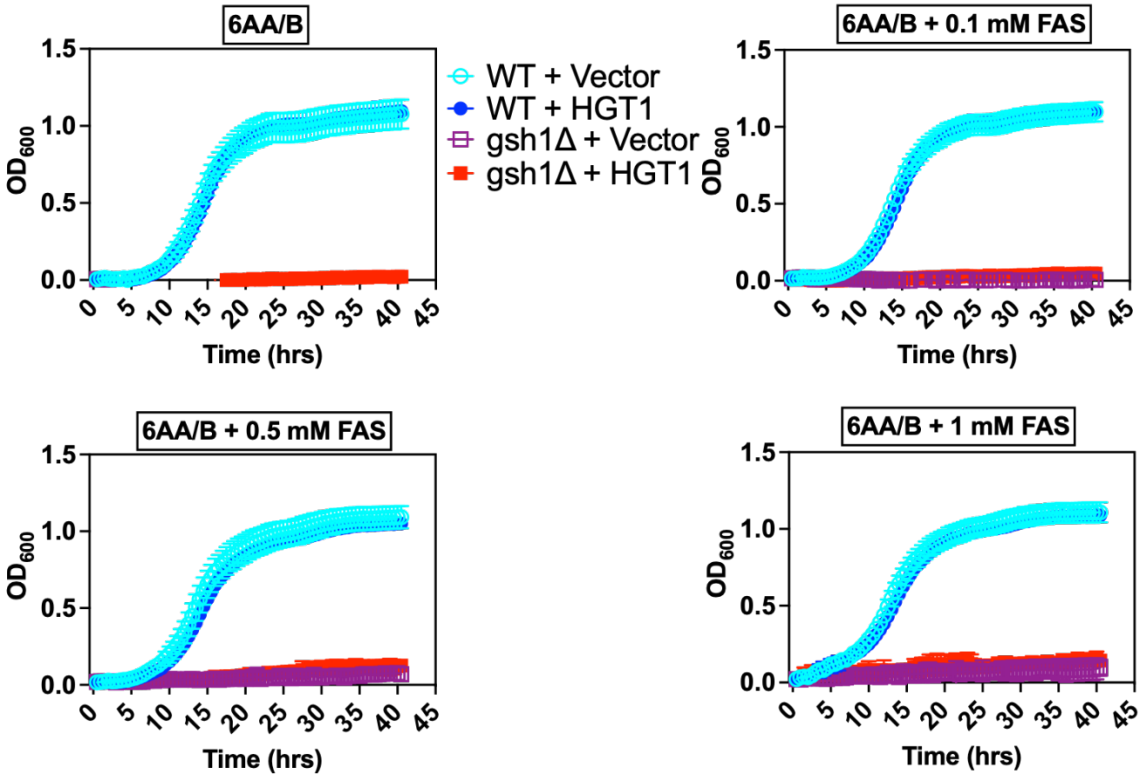

Figure 4.14: Presence of iron does not help in rescuing the inviability of *gsh1Δ* cells even with the Hgt1 transporter overexpression. Yeast strains (same as in Figure 4.1) were pre-grown on SC plates with 0.05 µM GSH for 2 days. *gsh1Δ* cells overexpressing *HGT1* do not grow in the presence of iron and minimal media. Iron is provided by adding ferrous ammonium sulfate (FAS) in the media. Growth was analyzed by using a Synergy H1 plate-reader. Data shown here are the means of 3 independent experiments with error bars representing standard deviation (SD).

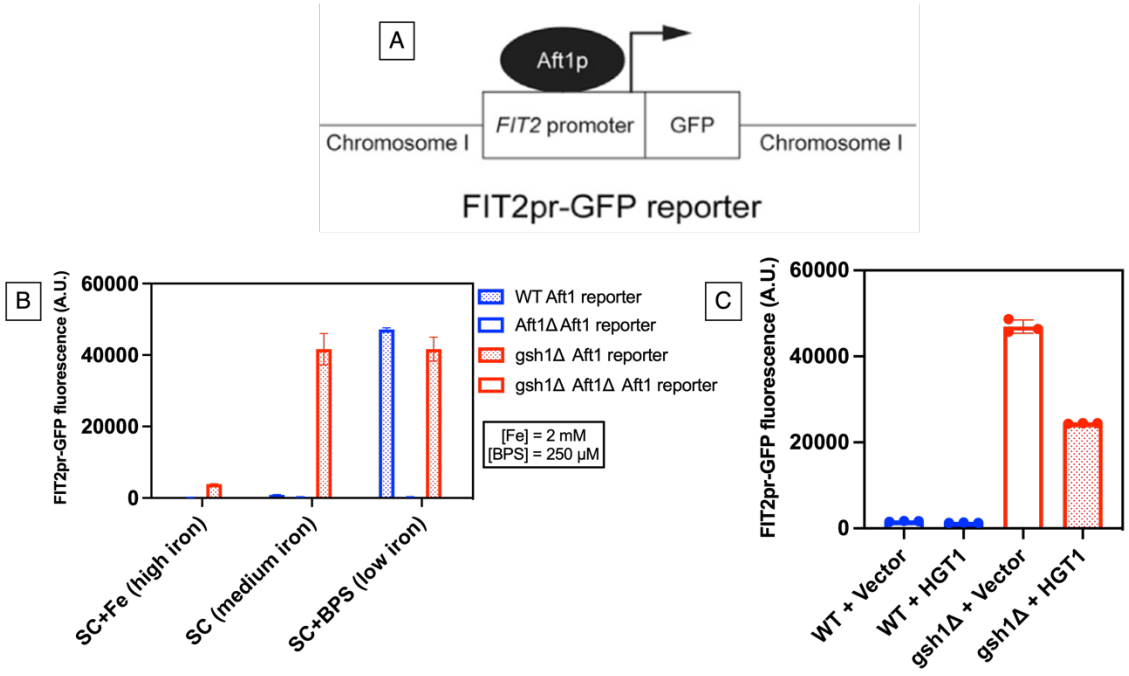

Figure 4.15: Defects in cellular iron homeostasis are partially rescued by *HGT1* overexpression. The indicated BY4741 yeast strains were pre-grown on SC complete plates with/without 0.05 µM GSH [for strains in (B)] or SC (-Leu) plates with/without 0.05 µM GSH for 2 days [for strains in (C)] and cultured overnight in low fluorescent SC complete media [for strains in (B)] or SC (-Leu) media [for strains in (C)] until mid-log phase. (A) Schematic of the Aft1 transcriptional reporter (143), (B) and (C) GFP was measured using the Biotek Synergy H1 plate reader, with excitation and emission wavelengths of 485 and 528 nm, respectively. In (C), WT and *gsh1*Δ Aft1 reporter strains are transformed with p315TEF (vector) or p315TEF-*HGT1*. Reported values are the means of three independent experiments and the error bars are standard deviations (SD).

experiment, we performed this analysis in *aft1*Δ strains to verify the Aft1-dependent activity of the GFP reporter. We made three different media conditions for growing these cells: high iron (SC media with FAS), medium iron (SC media), and low iron (SC media with BPS; an iron chelator). We saw that in all conditions, *aft1*Δ cells did not have any GFP signal, which was expected. In high iron condition, we saw that none of the strains had any GFP signal indicating that the iron regulon is turned off. In medium iron conditions the iron regulon is properly regulated in WT strain, while the *gsh1*Δ strain has a high GFP signal as expected due to disruption of the Fe-S dependent signaling pathways that inhibits Aft1 activity (140). With iron chelation, both the WT and *gsh1*Δ strains have high GFP signals as expected due to activation of the iron regulon by Aft1. These data (Figure 4.15B) suggested that Aft1 transcriptional reporter was working as expected. We also observed that the GFP signal of the *HGT1* overexpression cells was almost half of the vector control cells (Figure 4.15C). The GFP signal of the WT cells were almost negligible compared to the *gsh1Δ* cells. These results suggest that the Fe-S dependent signaling pathway that inhibits Aft1 activity (140-142) is partially restored in *gsh1Δ* cells overexpressing *HGT1*. This led to the dampening of the GFP fluorescence intensity in the *gsh1Δ* + *HGT1* cells compared to the vector control cells. We presume that cysteine present in the SC media is contributing to increased Fe-S cluster biogenesis activity which is required for inhibition of Aft1 activity.

Discussion

The dependence of eukaryotic cells on intracellular GSH has been well characterized using the *gsh1Δ* strain. These studies have shown that GSH is critical for maintaining the mitochondrial integrity and the maturation of extra-mitochondrial Fe-S

cluster proteins (11,36,75,158). After the Hgt1 transporter came into the picture, the damaging consequences of high intracellular GSH was also discovered (11,75). In our lab we have generated and presented a model that shows the consequences if the intracellular environment oscillates between low and high GSH. We accomplished this by simultaneously deleting the gene encoding the Gsh1 enzyme and overexpressing the Hgt1 transporter. We have repeatedly shown that *HGT1* overexpression can partially rescue the growth defect of GSH deficiency. This rescue has been observed in SC media, which has all the amino acids and nucleobases except the ones needed for the plasmid selection and maintenance. In order to isolate the component needed for this partial rescue, we also grew the *gsh1Δ + HGT1* strains on 6AA/B minimal media. Interestingly, we observed that the cells were not able to grow on minimal media without assistance from extracellular GSH (111). This raised an important question as to which component/amino acid is allowing growth of *gsh1Δ + HGT1* cells in SC media. Since the function of GSH is dependent on its redox-active thiol group (159), we focused on cysteine. We showed that cysteine partially rescues the growth of *gsh1Δ + HGT1* cells in 6AA/B minimal media, and this effect is more prominent during anaerobic growth, as seen during with anaerobic vs. aerobic plate growth assays. Surprisingly, Yct1 (a cysteine specific transporter) (146) was unable to rescue the GSH auxotrophy of the cells. Hgt1 is also a proton symporter and can import protons as well as GSH, while Yct1 is only a cysteine transporter. At this point, it is not clear whether this difference between the two transporters is the deciding factor. More experiments are warranted regarding the interaction of these transporters with their ligands and structural differences between them to have a clear conclusion. Liquid growth curve assays in minimal media with different concentrations of cysteine showed proper growth of *gsh1Δ*

+ *HGT1* cells at lower cysteine concentrations, validating the role of cysteine in replacing GSH. We also tested overexpression of a cysteine-degrading enzyme to break down cysteine and tried to show that cysteine's absence is hampering Hgt1's ability to rescue the cells from GSH auxotrophy. The data from the experiment looked promising but it probably needs some troubleshooting steps, like instead of using 5AA/B media plates, we could use SC media. Also, it would be helpful to have low levels of cysteine. Maybe we should not go beyond 0.5 mM cysteine concentration for these kinds of experiments, since cysteine's action can be observed within a narrow range of concentration. We also tried to grow the cells by adding methionine in the minimal media, since methionine has a thiol derivative group (thioether), but could not observe any growth of *gsh1Δ* + *HGT1* cells (111). In addition, we tested a Met+ BY4742 strain background (both WT and *gsh1Δ*) to completely rule out any effect of extracellular methionine that might come from the media. Cysteine could also rescue the *gsh1Δ* + *HGT1* cells, even after the cells were grown for 72 hours with repeated dilution. To test the effect of other cysteine derivatives, N-acetylcysteine (NAC) was added in the minimal media for assaying growth of *gsh1Δ* + *HGT1* cells. Surprisingly, NAC did not impart the toxicity of cysteine even at higher concentrations. My former lab mate Dr. Crystal Conaway McGee also used DTT (dithiothreitol; a commercially available thiol-containing reducing agent) instead of cysteine to test the growth of *gsh1Δ* + *HGT1* cells in minimal media, and observed the partial rescue of these cells as well (111). Although, the growth of cells was not as robust as with cysteine or NAC, since DTT is structurally different from cysteine and GSH, so it is likely that it cannot replace all their functions in the cell. Nevertheless, these observations implied that cysteine (present at approximately 1 mM concentration in SC media) might

be the responsible component for the partial rescue of the *gsh1Δ + HGT1* cells. It has been previously reported that cysteine can compete with GSH for import into the cell through the Hgt1 transporter (75). But the ability of Hgt1 transporter to rescue the *gsh1Δ* cells from their GSH auxotrophy, with assistance from cysteine, is surprising.

Recently, the role of GSH in Fe-S cluster assembly and its role in iron metabolism has been proposed as its primary function (11) and the reason for its essentiality in cellular functions (11,81). Over the past decade, the essential contributions of GSH to cellular iron metabolism have come more into focus. GSH is indispensable in mitochondrial Fe-S cluster biosynthesis and is required for the export of the yet undefined Fe-S cluster precursor from the mitochondrial to the cytosol. In the cytosol, it is an essential cofactor of the class II CGFS type Grxs, integral components in cellular iron and Fe-S trafficking (141). Therefore, subcellular iron levels were measured in WT and *gsh1Δ* cells and it was noted that in the cytosolic fraction, the iron levels in *gsh1Δ* cells overexpressing *HGT1* were on at par with WT levels. In the mitochondrial fraction, although the iron levels were decreased in the *gsh1Δ + HGT1* cells relative to the *gsh1Δ* + vector cells, they were still above the WT levels (111). This finding indicates that iron homeostasis is not fully restored in the *gsh1*Δ + *HGT1* even though cells are viable.

To determine how Fe-S cluster biogenesis is impacted in *gsh1*Δ + *HGT1* strains, we performed cytosolic and mitochondrial Fe-S enzymatic activity assays, both qualitatively and quantitatively. The cytosolic qualitative Fe-S enzymatic assay showed a partial but clear activity of the enzyme sulfite reductase with the *gsh1Δ + HGT1* cells, as demonstrated by the spot test on the BiG (Bismuth Sulfite-Glucose) plates. Expectedly, the WT cells showed brown colonies suggesting full enzymatic activity of the enzyme, while

the *gsh1Δ* + vector cells did not grow at all as expected. The quantitative cytosolic Fe-S enzymatic assay with Leu1 also did not show a big difference between the two different *gsh1Δ* cells, although the enzyme activity in *gsh1Δ* + *HGT1* cells was slightly higher than that of the *gsh1Δ* cells with the empty vector. The mitochondrial quantitative enzymatic assay included both aconitase and succinate dehydrogenase activity assay. With both, the *gsh1Δ* cells (both empty vector and *HGT1* overexpressed) showed negligible to low activity compared to the WT cells. Overall, the enzymatic activity data suggested that in the presence of cysteine, *HGT1* overexpression in *gsh1Δ* cells can probably revive the inactive Fe-S cluster enzymatic activity but it is likely not enough to be perceivable by enzymatic assays. Instead, Hgt1 transporter's more noticeable impact can be observed through it rescue of GSH auxotrophy.

Since we were looking to connect GSH auxotrophy and its effect on Fe-S cluster biogenesis and maturation, we wanted to see if the presence of iron in the media can rescue the cells where there is no GSH. Growth curves in SC liquid media remained inconclusive, since all the strains, except *gsh1Δ* + vector, grew well in SC media. Due to this, we shifted to 6AA/B minimal media and added FAS at different concentrations. We could not observe any growth in the *gsh1Δ* cells (both empty vector and *HGT1*) but the WT cells grew as expected. This conclusively proved that, the presence of excess iron in the media is not enough to rescue the GSH auxotrophy, even though the Hgt1 transporter is overexpressed. Additional nutrient supplements are equally important for the cells and in our case, cysteine is that supplement.

On a similar note, we also wanted to investigate whether Hgt1 overexpression impacted activity of the iron-responsive transcriptional repressor Aft1 since regulation of

this DNA binding protein is dependent on an unidentified sulfur-containing compound generated by the mitochondrial Fe-S cluster biogenesis machinery. We used a quantitative Aft1 transcriptional reporter strain with an integrated Aft1-responsive *FIT2* promoter (*FIT2pr*) driving expression of GFP (143). Aft1-dependent GFP expression as measured by fluorescence intensity was reduced by half in *gsh1Δ* + *HGT1* cells compared to the *gsh1Δ* + vector control cells. The WT cells (with or without *HGT1* overexpression) had negligible fluorescence intensity compared to the *gsh1Δ* cells. These results confirm that in a GSH-depleted system and in the presence of excess Hgt1, activation of the iron regulon by Aft1 is partially inhibited. All our previous experiments have suggested that this inhibition is probably mediated by cysteine (already present in the SC media) and it is likely that cysteine somehow increases Fe-S cluster biosynthesis in this strain which in turn leads to better Fe-S cluster dependent inhibition of Aft1 by Grx3/4-Fra2.

Going forward, the main riddle that needs to be solved is the movement of cysteine inside the cell. We also don't know why specifically Hgt1 overexpression is aiding the cells to survive and not Yct1, which is supposed to be a cysteine specific transporter (146). It might be because Hgt1 is a proton symporter as well and Yct1 is not. We are also not sure about the non-toxic nature of NAC at higher concentration, unlike cysteine. All these questions need to be answered to figure out the exact mechanism of Hgt1-mediated *gsh1Δ* cell survival.

References

4. Deponte, M. (2017) The Incomplete Glutathione Puzzle: Just Guessing at Numbers and Figures? *Antioxid Redox Signal* **27**, 1130-1161

9. Toledano, M. B., and Huang, M. E. (2017) The Unfinished Puzzle of Glutathione Physiological Functions, an Old Molecule That Still Retains Many Enigmas. *Antioxid Redox Signal* **27**, 1127-1129

11. Kumar, C., Igbaria, A., D'Autreaux, B., Planson, A. G., Junot, C., Godat, E., Bachhawat, A. K., Delaunay-Moisan, A., and Toledano, M. B. (2011) Glutathione revisited: a vital function in iron metabolism and ancillary role in thiol-redox control. *EMBO J* **30**, 2044-2056

34. Hwang, C., Sinskey, A. J., and Lodish, H. F. (1992) Oxidized redox state of glutathione in the endoplasmic reticulum. *Science* **257**, 1496-1502

36. Ayer, A., Tan, S. X., Grant, C. M., Meyer, A. J., Dawes, I. W., and Perrone, G. G. (2010) The critical role of glutathione in maintenance of the mitochondrial genome. *Free Radic Biol Med* **49**, 1956-1968

66. Sipos, K., Lange, H., Fekete, Z., Ullmann, P., Lill, R., and Kispal, G. (2002) Maturation of cytosolic iron-sulfur proteins requires glutathione. *J Biol Chem* **277**, 26944-26949

75. Bourbouloux, A., Shahi, P., Chakladar, A., Delrot, S., and Bachhawat, A. K. (2000) Hgt1p, a high affinity glutathione transporter from the yeast Saccharomyces cerevisiae. *J Biol Chem* **275**, 13259-13265

80. Banhegyi, G., Lusini, L., Puskas, F., Rossi, R., Fulceri, R., Braun, L., Mile, V., di Simplicio, P., Mandl, J., and Benedetti, A. (1999) Preferential transport of

glutathione versus glutathione disulfide in rat liver microsomal vesicles. *J Biol Chem* **274**, 12213-12216

81. Ponsero, A. J., Igbaria, A., Darch, M. A., Miled, S., Outten, C. E., Winther, J. R., Palais, G., D'Autréaux, B., Delaunay-Moisan, A., and Toledano, M. B. (2017) Endoplasmic Reticulum Transport of Glutathione by Sec61 Is Regulated by Ero1 and Bip. *Mol Cell* **67**, 962-973.e965

111. McGee, C. C. (2019) *Impact of Glutathione Transporters on Subcellular Glutathione Pools and Cell Survival in Saccharomyces Cerevisiae.* PhD Doctoral dissertation, University of South Carolina

132. Meister, A., and Anderson, M. E. (1983) Glutathione. *Annu Rev Biochem* **52**, 711-760

133. May, M. J., Vernoux, T., Sanchez-Fernandez, R., Van Montagu, M., and Inze, D. (1998) Evidence for posttranscriptional activation of gamma-glutamylcysteine synthetase during plant stress responses. *Proc Natl Acad Sci U S A* **95**, 12049-12054

134. Bachhawat, A. K., and Yadav, S. (2018) The glutathione cycle: Glutathione metabolism beyond the γ-glutamyl cycle. *IUBMB Life* **70**, 585-592

135. Smith, C. V., Jones, D. P., Guenthner, T. M., Lash, L. H., and Lauterburg, B. H. (1996) Compartmentation of glutathione: implications for the study of toxicity and disease. *Toxicol Appl Pharmacol* **140**, 1-12

136. Herzenberg, L. A., De Rosa, S. C., Dubs, J. G., Roederer, M., Anderson, M. T., Ela, S. W., Deresinski, S. C., and Herzenberg, L. A. (1997) Glutathione deficiency is associated with impaired survival in HIV disease. *Proc Natl Acad Sci U S A* **94**, 1967-1972

137. Oestreicher, J., and Morgan, B. (2018) Glutathione: subcellular distribution and membrane transport. *Biochemistry and Cell Biology* **97**, 270-289

138. Garcia-Ruiz, C., Morales, A., Colell, A., Rodes, J., Yi, J. R., Kaplowitz, N., and Fernandez-Checa, J. C. (1995) Evidence that the rat hepatic mitochondrial carrier is distinct from the sinusoidal and canalicular transporters for reduced glutathione. Expression studies in Xenopus laevis oocytes. *J Biol Chem* **270**, 15946-15949

139. Ballatori, N., and Dutczak, W. J. (1994) Identification and characterization of high and low affinity transport systems for reduced glutathione in liver cell canalicular membranes. *J Biol Chem* **269**, 19731-19737

140. Lill, R., Dutkiewicz, R., Freibert, S. A., Heidenreich, T., Mascarenhas, J., Netz, D. J., Paul, V. D., Pierik, A. J., Richter, N., Stümpfig, M., Srinivasan, V., Stehling, O., and Mühlenhoff, U. (2015) The role of mitochondria and the CIA machinery in the maturation of cytosolic and nuclear iron–sulfur proteins. *European Journal of Cell Biology* **94**, 280-291

141. Daniel, T., Faruq, H. M., Laura Magdalena, J., Manuela, G., and Christopher Horst, L. (2020) Role of GSH and Iron-Sulfur Glutaredoxins in Iron Metabolism—Review. *Molecules* **25**

142. Talib, E. A., and Outten, C. E. (2021) Iron-sulfur cluster biogenesis, trafficking, and signaling: Roles for CGFS glutaredoxins and BolA proteins. *Biochim Biophys Acta Mol Cell Res* **1868**, 118847

143. Hughes, C. E., Coody, T. K., Jeong, M. Y., Berg, J. A., Winge, D. R., and Hughes, A. L. (2020) Cysteine Toxicity Drives Age-Related Mitochondrial Decline by Altering Iron Homeostasis. *Cell* **180**, 296-310 e218

144. Ozer, H. K., Dlouhy, A. C., Thornton, J. D., Hu, J., Liu, Y., Barycki, J. J., Balk, J., and Outten, C. E. (2015) Cytosolic Fe-S Cluster Protein Maturation and Iron Regulation Are Independent of the Mitochondrial Erv1/Mia40 Import System. *J Biol Chem* **290**, 27829-27840

145. Thomas, D., Barbey, R., Henry, D., and Surdin-Kerjan, Y. (1992) Physiological analysis of mutants of Saccharomyces cerevisiae impaired in sulphate assimilation. *J Gen Microbiol* **138**, 2021-2028

146. Kaur, J., and Bachhawat, A. K. (2007) Yct1p, a novel, high-affinity, cysteine-specific transporter from the yeast Saccharomyces cerevisiae. *Genetics* **176**, 877-890

147. Daum, G., Bohni, P. C., and Schatz, G. (1982) Import of proteins into mitochondria. Cytochrome b2 and cytochrome c peroxidase are located in the intermembrane space of yeast mitochondria. *J Biol Chem* **257**, 13028-13033

148. Strain, J., Lorenz, C. R., Bode, J., Garland, S., Smolen, G. A., Ta, D. T., Vickery, L. E., and Culotta, V. C. (1998) Suppressors of superoxide dismutase (SOD1) deficiency in Saccharomyces cerevisiae. Identification of proteins predicted to mediate iron-sulfur cluster assembly. *J Biol Chem* **273**, 31138-31144

149. Pierik, A. J., Netz, D. J., and Lill, R. (2009) Analysis of iron-sulfur protein maturation in eukaryotes. *Nat Protoc* **4**, 753-766

150. Park, E. J., Min, K. J., Lee, T. J., Yoo, Y. H., Kim, Y. S., and Kwon, T. K. (2014) beta-Lapachone induces programmed necrosis through the RIP1-PARP-AIF-dependent pathway in human hepatocellular carcinoma SK-Hep1 cells. *Cell Death Dis* **5**, e1230

151. Irani, K., Xia, Y., Zweier, J. L., Sollott, S. J., Der, C. J., Fearon, E. R., Sundaresan, M., Finkel, T., and Goldschmidt-Clermont, P. J. (1997) Mitogenic signaling mediated by oxidants in Ras-transformed fibroblasts. *Science* **275**, 1649-1652

152. Le Gal, K., Ibrahim, M. X., Wiel, C., Sayin, V. I., Akula, M. K., Karlsson, C., Dalin, M. G., Akyürek, L. M., Lindahl, P., Nilsson, J., and Bergo, M. O. (2015) Antioxidants can increase melanoma metastasis in mice. *Science Translational Medicine* **7**, 308re308

153. Piskounova, E., Agathocleous, M., Murphy, M. M., Hu, Z., Huddlestun, S. E., Zhao, Z., Leitch, A. M., Johnson, T. M., DeBerardinis, R. J., and Morrison, S. J. (2015) Oxidative stress inhibits distant metastasis by human melanoma cells. *Nature* **527**, 186-191

154. Protchenko, O., Ferea, T., Rashford, J., Tiedeman, J., Brown, P. O., Botstein, D., and Philpott, C. C. (2001) Three cell wall mannoproteins facilitate the uptake of iron in Saccharomyces cerevisiae. *J Biol Chem* **276**, 49244-49250

155. Rutherford, J. C., Jaron, S., and Winge, D. R. (2003) Aft1p and Aft2p mediate iron-responsive gene expression in yeast through related promoter elements. *J Biol Chem* **278**, 27636-27643

156. Rutherford, J. C., Ojeda, L., Balk, J., Mühlenhoff, U., Lill, R., and Winge, D. R. (2005) Activation of the iron regulon by the yeast Aft1/Aft2 transcription factors depends on mitochondrial but not cytosolic iron-sulfur protein biogenesis. *J Biol Chem* **280**, 10135-10140

157. Outten, C. E., and Culotta, V. C. (2003) A novel NADH kinase is the mitochondrial source of NADPH in Saccharomyces cerevisiae. *Embo j* **22**, 2015-2024

158. Lill, R., Diekert, K., Kaut, A., Lange, H., Pelzer, W., Prohl, C., and Kispal, G. (1999) The essential role of mitochondria in the biogenesis of cellular iron-sulfur proteins. *Biol Chem* **380**, 1157-1166

159. Poole, L. B. (2015) The basics of thiols and cysteines in redox biology and chemistry. *Free Radic Biol Med* **80**, 148-157

CHAPTER 5

SUPPLEMENTARY METHODS

Introduction

This chapter describes experimental details used to obtain results specifically for this dissertation. Here you will find tips for analyzing genetically modified strains and information about plasmids used for this study. All procedures were adopted from published protocols to obtain results for our purposes. Techniques discussed in detail are the glutathione (GSH)/glutathione disulfide (GSSG) assay, redox western blots and monitoring growth of yeast using the Biotek Synergy H1 plate reader. To measure GSH and GSSG from whole cells, we utilized the 5,5'-dithiobis (2-nitrobenzoic acid) (DTNB) colorimetric enzyme cycling assay (129,160). Lastly, the method developed for monitoring yeast growth using a plate reader was created using the manufacturer's instructions.

Calibration and Measurement of pHluorin by using the Synergy H1 plate reader

This method has been adapted from Orij *et al*., (161) and slightly modified according to our needs.

Reagents in this method:

- Phosphate buffer saline (PBS) buffer: (for 1-liter 10X stock; 1.37 M NaCl, 27 mM KCl, 100 mM Na_2HPO_4, 18 mM KH_2PO_4. Dissolve the reagents in 800 ml of water. Adjust the pH to 7.4 or 7.2 with HCl and then add the rest of the water to 1 liter).
- Low fluorescence selection media: for 500 ml media add 3.35 g of YNB-Folic Acid-Riboflavin powder (Sunrise Science Products, Catalog # 1535-050) and 1 g of the appropriate dropout mix. This media is always sterile-filtered, never autoclaved.
- 10 mg/ml digitonin (dissolved in DMSO, aliquoted and stored at -20 °C).

Procedures:

1. Prepare the McIlvaine's buffer system (162) [0.2 M Na_2HPO_4 (2.839 g/100 ml), FW: 141.96 g/mol) and 0.1 M citric acid (1.921 g/100ml, FW: 192.12 g/mol)] to prepare the 10 ml buffer for each pH. Mix 0.2 M sodium phosphate dibasic and 0.1 M citric acid in 15 ml centrifuge tubes.
2. Grow the pHluorin transformed cells (along with the WT cells without pHluorin as a background fluorescence control). Get a loop full of cells from a fresh plate and grow them overnight (10 ml is enough) in sterile-filtered low fluorescent selection media containing 2% glucose, at 30°C. Grow the cells in such a way that the next morning, the OD_{600} is around 1-1.5.
3. Next morning, harvest the cells and resuspend the cells in 5 ml PBS buffer containing 100 µg/ml digitonin for 10 minutes.
4. After 10 minutes, spin the cells at 3000 rpm for 5 minutes. Wash the cells with the same amount of PBS.

5. Concentrate the cells 10 times by centrifuging down the cells and resuspending them in 1/10th the original volume (OD_{600} = 10). Keep them on ice.
6. Add 180 µl of buffer into each well of a 96-well black microplate and add 20 µl of cells into each buffer.
7. Measure the fluorescence with an excitation wavelength at 390 nm and 470 nm, with the emission wavelength set at 512 nm. I used filter cubes for this measurement. The cube's fluorescence parameters would be labelled as 400/30, 516/20, 460/40, 516/20. In the plate reader, go to set filter cube > place the mentioned filter cube > choose pHluorin filter and click update reader. This would give a prompt stating "filter cube was updated successfully". After this prompt, set up the protocol (Protocol tab under Task Manager). Choose the pHluorin protocol. I usually set the gain to 50 and the read to top read. I always use a black plate.
8. Record the fluorescence intensity values of the pHluorin-transformed cells to generate a sigmoidal calibration curve using the GraphPad Prism software, which will calculate the pK_a, R_{min} and R_{max} values. R_{min} is the ratio (R_{390}/R_{470}) of cells in pH 4.8 buffer, R_{max} is the ratio (R_{390}/R_{470}) of cells in pH 8.4 buffer.
9. Record the fluorescence intensity values for the WT and the transformed cells and calculate the background corrected values (pHluorin transformed cells – non transformed cells). Make sure to record the intensity values for both the excitation wavelengths by using the drop-down menu.
10. Transfer the data to a MS Excel spreadsheet and calculate the ratio of excitation wavelengths, i.e. 400/460. Then put the values into the Henderson-Hasselbalch

equation [pH = pK_a + log (R – R_{min})/ (R_{max} – R)] to calculate the measured pH values.

GSH/GSSG Assay using Synergy H1 plate reader

The GSH/GSSG assay described here was developed with the help of Dr. Crystal Conway and Dr. Malini Gupta to measure GSH and GSSG using a Biotek Synergy H1 plate reader. Here, we successfully measured yeast lysates using previously published procedures (160). Whole cell lysates were made according to published methods (129). A notable difference in the previously published method (160) was the use of sodium phosphate buffer with 1 mM EDTA (NaPE), while the published protocol suggested potassium phosphate buffer with 5 mM EDTA (KPE). This change was made so that all the reagents were the same as previously published methods by the C. Outten group (106,163). The combined protocols and changes produced results comparable to the published data from the laboratory.

Reagents in this method:

- **0.1 M NaPE buffer**: 100 mM sodium phosphate, 1 mM EDTA sodium salt, pH 7.5
- **1 mM NADPH** (prepared in NaPE buffer): Make fresh and keep out of light
- **2 mM DTNB** (prepared in NaPE buffer): Make fresh and keep out of light
- **3 U/ml GSSG reductase (GLR)**: (prepared fresh in NaPE buffer)
- **5-sulfosalicylic acid (SSA)**
- **2-vinylpyridine**: do not dilute this product and use under the fume hood
- **25% triethanolamine** (prepared fresh in NaPE buffer)

Whole cell GSH sample preparation:

1. Grow cells in YPD or SC selection media until mid-log phase (~ 0.5 – 2 OD) in desired volume.
2. Collect 2 x 10^7 cells (2 ml at 1 O.D.) by spinning at 12000 rpm for 30 s at room temperature. This amount is assuming 1 O.D. = 1 x 10^7 cells. For *gsh1Δ* strains harvest 2 x 10^9 cells since [GSH] is low.
3. Wash cells twice with water and aspirate off SN. Be careful not to disturb the pellet.
4. Prepare 1 ml 10% 5-sulfosalicylic acid (SSA) by dissolving 100 mg of SSA into 1 ml of water. Prepare 5-10 ml 1% SSA depending on amount needed for the assay.
5. Resuspend cells in 50 µl of ice-cold 1% SSA and lyse with approximately 20 µl of glass beads in the bead beater or with vigorous vortexing. For *gsh1Δ* strains, use 250 µl of ice-cold 1% SSA with 100 µl of glass beads.
6. Bring extract to a final volume of 250 µl using ice-cold 1% SSA. Do not dilute *gsh1Δ* extracts.
7. Allow cells to incubate on ice for 30 minutes.
8. Spin extract at 13000 g for 5 minutes at 4 °C.
9. Samples can be measured immediately or frozen and stored at -80 °C until ready for the assay.

<u>Enzyme Assay Protocol</u>:

1. Prepare a 100 mM GSH stock solution with water (can be stored at -20 °C) and dilute it to 1 mM GSH.
2. Make GSH standards of 0, 1, 2.5, 5, 7.5, 15 and 25 µM GSH using 1% SSA by serially diluting each standard from the 1 mM GSH stock (need at least 20 µl for each standard).

3. Mix equal volumes of freshly prepared DTNB and GLR solutions in reagent reservoir. Keep the reservoir covered with aluminum foil while working with lights on. Need at least 60 µl of each reagent for each well.
4. In a separate reservoir add freshly prepared NADPH solution. Keep it covered with aluminum foil while working with lights on.
5. Add 20 µl of the blank, standards and sample into individual wells of a clear non-sterile 96-well plate.
6. Add 120 µl of the DTNB/GLR mixture into each well and pipet up and down to mix.
7. Allow 30 s for the conversion of GSSG to GSH, then add 60 µl of NADPH and pipet up and down to mix.
8. Read the absorbance at 412 nm every 15 s for 2 minutes.

Preparation of GSSG samples:

1. Prepare a 50 mM GSSG stock solution in NaPE buffer and dilute to 0.5 mM GSSG in 1% SSA.
2. Make GSSG standards of 0, 0.5, 1, 2.5, 5, 7.5 and 12.5 µM in 1% SSA by serially diluting each standard from the 0.5 mM GSSG stock.
3. Transfer 50 µl of the acidified cell extract into a 1.5 ml Eppendorf tube.
4. Add 1 µl 2-vinylpyridine to the 50 µl acidified cell extract and vortex the mixture. Use the fume hood when working with 2-vinylpyridine.
5. To the 2-vinylpyridine treated samples add 1 µl of 25% triethanolamine.
6. Incubate the samples under the fume hood for 1 hour at room temperature.
7. Prepare reagents and read GSSG samples as described above for GSH.

Growth Curve Assay – Synergy H1 plate reader

Yeast cell growth was analyzed using a Synergy H1 plate reader. The manufacturer's instructions were followed to establish the protocol. The procedure outlined below details the assay and subsequent analysis of growth. We found that yeast started at O.D. lower than 0.05 could not be detected. Thus, all strains grown using this method were blank corrected from cells started at O.D. = 0.05.

Procedure:

1. Grow cells on a plate until a patch of cells form. This normally takes about 2-3 days.
2. Resuspend a loopful of cells into 1 ml of sterile water and take O.D. in a clear 96-well plate using the plate reader. This 96-well plate does not have to be sterile.
3. After taking the O.D., dilute each strain to 0.5 O.D. in new sterile micro-centrifuge tubes.
4. Add 20 µl of the 0.5 O.D. of cell stock into a sterile flat-bottomed clear 96-well microplate (Corning 96-well plates # 3596 were used in this study).
5. To the cells, add 180 µl of autoclaved media so that the starting O.D. is 0.05 (starting cells at O.D. less than 0.05 is difficult to detect using this method and may yield negative values when subtracted from blank).
6. Leaving the clear plastic top off, seal the top of the 96-well plate with a clear membrane. This allows cells to have aeration during growth while reducing contamination and evaporation (the Breath Easy sealing membranes from Sigma Aldrich # Z380059 were used for all growth curves).
7. Place the sealed 96-well plate in the plate reader without the lid.

8. Select wells to be read in the procedure and the plate layout sections (the software used for this experiment is Gen5 2.09).
9. Allow the temperature to reach 30 °C before taking initial readings. Measurements were taken every 30 minutes with the continuous orbital shaking mode set over a course of 24 hours. The shaking speed was set to slow and frequency set at 559 (1 mm amplitude).
10. Analyze growth curves by plotting the blank corrected OD_{600} values of each strain over time on a logarithmic scale.

***FIT2* promoter Aft1 reporter strains**

To investigate the relationship between GSH and iron metabolism and to show the connection between cysteine import and the rescue of *gsh1Δ* with HGT1 overexpressed cells, a quantitative Aft1 transcriptional reporter composed of the Aft1-responsive *FIT2* promoter (*FIT2pr*) driving expression of GFP was used (143). The strains bearing this specific reporter were kindly and generously provided by the lab of Dr. Adam Hughes, Department of Biochemistry, University of Utah. Four different strains were given to us by the lab (Table 5.1):

Aft1 reporter assay

This protocol has been adapted and almost exactly followed from the source (143). The only difference is that I used a the Biotek Synergy H1 plate reader and the Hughes's lab used FACS for measuring the fluorescence intensity. I used the low fluorescent SC

Table 5.1: List of strains bearing the Aft1 transcriptional reporter. The strains were kindly provided by the lab of Dr. Adam Hughes, Department of Biochemistry, University of Utah.

Strains	**Identifier**
S. cerevisiae: wild type Aft1 reporter: BY4741chrI(199456-199457)::P_{FIT2}-yeGFP-$Term_{ADH1}$:KanMX	AHY2993
S. cerevisiae: wild type Aft1 reporter: BY4741chrI(199456-199457)::P_{FIT2}-yeGFP-$Term_{ADH1}$:HphMX	AHY5005
S. cerevisiae: *aft1Δ* Aft1 reporter: BY4741chrI(199456-199457)::P_{FIT2}-yeGFP-$Term_{ADH1}$-HphMX *aft1Δ*::KanMX	AHY5007
S. cerevisiae: *cys3Δ* Aft1 reporter: BY4741chrI(199456-199457)::P_{FIT2}-yeGFP-$Term_{ADH1}$-KanMX *cys3*::URA3	AHY5020

media (Sunrise Pharmaceuticals) for this protocol ((see pHluorin measurements above for more details).

Protocol:

1. Grow cells overnight until mid-log phase (OD_{600} ~ 1). I would suggest not to work with cells which have grown beyond OD_{600} – 2. A 10 ml volume (for overnight growth) in conical flasks is enough.
2. Harvest the cells at 3000 rpm for 5 min.
3. Wash the cells twice with the same amount of sterile MQH_2O.
4. Resuspend the cells with the same media. At this stage, you can dilute the cells back to OD 1 if they are a little overgrown (always below OD 2).
5. Add 200 µl of these cells in a 96-well black plate.
6. Go the plate reader and the use the protocol saved in Documents>Tirthankar> "template protocol for measuring fluorescence intensity in *FIT2pr*-GFP Aft1 reporter". The pattern of wells is selected according to my experiment set up. Change them according to the user's preference. The excitation and emission wavelengths are set as 485 and 528 nm. The gain is automatic, and the reading should be top read. I used the monochromator for this experiment.

** Always use the proper control strains for background subtraction. For example, Aft1 reporter *gsh1*Δ + *HGT1* strain should have a *gsh1*Δ + *HGT1* strain without the reporter. Use low fluorescent media for both the sample and the control strains.

Cloning of the p315TEF vector and p315TEF-*HGT1* overexpression plasmids

Creation of the overexpression plasmids (p315TEF vector and p315TEF-*HGT1*) were performed using the NEBuilder High-Fidelity DNA Assembly protocol (New England Biolabs). The idea was to cut and insert the region with the *TEF1* promoter, *HGT1* coding sequence and the *CYC1* terminator from p416TEF-*HGT1* into pRS315. pRS315 was an empty vector with *LEU2* selection marker. The reason for changing the selection marker from *URA3* to *LEU2* was to avoid having two overexpression plasmids with the same selection marker, since the *CYS3* overexpression plasmid (generously provided by the Adam Hughes lab, University of Utah) had a *URA3* selection marker too. These two plasmids together, would have been impossible to transform in yeast. Below is a summary of the Assembly protocol that I followed:

1. Generate primers for the amplification of the insert region. The forward and reverse primers for amplifying the *TEF1* promoter and the *CYC1* terminator region (with or without the *HGT1* coding sequence in between) are 5'-CTATAGGGCGAATTGGAGCTCATAGCTTCAAAATGTTTCTACTC–3' and 5'-GGATCCACTAGTTCTAGAGCGGCCGCAAATTAAAGCCTTCGAGC-3', respectively.
2. Amplify the inserts using PCR (Table 5.2 and 5.3).
3. After the PCR is done, add 1 µl of DpnI enzyme in each of the PCR tubes to digest the template DNA and incubate for an hour.
4. Run agarose gels to confirm that the PCR worked (the size of the insert must be known for that). If the correct bands are observed, use a kit to clean up the PCR products,

Table 5.2: Composition of the PCR (polymerase chain reaction) mixture used for the creation of p315TEF empty vector and p315TEF-*HGT1*

5x Q5 reaction buffer	10 µl
5 mM dNTPs	2 µl
10 µM forward primer	2.5 µl
10 µM reverse primer	2.5 µl
Template DNA (I used 50 ng/µl working stock)	2 µl
Q5 high fidelity DNA polymerase	0.5 µl
Nuclease free water	30.5 µl
Total	50 µl

Table 5.3: Thermal Cycler program used for the creation of p315TEF empty vector and p315TEF-*HGT1*.

STEP	TEMPERATURE	TIME
Initial denaturation	98 °C	30 seconds (I paused the machine, added the DNA polymerase, and then resumed)
25-35 cycles	98 °C 56 °C - 60 °C 72 °C	10 seconds 20 seconds 25 seconds/kb
Final extension	72 °C	2 minutes
Hold	4 °C	

measure their DNA concentration and set up the NEBuilder High-Fidelity DNA Assembly mixture according to the protocol.

Small scale mitochondria isolation

Isolation of cytosolic and mitochondrial fractions was done to determine the activity of Fe-S cluster enzymes, like aconitase and succinate dehydrogenase. To prepare extracts for analyzing the enzymatic activity, the mitochondrial isolation protocol from Outten *et al*., and Strain *et al*., was followed (148,157). The only modification was the increase in culture volume for *gsh1Δ* cells (especially for *gsh1Δ* + p416TEF empty vector cells to obtain enough mitochondria to measure the enzymatic activity). The resuspension volume for isolated mitochondria in the buffer was also adjusted for *gsh1Δ* cells used for the enzymatic assays.

Buffers needed (sterile filter or autoclave buffers and store at 4 °C):

SOR buffer: 1.2 M sorbitol, 20 mM Hepes, pH 7.5.

SM buffer: 250 mM sucrose, 10 mM MOPS, pH 7.2.

Enzyme stocks

Zymolyase 20T: 20 mg/ml in water (zymolyase was prepared before use and stored at -20 °C. The enzyme is more effective if it is thawed from a frozen stock).

Fractionation Protocol:

1. Grow cells overnight in 50-100 ml culture (SC or YPD) to mid-log phase (larger cultures of approximately 300-500 ml were used when working with *gsh1Δ* +

p416TEF empty vector cells to obtain enough mitochondria to measure the enzymatic activity).

2. Harvest cells at 3000 rpm for 5 minutes.
3. Pre-weigh 1.5 ml microcentrifuge tubes and record the values.
4. Pour off the supernatant (SN), wash the cell pellet with 1 ml water and transfer to pre-weighed microcentrifuge tubes.
5. Spin 10 s at 12000 rpm. Aspirate off the SN.
6. Wash the cells with 1 ml SOR buffer and spin 10 s at 12000 rpm.
7. Aspirate off the SN and measure the net weight of the cell pellet.
8. Resuspend the pellet in SOR buffer (1 ml/150 mg cells).
9. Add 3 mg of zymolyase per gram of cells.
10. Mix by inverting 5 times and incubate in 30 °C water bath for 30 min to 1 hr.
11. Check spheroplasts after 40-45 min by adding 10 µl into a plastic cuvette and flush with 1 ml water. In another cuvette, flush 10 µl with 1 ml SOR buffer. If the cell wall of the yeast is no longer intact, the spheroplasts should lyse in water but not in SOR buffer. Therefore, the sample should look clear in water and cloudy in SOR buffer.
12. Spin samples at 3500 rpm for 5 min at 4 °C. Aspirate off the SN.
13. Wash the spheroplasts with 1 ml SOR buffer (careful with this step to avoid bursting the spheroplasts).
14. Spin for 5 min at 3500 rpm at 4 °C and aspirate off the SN.
15. Resuspend the spheroplasts in SM buffer (2 µl SM buffer per mg cells). Samples should be kept on ice from this step forward to prevent protein degradation.

16. Add phenylmethanesulfonyl fluoride (PMSF) to a final concentration of 0.5 mM and protease inhibitors at 1:100 dilution to the SM buffer of samples used for western blot analysis and Fe-S enzymatic activity measurement.
17. Disrupt the plasma membrane of the spheroplasts with 30 strokes in a 1 ml Dounce homogenizer using a loose-fitting pestle.
18. Spin 5 min at 3000 rpm at 4 °C and carefully transfer the SN to a new tube.
19. Repeat step 18 with the SN to completely remove all pellet debris.
20. Measure the volume of the SN extract after the second spin and record.
21. Save some of this SN extract (total extract) for western blot analysis if required.
22. Spin the remaining total extract at 12000 rpm for 10 min at 4 °C.
23. Transfer the SN containing the post-mitochondrial supernatant to a new tube.
24. Gently wash the pellet which comprises the crude mitochondria with 500 µl SM buffer.
25. Spin at 12000 rpm for 10 min at 4 °C and aspirate off the SN.
26. Resuspend the crude mitochondrial pellet in a desired volume of SM buffer. For western blot analysis and Fe-S enzymatic activity assays, the mitochondria were resuspended in 1/5 volume of the total extract and protease inhibitors were included in the SM buffer.
27. Measure the protein concentration of subcellular extract using the Bradford assay.

Aconitase assay

This protocol has been previously published by Outten *et al*., (157) and Strain *et al*., (148) and has been adapted here exactly as it was performed.

Reagents needed:

- Lysis buffer: 50 mM potassium phosphate, pH 7.4, 1:100 PMSF (0.5 mM).
- Assay buffer (make fresh and store and RT)
    - 10 mM cis-aconitate (made in 50 mM Tris-HCl buffer, must be pHed to 7.4).
    - 50 mM Tris, pH 7.4, 100 mM NaCl.
- For making a volume of 20 ml of assay buffer, add 1 ml 10 mM cis-aconitate + 19 ml 50 mM Tris, pH 7.4, 100 mM NaCl.

Preparation of cell extracts:

1. Grow 10 ml of cells in the specified media overnight ~24-27 hours until they stationary phase. OD 6-7 is enough.
2. Harvest the cells. Thicker pellet means, cells will be more difficult to break apart. Try to divide the pellet in 2-3 parts, if the pellet is quite thick.
3. Wash one time with water and transfer to microcentrifuge tube. Estimate the volume of the pellet.
4. Resuspend the pellet in ice-cold lysis buffer. Use 250 µl lysis buffer for every 150 µl of cell pellet.
5. Add glass beads in the microcentrifuge tube containing cells. Volume of glass beads used should be equal to the volume of the cell pellet.
6. Vortex for 1 minute 4 – 5 times, with intermittent 1 minute wait on ice (or vortex for 4 minutes in the cold room).
7. Spin down at 13000 rpm, 10 minutes. Remove the supernatant and place in another tube on ice quickly, cap immediately.

8. Spin the supernatant again for 5 – 10 minutes and remove it carefully (to avoid the debris at the bottom). Put it in a new tube and cap quickly to avoid oxidation.
9. Take 1 – 2 µl for Bradford assay for measuring the protein concentration.

Enzymatic assay:

- Kinetic reading – scan at 15 second cycles for a total of 3 minutes (180 seconds) at 240 nm. Use quartz cuvettes.
- For the cell extracts samples, set up the cuvettes with 750 µl of assay buffer. Add 75 µg of protein extract in each cuvette, quickly mix by inverting and start the measurements.
- Control: run assay buffer with no extract added. Measure rate of background cis-aconitate disappearance and subtract from samples.
- Use extinction coefficient of cis-aconitate (4.88 mM^{-1} cm^{-1}) to calculate the enzymatic activity. 1 unit of enzymatic activity is 1 nmol cis-aconitate converted/min/mg protein.
- Activity = $\frac{\text{rate}\left(dA/_{\text{min}}\right) * \text{rxn mix vol } (\mu L)}{4.88\ mM^{-1} \cdot cm^{-1} * 0.075 mg}$ nmol/min/mg.

Some important points to remember during the assay:

1. Try not to dilute the concentration of the protein after Bradford. Use from the same tube. Diluted proteins might get oxidized faster. Directly add the protein extract to the assay buffer in the cuvette.
2. Mix everything in the cuvettes themselves. Do it gently.
3. One can keep the assay buffer in the room temperature. No need to keep that on ice. Always keep the proteins on ice.

Succinate Dehydrogenase (SDH) assay

The succinate dehydrogenase assay protocol comprises two parts and has been adapted from Outten *et al*., (157) and Strain *et al*., (148) . The first part is the small-scale mitochondria isolation, and the second part is the actual assay. Following are some points regarding the assay, which I found useful:

1. All the strains that I have worked with grow fine except *gsh1Δ* + vector. This specific strain is really difficult to grow. For the SDH assay, the media needs to have 0.6% glucose, to stimulate the respiratory pathway. It's better to use 100 ml media for growing these cells (for this specific assay). Starting OD should be around 1. That way, even with very slow growth rate, after 24-27 hours, the OD would probably reach around 3, which after harvesting, one can work with. Also, one can use multiple 100 ml volume of cells for overnight growth and pool them together during the mitochondrial isolation procedure.
2. Be very careful with KCN (Potassium Cyanide). Always weigh KCN wearing a face shield, gloves, and masks. Add the HEPES buffer in the hood to make the KCN solution.
3. Add the succinate and the mitochondrial extract last in the cuvette. Immediately, seal the cuvette with parafilm, gently mix by inverting 2 – 3 times and take the measurement.
4. If the cell pellet is too big, one can divide it in 2 – 3 microcentrifuge tubes. Too big a pellet will be difficult to handle and the spheroplasts would not form properly.
5. Add 10 µg mitochondrial protein extract and succinate just before starting the reaction and monitor the decrease in absorbance at 600 nm.

6. All the reagents need to be made fresh every time.

The contents of the quartz cuvette, with concentrations and volumes is shown in Table 5.4.

Leu1 (isopropylmalate isomerase) assay

The cell lysis protocol for this assay is a bit different from what I have used for aconitase assay. Although, I do not think it matters what buffer one uses for cell lysis, especially in these assays, but nobody did this assay before in our lab, so I followed the following published protocol (164).

Buffers and reagents needed:

1. TNETG buffer (for cell lysis): 10 mM Tris/Cl pH 7.4, 2.5 mM EDTA, 150 mM NaCl, 10% (vol/vol) glycerol, 0.5% (vol/vol) Triton X-100.
    - For 500 ml use 5 ml of 1 M Tris-HCl pH 7.4, 2.5 ml of 0.5 M EDTA (pH 7.4), 37.5 ml of 2 M NaCl, 50 ml of glycerol and 25 ml of 10% (wt/vol) Triton X-100100 mM PMSF in 100% ethanol.
2. Isopropylmalate isomerase (Leu1) buffer: 20 mM Tris Tris-Cl pH 7.4, 50 mM NaCl.
3. Substrate: 10 mM of 3-isopropylmalic acid (Sigma, Catalog # 02339) is water, dilute freshly from a 100 mM stock solution in water stored frozen at -20°C.

Cell extract preparation:

1. Grow a 50-ml yeast culture in appropriate media by shaking overnight at 30 °C.
2. Harvest cells by centrifugation for 5 min at 2000g, room temperature. Remove the supernatant and resuspend the cell pellet with 10 ml of H_2O, transfer to a 15-ml Falcon tube and repeat the centrifugation.

Table 5.4: Components of the reaction mixture prepared in a 1-ml quartz cuvette for the Succinate Dehydrogenase assay.

Reagents	**Final concentration**	**Stock concentration**
HEPES; pH 7.4 (can keep at room temperature)	50 mM (100 µl)	0.5 M
EDTA (can keep at room temperature)	0.1 mM (10 µl)	10 mM
KCN (dissolve in 0.5 M HEPES)	1 mM (100 µl)	10 mM
Phenazine Methosulfate (dissolve in water)	100 µM (10 µl)	10 mM
Dichlorophenol indophenol (dissolve in water)	50 µM (5 µl)	10 mM
Sodium Succinate (dissolve in 0.5 M HEPES)	20 mM (100 µl)	200 mM
Water	675 µl	

3. All subsequent steps should be carried out at 4°C. Resuspend the pellet in 500 µl of ice-cold TNETG buffer; add 20 µl of 100 mM PMSF and 1 ml of glass beads. Close the lid tightly. Vortex at maximum speed with the lid side of the tubes contacting the rotating plate for 1 min, repeat the vortexing five times with intermittent 1 min cooling periods on ice.
4. Centrifuge for 5 min at 2000g. Transfer the supernatant to 1.5 ml microfuge tubes and centrifuge for 10 min at 13000g. Transfer the supernatant to a new microfuge tube and repeat the centrifugation. Transfer the supernatant again to a new tube and use 1-5 µl for protein determination.

Enzymatic assay:

1. Mix 970 µl of Leu1 buffer, 20 µl of 10 mM 3-isopropylmalic acid and 60-75 µg of cell extract in a quartz cuvette.
2. Measure the increase in absorbance at 235 nm for 3 min at 15 sec intervals. The extinction coefficient of 3-isopropylmalic acid is 4530 M^{-1} cm^{-1}.

BiG (Bismuth Sulfite-Glucose) plate assay

This protocol has been adapted from two different sources. The original source is the article that first showed how to make these plates (145) and the second source is the Ozer *et al*., article from our lab that came out in 2015 (144). I have included comments on how to mix and prepare the plate solution.

For a total of 100 ml of media, I prepare two separate solutions that are each 50 ml and mix them together after both are separately heated and dissolved.

Solution (A) – 50-ml mixture of YNB, assay reagents and glucose.

- 0.67 g YNB (yeast nitrogen base) – ours is the version where ammonium sulfate is included, so we do not need to add it separately.
- 0.2 g SC dropout mix (any combination but always without methionine), use the combination according to the strain you are working with.
- 1 g β-Alanine.
- 0.1 g Bismuth ammonium citrate.
- 0.3 g Sodium sulfite.
- Sterile water – calculate how much you need, keeping in mind that you need to add glucose and the amino acids (that you may need to add back) after microwaving.
- Amino acids that need to be added back – calculate how much you need (add after microwaving).
- 10 ml 20% glucose (add after microwaving).

** The total volume of this mixture would be 50 ml, so calculate accordingly (especially the water; that is the only variable). I usually prepare this mix in 1 250 ml flask. Make sure that the mix does not boil much in the microwave. Gentle boiling is okay, and you have to monitor continuously, with intermittent swirling. The mix will remain turbid and would seem that nothing has dissolved (THAT IS OKAY). That is how it supposed to look like. I usually weigh the YNB and the dropout mix, add them in the water and usually dissolve them first just by gentle swirling (some particles remain but that is inconsequential) and then add the rest. YNB and dropout mix usually dissolve just by swirling (no heating is needed).

Solution (B) - Agar (bacteriological) – 1.6 g in 50 ml sterile water.

** Microwave this as well. DO NOT EVER AUTOCLAVE THIS. For some reason, autoclaving the agar (especially for making BiG plates) destroys the properties of the reagents that are needed for this assay to work. This mixture will boil in the microwave. You will have to monitor it continuously with intermittent swirling. It will become very frothy while boiling (make sure to not spill it inside the microwave). The froth will go away eventually. Make sure to cool it a little bit before mixing with the other flask.

Once both the flasks (A and B) are done, I usually pour B (agar) into A (YNB/Bismuth). That way, I know that nothing is left behind from A; remember that A will be turbid even after microwaving. Gently swirl the flask A, so that the agar and the other solution mix well (make sure that there are no bubbles). Pour the mix in 4 plates (100 ml is just enough for 4 plates). I do not use any pipette for plating because I fear that the heat dissipation will solidify the mixture quicker. Just make sure that the plates are fully covered and there are no air bubbles.

Site-Directed Mutagenesis of Hgt1 transporter

Some important points before the actual protocol:

- Spin down primers – make 1 µg/µl stock and then make 50 ng/µl working stocks for a total of 100 µl.
- Make 50 ng/µl template DNA stock.

QuickChange II Mutagenesis protocol:

1. Design primers for PCR using template DNA and Agilent Primer Design program.
2. Set up the PCR reaction with the mutagenesis primers.
3. Run 5 µl of PCR product on agarose gel to make sure that the PCR worked.

4. Add 1 µl of DpnI to the remaining PCR reaction mix and incubate at 37 °C for 1 – 1.5 hour to digest the template DNA.
5. Transform 1 µl DpnI digested DNA into 100 µl competent *E. coli* cells and spread the cells with glass beads on LB plates with appropriate antibiotic.
6. The reaction conditions are listed in Table 5.5 and 5.6.

Table 5.5: Reaction mixture for a single PCR (Polymerase Chain Reaction) mix.

Reagents	**Volume (µl)**
10X Pfu AD/Ultra buffer	5
DNA template	1 (Stock 50 ng/µl)
dNTP	1 (Stock 10 mM)
Forward primer	2.5
Reverse primer	2.5
Enzyme (Pfu)	1
MilliQ Water	37

Table 5.6: Thermal Cycler program used for the site directed mutagenesis of Hgt1 transporter using the QuickChange II mutagenesis protocol.

Serial number	**Temperature (°C)**	**Time**
1	95	30 sec
2	95	30 sec
3	55	1 min
4	68	1 min/kb plasmid length
5	Repeat 2 - 4	15 times
6	68	10 min
7	4	hold

References

106. Hu, J., Dong, L., and Outten, C. E. (2008) The redox environment in the mitochondrial intermembrane space is maintained separately from the cytosol and matrix. *J Biol Chem* **283**, 29126-29134

129. Anderson, M. E. (1985) Determination of glutathione and glutathione disulfide in biological samples. *Methods Enzymol* **113**, 548-555

143. Hughes, C. E., Coody, T. K., Jeong, M. Y., Berg, J. A., Winge, D. R., and Hughes, A. L. (2020) Cysteine Toxicity Drives Age-Related Mitochondrial Decline by Altering Iron Homeostasis. *Cell* **180**, 296-310 e218

144. Ozer, H. K., Dlouhy, A. C., Thornton, J. D., Hu, J., Liu, Y., Barycki, J. J., Balk, J., and Outten, C. E. (2015) Cytosolic Fe-S Cluster Protein Maturation and Iron Regulation Are Independent of the Mitochondrial Erv1/Mia40 Import System. *J Biol Chem* **290**, 27829-27840

145. Thomas, D., Barbey, R., Henry, D., and Surdin-Kerjan, Y. (1992) Physiological analysis of mutants of Saccharomyces cerevisiae impaired in sulphate assimilation. *J Gen Microbiol* **138**, 2021-2028

148. Strain, J., Lorenz, C. R., Bode, J., Garland, S., Smolen, G. A., Ta, D. T., Vickery, L. E., and Culotta, V. C. (1998) Suppressors of superoxide dismutase (SOD1) deficiency in Saccharomyces cerevisiae. Identification of proteins predicted to mediate iron-sulfur cluster assembly. *J Biol Chem* **273**, 31138-31144

157. Outten, C. E., and Culotta, V. C. (2003) A novel NADH kinase is the mitochondrial source of NADPH in Saccharomyces cerevisiae. *Embo j* **22**, 2015-2024

160. Rahman, I., Kode, A., and Biswas, S. K. (2006) Assay for quantitative determination of glutathione and glutathione disulfide levels using enzymatic recycling method. *Nat Protoc* **1**, 3159-3165

161. Orij, R., Postmus, J., Ter Beek, A., Brul, S., and Smits, G. J. (2009) In vivo measurement of cytosolic and mitochondrial pH using a pH-sensitive GFP derivative in Saccharomyces cerevisiae reveals a relation between intracellular pH and growth. *Microbiology (Reading)* **155**, 268-278

162. McIlvaine, T. C. (1921) A BUFFER SOLUTION FOR COLORIMETRIC COMPARISON. *Journal of Biological Chemistry* **49**, 183-186

163. Outten, C. E., and Culotta, V. C. (2004) Alternative start sites in the Saccharomyces cerevisiae GLR1 gene are responsible for mitochondrial and cytosolic isoforms of glutathione reductase. *J Biol Chem* **279**, 7785-7791

164. Pierik, A. J., Netz, D. J. A., and Lill, R. (2009) Analysis of iron–sulfur protein maturation in eukaryotes. *Nature Protocols* **4**, 753-766

COMPLETE BIBLIOGRAPHY

1. Aller, I., Rouhier, N., and Meyer, A. J. (2013) Development of roGFP2-derived redox probes for measurement of the glutathione redox potential in the cytosol of severely glutathione-deficient rml1 seedlings. Front Plant Sci 4, 506

2. Mari, M., Morales, A., Colell, A., Garcia-Ruiz, C., and Fernandez-Checa, J. C. (2009) Mitochondrial glutathione, a key survival antioxidant. *Antioxid Redox Signal* **11**, 2685-2700

3. Herrero, E., Belli, G., and Casa, C. (2010) Structural and functional diversity of glutaredoxins in yeast. *Curr Protein Pept Sci* **11**, 659-668

4. Deponte, M. (2017) The Incomplete Glutathione Puzzle: Just Guessing at Numbers and Figures? *Antioxid Redox Signal* **27**, 1130-1161

5. Hanschmann, E. M., Godoy, J. R., Berndt, C., Hudemann, C., and Lillig, C. H. (2013) Thioredoxins, glutaredoxins, and peroxiredoxins--molecular mechanisms and health significance: from cofactors to antioxidants to redox signaling. *Antioxid Redox Signal* **19**, 1539-1605

6. Jacquot, J. P., and Zaffagnini, M. (2019) Thioredoxin and Glutaredoxin Systems Antioxidants Special Issue. *Antioxidants (Basel)* **8**

7. Lillig, C. H., and Berndt, C. (2013) Glutaredoxins in thiol/disulfide exchange. *Antioxid Redox Signal* **18**, 1654-1665

8. Lillig, C. H., Berndt, C., and Holmgren, A. (2008) Glutaredoxin systems. *Biochim Biophys Acta* **1780**, 1304-1317

9. Toledano, M. B., and Huang, M. E. (2017) The Unfinished Puzzle of Glutathione Physiological Functions, an Old Molecule That Still Retains Many Enigmas. *Antioxid Redox Signal* **27**, 1127-1129

10. Herrero, E., Ros, J., Belli, G., and Cabiscol, E. (2008) Redox control and oxidative stress in yeast cells. *Biochim Biophys Acta* **1780**, 1217-1235

11. Kumar, C., Igbaria, A., D'Autreaux, B., Planson, A. G., Junot, C., Godat, E., Bachhawat, A. K., Delaunay-Moisan, A., and Toledano, M. B. (2011) Glutathione revisited: a vital function in iron metabolism and ancillary role in thiol-redox control. *EMBO J* **30**, 2044-2056

12. Li, J., and Cowan, J. A. (2015) Glutathione-coordinated [2Fe-2S] cluster: a viable physiological substrate for mitochondrial ABCB7 transport. *Chem Commun (Camb)* **51**, 2253-2255

13. Lill, R., Dutkiewicz, R., Freibert, S. A., Heidenreich, T., Mascarenhas, J., Netz, D. J., Paul, V. D., Pierik, A. J., Richter, N., Stumpfig, M., Srinivasan, V., Stehling, O., and Muhlenhoff, U. (2015) The role of mitochondria and the CIA machinery in the maturation of cytosolic and nuclear iron-sulfur proteins. *Eur J Cell Biol* **94**, 280-291

14. Balk, J., and Schaedler, T. A. (2014) Iron cofactor assembly in plants. *Annu Rev Plant Biol* **65**, 125-153

15. Schaedler, T. A., Faust, B., Shintre, C. A., Carpenter, E. P., Srinivasan, V., van Veen, H. W., and Balk, J. (2015) Structures and functions of mitochondrial ABC transporters. *Biochem Soc Trans* **43**, 943-951

16. Srinivasan, V., Pierik, A. J., and Lill, R. (2014) Crystal structures of nucleotide-free and glutathione-bound mitochondrial ABC transporter Atm1. *Science* **343**, 1137-1140

17. Berndt, C., and Lillig, C. H. (2017) Glutathione, Glutaredoxins, and Iron. *Antioxid Redox Signal* **27**, 1235-1251

18. Braymer, J. J., and Lill, R. (2017) Iron-sulfur cluster biogenesis and trafficking in mitochondria. *J Biol Chem* **292**, 12754-12763

19. Jia, M., Sen, S., Wachnowsky, C., Fidai, I., Cowan, J. A., and Wysocki, V. H. (2020) Characterization of [2Fe-2S]-Cluster-Bridged Protein Complexes and Reaction Intermediates by use of Native Mass Spectrometric Methods. *Angew Chem Int Ed Engl* **59**, 6724-6728

20. Lill, R., and Freibert, S. A. (2020) Mechanisms of Mitochondrial Iron-Sulfur Protein Biogenesis. *Annu Rev Biochem* **89**, 471-499

21. Abdalla, M., Dai, Y. N., Chi, C. B., Cheng, W., Cao, D. D., Zhou, K., Ali, W., Chen, Y., and Zhou, C. Z. (2016) Crystal structure of yeast monothiol glutaredoxin Grx6 in complex with a glutathione-coordinated [2Fe-2S] cluster. *Acta Crystallogr F Struct Biol Commun* **72**, 732-737

22. Izquierdo, A., Casas, C., Muhlenhoff, U., Lillig, C. H., and Herrero, E. (2008) Saccharomyces cerevisiae Grx6 and Grx7 are monothiol glutaredoxins associated with the early secretory pathway. *Eukaryot Cell* **7**, 1415-1426

23. Mesecke, N., Mittler, S., Eckers, E., Herrmann, J. M., and Deponte, M. (2008) Two novel monothiol glutaredoxins from Saccharomyces cerevisiae provide further insight into iron-sulfur cluster binding, oligomerization, and enzymatic activity of glutaredoxins. *Biochemistry* **47**, 1452-1463

24. Schafer, F. Q., and Buettner, G. R. (2001) Redox environment of the cell as viewed through the redox state of the glutathione disulfide/glutathione couple. *Free Radic Biol Med* **30**, 1191-1212

25. Dalvi, S. M., Patil, V. W., and Ramraje, N. N. (2012) The roles of glutathione, glutathione peroxidase, glutathione reductase and the carbonyl protein in pulmonary and extra pulmonary tuberculosis. *J Clin Diagn Res* **6**, 1462-1465

26. Couto, N., Wood, J., and Barber, J. (2016) The role of glutathione reductase and related enzymes on cellular redox homoeostasis network. *Free Radic Biol Med* **95**, 27-42

27. Aquilano, K., Baldelli, S., and Ciriolo, M. R. (2014) Glutathione: new roles in redox signaling for an old antioxidant. *Front Pharmacol* **5**, 196

28. Lill, R. (2009) Function and biogenesis of iron-sulphur proteins. *Nature* **460**, 831-838

29. Ribas, V., Garcia-Ruiz, C., and Fernandez-Checa, J. C. (2014) Glutathione and mitochondria. *Front Pharmacol* **5**, 151

30. Pompella, A., Visvikis, A., Paolicchi, A., De Tata, V., and Casini, A. F. (2003) The changing faces of glutathione, a cellular protagonist. *Biochem Pharmacol* **66**, 1499-1503

31. Valko, M., Leibfritz, D., Moncol, J., Cronin, M. T., Mazur, M., and Telser, J. (2007) Free radicals and antioxidants in normal physiological functions and human disease. *Int J Biochem Cell Biol* **39**, 44-84

32. Bien, M., Longen, S., Wagener, N., Chwalla, I., Herrmann, J. M., and Riemer, J. (2010) Mitochondrial disulfide bond formation is driven by intersubunit electron transfer in Erv1 and proofread by glutathione. *Mol Cell* **37**, 516-528

33. Chakravarthi, S., and Bulleid, N. J. (2004) Glutathione is required to regulate the formation of native disulfide bonds within proteins entering the secretory pathway. *J Biol Chem* **279**, 39872-39879

34. Hwang, C., Sinskey, A. J., and Lodish, H. F. (1992) Oxidized redox state of glutathione in the endoplasmic reticulum. *Science* **257**, 1496-1502

35. Molteni, S. N., Fassio, A., Ciriolo, M. R., Filomeni, G., Pasqualetto, E., Fagioli, C., and Sitia, R. (2004) Glutathione limits Ero1-dependent oxidation in the endoplasmic reticulum. *J Biol Chem* **279**, 32667-32673

36. Ayer, A., Tan, S. X., Grant, C. M., Meyer, A. J., Dawes, I. W., and Perrone, G. G. (2010) The critical role of glutathione in maintenance of the mitochondrial genome. *Free Radic Biol Med* **49**, 1956-1968

37. Schaedler, T. A., Thornton, J. D., Kruse, I., Schwarzlander, M., Meyer, A. J., van Veen, H. W., and Balk, J. (2014) A conserved mitochondrial ATP-binding cassette transporter exports glutathione polysulfide for cytosolic metal cofactor assembly. *J Biol Chem* **289**, 23264-23274

38. Montero, D., Tachibana, C., Rahr Winther, J., and Appenzeller-Herzog, C. (2013) Intracellular glutathione pools are heterogeneously concentrated. *Redox Biol* **1**, 508-513

39. Toledano, M. B., Delaunay-Moisan, A., Outten, C. E., and Igbaria, A. (2013) Functions and cellular compartmentation of the thioredoxin and glutathione pathways in yeast. *Antioxid Redox Signal* **18**, 1699-1711

40. Murphy, E. R., Sacco, R. E., Dickenson, A., Metzger, D. J., Hu, Y., Orndorff, P. E., and Connell, T. D. (2002) BhuR, a virulence-associated outer membrane protein of Bordetella avium, is required for the acquisition of iron from heme and hemoproteins. *Infect Immun* **70**, 5390-5403

41. Ribbe, M. W., Hu, Y., Hodgson, K. O., and Hedman, B. (2014) Biosynthesis of nitrogenase metalloclusters. *Chem Rev* **114**, 4063-4080

42. Freibert, S. A., Goldberg, A. V., Hacker, C., Molik, S., Dean, P., Williams, T. A., Nakjang, S., Long, S., Sendra, K., Bill, E., Heinz, E., Hirt, R. P., Lucocq, J. M., Embley, T. M., and Lill, R. (2017) Evolutionary conservation and in vitro reconstitution of microsporidian iron-sulfur cluster biosynthesis. *Nat Commun* **8**, 13932

43. Zheng, L., Cash, V. L., Flint, D. H., and Dean, D. R. (1998) Assembly of iron-sulfur clusters. Identification of an iscSUA-hscBA-fdx gene cluster from Azotobacter vinelandii. *J Biol Chem* **273**, 13264-13272

44. Boniecki, M. T., Freibert, S. A., Muhlenhoff, U., Lill, R., and Cygler, M. (2017) Structure and functional dynamics of the mitochondrial Fe/S cluster synthesis complex. *Nat Commun* **8**, 1287

45. Fox, N. G., Yu, X., Feng, X., Bailey, H. J., Martelli, A., Nabhan, J. F., Strain-Damerell, C., Bulawa, C., Yue, W. W., and Han, S. (2019) Structure of the human frataxin-bound iron-sulfur cluster assembly complex provides insight into its activation mechanism. *Nat Commun* **10**, 2210

46. Uzarska, M. A., Dutkiewicz, R., Freibert, S. A., Lill, R., and Muhlenhoff, U. (2013) The mitochondrial Hsp70 chaperone Ssq1 facilitates Fe/S cluster transfer from Isu1 to Grx5 by complex formation. *Mol Biol Cell* **24**, 1830-1841

47. Kispal, G., Csere, P., Prohl, C., and Lill, R. (1999) The mitochondrial proteins Atm1p and Nfs1p are essential for biogenesis of cytosolic Fe/S proteins. *EMBO J* **18**, 3981-3989

48. Ciofi-Baffoni, S., Nasta, V., and Banci, L. (2018) Protein networks in the maturation of human iron-sulfur proteins. *Metallomics* **10**, 49-72

49. Netz, D. J., Mascarenhas, J., Stehling, O., Pierik, A. J., and Lill, R. (2014) Maturation of cytosolic and nuclear iron-sulfur proteins. *Trends Cell Biol* **24**, 303-312

50. Paul, V. D., and Lill, R. (2015) Biogenesis of cytosolic and nuclear iron-sulfur proteins and their role in genome stability. *Biochim Biophys Acta* **1853**, 1528-1539

51. Balk, J., Aguilar Netz, D. J., Tepper, K., Pierik, A. J., and Lill, R. (2005) The essential WD40 protein Cia1 is involved in a late step of cytosolic and nuclear iron-sulfur protein assembly. *Mol Cell Biol* **25**, 10833-10841

52. Balk, J., Pierik, A. J., Netz, D. J., Muhlenhoff, U., and Lill, R. (2004) The hydrogenase-like Nar1p is essential for maturation of cytosolic and nuclear iron-sulphur proteins. *EMBO J* **23**, 2105-2115

53. Gari, K., Leon Ortiz, A. M., Borel, V., Flynn, H., Skehel, J. M., and Boulton, S. J. (2012) MMS19 links cytoplasmic iron-sulfur cluster assembly to DNA metabolism. *Science* **337**, 243-245

54. Song, D., and Lee, F. S. (2008) A role for IOP1 in mammalian cytosolic iron-sulfur protein biogenesis. *J Biol Chem* **283**, 9231-9238

55. Srinivasan, V., Netz, D. J., Webert, H., Mascarenhas, J., Pierik, A. J., Michel, H., and Lill, R. (2007) Structure of the yeast WD40 domain protein Cia1, a component acting late in iron-sulfur protein biogenesis. *Structure* **15**, 1246-1257

56. Stehling, O., Mascarenhas, J., Vashisht, A. A., Sheftel, A. D., Niggemeyer, B., Rosser, R., Pierik, A. J., Wohlschlegel, J. A., and Lill, R. (2013) Human CIA2A-FAM96A and CIA2B-FAM96B integrate iron homeostasis and maturation of different subsets of cytosolic-nuclear iron-sulfur proteins. *Cell Metab* **18**, 187-198

57. Bernard, D. G., Cheng, Y., Zhao, Y., and Balk, J. (2009) An allelic mutant series of ATM3 reveals its key role in the biogenesis of cytosolic iron-sulfur proteins in Arabidopsis. *Plant Physiol* **151**, 590-602

58. Cavadini, P., Biasiotto, G., Poli, M., Levi, S., Verardi, R., Zanella, I., Derosas, M., Ingrassia, R., Corrado, M., and Arosio, P. (2007) RNA silencing of the mitochondrial ABCB7 transporter in HeLa cells causes an iron-deficient phenotype with mitochondrial iron overload. *Blood* **109**, 3552-3559

59. Garcia-Santamarina, S., Uzarska, M. A., Festa, R. A., Lill, R., and Thiele, D. J. (2017) Cryptococcus neoformans Iron-Sulfur Protein Biogenesis Machinery Is a Novel Layer of Protection against Cu Stress. *mBio* **8**

60. Kushnir, S., Babiychuk, E., Storozhenko, S., Davey, M. W., Papenbrock, J., De Rycke, R., Engler, G., Stephan, U. W., Lange, H., Kispal, G., Lill, R., and Van Montagu, M. (2001) A mutation of the mitochondrial ABC transporter Sta1 leads to dwarfism and chlorosis in the Arabidopsis mutant starik. *Plant Cell* **13**, 89-100

61. Pondarre, C., Antiochos, B. B., Campagna, D. R., Clarke, S. L., Greer, E. L., Deck, K. M., McDonald, A., Han, A. P., Medlock, A., Kutok, J. L., Anderson, S. A., Eisenstein, R. S., and Fleming, M. D. (2006) The mitochondrial ATP-binding cassette transporter Abcb7 is essential in mice and participates in cytosolic iron-sulfur cluster biogenesis. *Hum Mol Genet* **15**, 953-964

62. Wang, Z., Ma, T., Huang, Y., Wang, J., Chen, Y., Kistler, H. C., Ma, Z., and Yin, Y. (2019) A fungal ABC transporter FgAtm1 regulates iron homeostasis via the transcription factor cascade FgAreA-HapX. *PLoS Pathog* **15**, e1007791

63. Zuo, J., Wu, Z., Li, Y., Shen, Z., Feng, X., Zhang, M., and Ye, H. (2017) Mitochondrial ABC Transporter ATM3 Is Essential for Cytosolic Iron-Sulfur Cluster Assembly. *Plant Physiol* **173**, 2096-2109

64. Kispal, G., Csere, P., Guiard, B., and Lill, R. (1997) The ABC transporter Atm1p is required for mitochondrial iron homeostasis. *FEBS Lett* **418**, 346-350

65. Miao, R., Kim, H., Koppolu, U. M., Ellis, E. A., Scott, R. A., and Lindahl, P. A. (2009) Biophysical characterization of the iron in mitochondria from Atm1p-depleted Saccharomyces cerevisiae. *Biochemistry* **48**, 9556-9568

66. Sipos, K., Lange, H., Fekete, Z., Ullmann, P., Lill, R., and Kispal, G. (2002) Maturation of cytosolic iron-sulfur proteins requires glutathione. *J Biol Chem* **277**, 26944-26949

67. Braymer, J. J., Stumpfig, M., Thelen, S., Muhlenhoff, U., and Lill, R. (2019) Depletion of thiol reducing capacity impairs cytosolic but not mitochondrial iron-sulfur protein assembly machineries. *Biochim Biophys Acta Mol Cell Res* **1866**, 240-251

68. Balijepalli, S., Boyd, M. R., and Ravindranath, V. (1999) Inhibition of mitochondrial complex I by haloperidol: the role of thiol oxidation. *Neuropharmacology* **38**, 567-577

69. Qi, W., Li, J., and Cowan, J. A. (2014) A structural model for glutathione-complexed iron-sulfur cluster as a substrate for ABCB7-type transporters. *Chem Commun (Camb)* **50**, 3795-3798

70. Kuhnke, G., Neumann, K., Muhlenhoff, U., and Lill, R. (2006) Stimulation of the ATPase activity of the yeast mitochondrial ABC transporter Atm1p by thiol compounds. *Mol Membr Biol* **23**, 173-184

71. Li, L., Lee, T. K., Meier, P. J., and Ballatori, N. (1998) Identification of glutathione as a driving force and leukotriene C4 as a substrate for oatp1, the hepatic sinusoidal organic solute transporter. *J Biol Chem* **273**, 16184-16191

72. Rebbeor, J. F., Connolly, G. C., Dumont, M. E., and Ballatori, N. (1998) ATP-dependent transport of reduced glutathione on YCF1, the yeast orthologue of mammalian multidrug resistance associated proteins. *J Biol Chem* **273**, 33449-33454

73. Rebbeor, J. F., Connolly, G. C., Dumont, M. E., and Ballatori, N. (1998) ATP-dependent transport of reduced glutathione in yeast secretory vesicles. *Biochem J* **334 (Pt 3)**, 723-729

74. Rappa, G., Lorico, A., Flavell, R. A., and Sartorelli, A. C. (1997) Evidence that the multidrug resistance protein (MRP) functions as a co-transporter of glutathione and natural product toxins. *Cancer Res* **57**, 5232-5237

75. Bourbouloux, A., Shahi, P., Chakladar, A., Delrot, S., and Bachhawat, A. K. (2000) Hgt1p, a high affinity glutathione transporter from the yeast Saccharomyces cerevisiae. *J Biol Chem* **275**, 13259-13265

76. Bachhawat, A. K., Thakur, A., Kaur, J., and Zulkifli, M. (2013) Glutathione transporters. *Biochim Biophys Acta* **1830**, 3154-3164

77. Curie, C., Panaviene, Z., Loulergue, C., Dellaporta, S. L., Briat, J. F., and Walker, E. L. (2001) Maize yellow stripe1 encodes a membrane protein directly involved in Fe(III) uptake. *Nature* **409**, 346-349

78. Thakur, A., and Bachhawat, A. K. (2010) The role of transmembrane domain 9 in substrate recognition by the fungal high-affinity glutathione transporters. *Biochem J* **429**, 593-602

79. Kaur, J., and Bachhawat, A. K. (2009) Gln-222 in transmembrane domain 4 and Gln-526 in transmembrane domain 9 are critical for substrate recognition in the yeast high affinity glutathione transporter, Hgt1p. *J Biol Chem* **284**, 23872-23884

80. Banhegyi, G., Lusini, L., Puskas, F., Rossi, R., Fulceri, R., Braun, L., Mile, V., di Simplicio, P., Mandl, J., and Benedetti, A. (1999) Preferential transport of glutathione versus glutathione disulfide in rat liver microsomal vesicles. *J Biol Chem* **274**, 12213-12216

81. Ponsero, A. J., Igbaria, A., Darch, M. A., Miled, S., Outten, C. E., Winther, J. R., Palais, G., D'Autréaux, B., Delaunay-Moisan, A., and Toledano, M. B. (2017)

Endoplasmic Reticulum Transport of Glutathione by Sec61 Is Regulated by Ero1 and Bip. *Mol Cell* **67**, 962-973.e965

82. Preston, R. A., Murphy, R. F., and Jones, E. W. (1989) Assay of vacuolar pH in yeast and identification of acidification-defective mutants. *Proc Natl Acad Sci U S A* **86**, 7027-7031

83. Brett, C. L., Tukaye, D. N., Mukherjee, S., and Rao, R. (2005) The yeast endosomal Na+K+/H+ exchanger Nhx1 regulates cellular pH to control vesicle trafficking. *Mol Biol Cell* **16**, 1396-1405

84. Martinez-Munoz, G. A., and Kane, P. (2008) Vacuolar and plasma membrane proton pumps collaborate to achieve cytosolic pH homeostasis in yeast. *J Biol Chem* **283**, 20309-20319

85. Nishimura, K., Igarashi, K., and Kakinuma, Y. (1998) Proton gradient-driven nickel uptake by vacuolar membrane vesicles of Saccharomyces cerevisiae. *J Bacteriol* **180**, 1962-1964

86. Ohsumi, Y., and Anraku, Y. (1981) Active transport of basic amino acids driven by a proton motive force in vacuolar membrane vesicles of Saccharomyces cerevisiae. *J Biol Chem* **256**, 2079-2082

87. Llopis, J., McCaffery, J. M., Miyawaki, A., Farquhar, M. G., and Tsien, R. Y. (1998) Measurement of cytosolic, mitochondrial, and Golgi pH in single living cells with green fluorescent proteins. *Proc Natl Acad Sci U S A* **95**, 6803-6808

88. van Roermund, C. W., de Jong, M., L, I. J., van Marle, J., Dansen, T. B., Wanders, R. J., and Waterham, H. R. (2004) The peroxisomal lumen in Saccharomyces cerevisiae is alkaline. *J Cell Sci* **117**, 4231-4237

89. Paroutis, P., Touret, N., and Grinstein, S. (2004) The pH of the secretory pathway: measurement, determinants, and regulation. *Physiology (Bethesda)* **19**, 207-215

90. Dancourt, J., and Barlowe, C. (2010) Protein sorting receptors in the early secretory pathway. *Annu Rev Biochem* **79**, 777-802

91. Appenzeller-Herzog, C., Roche, A. C., Nufer, O., and Hauri, H. P. (2004) pH-induced conversion of the transport lectin ERGIC-53 triggers glycoprotein release. *J Biol Chem* **279**, 12943-12950

92. Scheel, A. A., and Pelham, H. R. (1996) Purification and characterization of the human KDEL receptor. *Biochemistry* **35**, 10203-10209

93. Wilson, D. W., Lewis, M. J., and Pelham, H. R. (1993) pH-dependent binding of KDEL to its receptor in vitro. *J Biol Chem* **268**, 7465-7468

94. Vavassori, S., Cortini, M., Masui, S., Sannino, S., Anelli, T., Caserta, I. R., Fagioli, C., Mossuto, M. F., Fornili, A., van Anken, E., Degano, M., Inaba, K., and Sitia, R. (2013) A pH-regulated quality control cycle for surveillance of secretory protein assembly. *Mol Cell* **50**, 783-792

95. Sannino, S., Anelli, T., Cortini, M., Masui, S., Degano, M., Fagioli, C., Inaba, K., and Sitia, R. (2014) Progressive quality control of secretory proteins in the early secretory compartment by ERp44. *J Cell Sci* **127**, 4260-4269

96. Watanabe, S., Harayama, M., Kanemura, S., Sitia, R., and Inaba, K. (2017) Structural basis of pH-dependent client binding by ERp44, a key regulator of protein secretion at the ER-Golgi interface. *Proc Natl Acad Sci U S A* **114**, E3224-E3232

97. Shibuya, A., Margulis, N., Christiano, R., Walther, T. C., and Barlowe, C. (2015) The Erv41-Erv46 complex serves as a retrograde receptor to retrieve escaped ER proteins. *J Cell Biol* **208**, 197-209

98. Gillies, R. J., Ugurbil, K., den Hollander, J. A., and Shulman, R. G. (1981) 31P NMR studies of intracellular pH and phosphate metabolism during cell division cycle of Saccharomyces cerevisiae. *Proc Natl Acad Sci U S A* **78**, 2125-2129

99. Bracey, D., Holyoak, C. D., and Coote, P. J. (1998) Comparison of the inhibitory effect of sorbic acid and amphotericin B on Saccharomyces cerevisiae: is growth inhibition dependent on reduced intracellular pH? *J Appl Microbiol* **85**, 1056-1066

100. Lanz, E., Slavik, J., and Kotyk, A. (1999) 2',7'-bis-(2-carboxyethyl)-5(6)-carboxyfluorescein as a dual-emission fluorescent indicator of intracellular pH suitable for argon laser confocal microscopy. *Folia Microbiol (Praha)* **44**, 429-434

101. Krebs, H. A., Wiggins, D., Stubbs, M., Sols, A., and Bedoya, F. (1983) Studies on the mechanism of the antifungal action of benzoate. *Biochem J* **214**, 657-663

102. Kresnowati, M. T., Suarez-Mendez, C., Groothuizen, M. K., van Winden, W. A., and Heijnen, J. J. (2007) Measurement of fast dynamic intracellular pH in Saccharomyces cerevisiae using benzoic acid pulse. *Biotechnol Bioeng* **97**, 86-98

103. Ostergaard, H., Henriksen, A., Hansen, F. G., and Winther, J. R. (2001) Shedding light on disulfide bond formation: engineering a redox switch in green fluorescent protein. *EMBO J* **20**, 5853-5862

104. Dooley, C. T., Dore, T. M., Hanson, G. T., Jackson, W. C., Remington, S. J., and Tsien, R. Y. (2004) Imaging dynamic redox changes in mammalian cells with green fluorescent protein indicators. *J Biol Chem* **279**, 22284-22293

105. Miesenbock, G., De Angelis, D. A., and Rothman, J. E. (1998) Visualizing secretion and synaptic transmission with pH-sensitive green fluorescent proteins. *Nature* **394**, 192-195

106. Hu, J., Dong, L., and Outten, C. E. (2008) The redox environment in the mitochondrial intermembrane space is maintained separately from the cytosol and matrix. *J Biol Chem* **283**, 29126-29134

107. Ostergaard, H., Tachibana, C., and Winther, J. R. (2004) Monitoring disulfide bond formation in the eukaryotic cytosol. *J Cell Biol* **166**, 337-345

108. Wachter, R. M., Yarbrough, D., Kallio, K., and Remington, S. J. (2000) Crystallographic and energetic analysis of binding of selected anions to the yellow variants of green fluorescent protein. *J Mol Biol* **301**, 157-171

109. Hanson, G. T., Aggeler, R., Oglesbee, D., Cannon, M., Capaldi, R. A., Tsien, R. Y., and Remington, S. J. (2004) Investigating mitochondrial redox potential with redox-sensitive green fluorescent protein indicators. *J Biol Chem* **279**, 13044-13053

110. Gietz, R. D., and Schiestl, R. H. (1991) Applications of high efficiency lithium acetate transformation of intact yeast cells using single-stranded nucleic acids as carrier. *Yeast* **7**, 253-263

111. McGee, C. C. (2019) *Impact of Glutathione Transporters on Subcellular Glutathione Pools and Cell Survival in Saccharomyces Cerevisiae.* PhD Doctoral dissertation, University of South Carolina

112. Orij, R., Postmus, J., Ter Beek, A., Brul, S., and Smits, G. J. (2009) In vivo measurement of cytosolic and mitochondrial pH using a pH-sensitive GFP

derivative in Saccharomyces cerevisiae reveals a relation between intracellular pH and growth. *Microbiology* **155**, 268-278

113. Hu, J. (2010) Investigating Subcellular Thiol Redox Chemistry with GFP-based Sensors. *Doctoral dissertation*

114. Darch, A. M. (2015) Subcellular glutathione distribution during severe redox stress and characterizing thiol redox control of human Cu, Zn superoxide dismutase. *Doctoral dissertation*

115. Bagar, T., Altenbach, K., Read, N. D., and Bencina, M. (2009) Live-Cell imaging and measurement of intracellular pH in filamentous fungi using a genetically encoded ratiometric probe. *Eukaryot Cell* **8**, 703-712

116. Martinière, A., Desbrosses, G., Sentenac, H., and Paris, N. (2013) Development and properties of genetically encoded pH sensors in plants. *Frontiers in Plant Science* **4**

117. Jamai, A., Tommasini, R., Martinoia, E., and Delrot, S. (1996) Characterization of Glutathione Uptake in Broad Bean Leaf Protoplasts. *Plant Physiol* **111**, 1145-1152

118. Cortese, J. D., Voglino, A. L., and Hackenbrock, C. R. (1992) The ionic strength of the intermembrane space of intact mitochondria is not affected by the pH or volume of the intermembrane space. *Biochim Biophys Acta* **1100**, 189-197

119. Morth, J. P., Pedersen, B. P., Buch-Pedersen, M. J., Andersen, J. P., Vilsen, B., Palmgren, M. G., and Nissen, P. (2011) A structural overview of the plasma membrane Na+,K+-ATPase and H+-ATPase ion pumps. *Nat Rev Mol Cell Biol* **12**, 60-70

120. Osawa, H., Stacey, G., and Gassmann, W. (2006) ScOPT1 and AtOPT4 function as proton-coupled oligopeptide transporters with broad but distinct substrate specificities. *Biochem J* **393**, 267-275

121. Sze, H., Li, X., and Palmgren, M. G. (1999) Energization of plant cell membranes by H+-pumping ATPases. Regulation and biosynthesis. *Plant Cell* **11**, 677-690

122. Bogs, J., Bourbouloux, A., Cagnac, O., Wachter, A., Rausch, T., and Delrot, S. (2003) Functional characterization and expression analysis of a glutathione transporter, BjGT1, from Brassica juncea: evidence for regulation by heavy metal exposure. *Plant, Cell & Environment* **26**, 1703-1711

123. Koh, S., Wiles, A. M., Sharp, J. S., Naider, F. R., Becker, J. M., and Stacey, G. (2002) An oligopeptide transporter gene family in Arabidopsis. *Plant Physiol* **128**, 21-29

124. Vasconcelos, M. W., Li, G. W., Lubkowitz, M. A., and Grusak, M. A. (2008) Characterization of the PT Clade of Oligopeptide Transporters in Rice. *The Plant Genome* **1**

125. Zulkifli, M., Yadav, S., Thakur, A., Singla, S., Sharma, M., and Bachhawat, A. K. (2016) Substrate specificity and mapping of residues critical for transport in the high-affinity glutathione transporter Hgt1p. *Biochem J* **473**, 2369-2382

126. Kaur, J., Srikanth, C. V., and Bachhawat, A. K. (2009) Differential roles played by the native cysteine residues of the yeast glutathione transporter, Hgt1p. *FEMS Yeast Res* **9**, 849-866

127. Cubitt, A. B., Heim, R., Adams, S. R., Boyd, A. E., Gross, L. A., and Tsien, R. Y. (1995) Understanding, improving and using green fluorescent proteins. *Trends Biochem Sci* **20**, 448-455

128. Sikorski, R. S., and Hieter, P. (1989) A system of shuttle vectors and yeast host strains designed for efficient manipulation of DNA in Saccharomyces cerevisiae. *Genetics* **122**, 19-27

129. Anderson, M. E. (1985) Determination of glutathione and glutathione disulfide in biological samples. *Methods Enzymol* **113**, 548-555

130. Zulkifli, M., and Bachhawat, A. K. (2017) Identification of residues critical for proton-coupled glutathione translocation in the yeast glutathione transporter, Hgt1p. *Biochemical Journal* **474**, 1807-1821

131. Kaur, H., Ganguli, D., and Bachhawat, A. K. (2012) Glutathione degradation by the alternative pathway (DUG pathway) in Saccharomyces cerevisiae is initiated by (Dug2p-Dug3p)2 complex, a novel glutamine amidotransferase (GATase) enzyme acting on glutathione. *J Biol Chem* **287**, 8920-8931

132. Meister, A., and Anderson, M. E. (1983) Glutathione. *Annu Rev Biochem* **52**, 711-760

133. May, M. J., Vernoux, T., Sanchez-Fernandez, R., Van Montagu, M., and Inze, D. (1998) Evidence for posttranscriptional activation of gamma-glutamylcysteine synthetase during plant stress responses. *Proc Natl Acad Sci U S A* **95**, 12049-12054

134. Bachhawat, A. K., and Yadav, S. (2018) The glutathione cycle: Glutathione metabolism beyond the γ-glutamyl cycle. *IUBMB Life* **70**, 585-592

135. Smith, C. V., Jones, D. P., Guenthner, T. M., Lash, L. H., and Lauterburg, B. H. (1996) Compartmentation of glutathione: implications for the study of toxicity and disease. *Toxicol Appl Pharmacol* **140**, 1-12

136. Herzenberg, L. A., De Rosa, S. C., Dubs, J. G., Roederer, M., Anderson, M. T., Ela, S. W., Deresinski, S. C., and Herzenberg, L. A. (1997) Glutathione deficiency is associated with impaired survival in HIV disease. *Proc Natl Acad Sci U S A* **94**, 1967-1972

137. Oestreicher, J., and Morgan, B. (2018) Glutathione: subcellular distribution and membrane transport. *Biochemistry and Cell Biology* **97**, 270-289

138. Garcia-Ruiz, C., Morales, A., Colell, A., Rodes, J., Yi, J. R., Kaplowitz, N., and Fernandez-Checa, J. C. (1995) Evidence that the rat hepatic mitochondrial carrier is distinct from the sinusoidal and canalicular transporters for reduced glutathione. Expression studies in Xenopus laevis oocytes. *J Biol Chem* **270**, 15946-15949

139. Ballatori, N., and Dutczak, W. J. (1994) Identification and characterization of high and low affinity transport systems for reduced glutathione in liver cell canalicular membranes. *J Biol Chem* **269**, 19731-19737

140. Lill, R., Dutkiewicz, R., Freibert, S. A., Heidenreich, T., Mascarenhas, J., Netz, D. J., Paul, V. D., Pierik, A. J., Richter, N., Stümpfig, M., Srinivasan, V., Stehling, O., and Mühlenhoff, U. (2015) The role of mitochondria and the CIA machinery in the maturation of cytosolic and nuclear iron–sulfur proteins. *European Journal of Cell Biology* **94**, 280-291

141. Daniel, T., Faruq, H. M., Laura Magdalena, J., Manuela, G., and Christopher Horst, L. (2020) Role of GSH and Iron-Sulfur Glutaredoxins in Iron Metabolism—Review. *Molecules* **25**

142. Talib, E. A., and Outten, C. E. (2021) Iron-sulfur cluster biogenesis, trafficking, and signaling: Roles for CGFS glutaredoxins and BolA proteins. *Biochim Biophys Acta Mol Cell Res* **1868**, 118847

143. Hughes, C. E., Coody, T. K., Jeong, M. Y., Berg, J. A., Winge, D. R., and Hughes, A. L. (2020) Cysteine Toxicity Drives Age-Related Mitochondrial Decline by Altering Iron Homeostasis. *Cell* **180**, 296-310 e218

144. Ozer, H. K., Dlouhy, A. C., Thornton, J. D., Hu, J., Liu, Y., Barycki, J. J., Balk, J., and Outten, C. E. (2015) Cytosolic Fe-S Cluster Protein Maturation and Iron Regulation Are Independent of the Mitochondrial Erv1/Mia40 Import System. *J Biol Chem* **290**, 27829-27840

145. Thomas, D., Barbey, R., Henry, D., and Surdin-Kerjan, Y. (1992) Physiological analysis of mutants of Saccharomyces cerevisiae impaired in sulphate assimilation. *J Gen Microbiol* **138**, 2021-2028

146. Kaur, J., and Bachhawat, A. K. (2007) Yct1p, a novel, high-affinity, cysteine-specific transporter from the yeast Saccharomyces cerevisiae. *Genetics* **176**, 877-890

147. Daum, G., Bohni, P. C., and Schatz, G. (1982) Import of proteins into mitochondria. Cytochrome b2 and cytochrome c peroxidase are located in the intermembrane space of yeast mitochondria. *J Biol Chem* **257**, 13028-13033

148. Strain, J., Lorenz, C. R., Bode, J., Garland, S., Smolen, G. A., Ta, D. T., Vickery, L. E., and Culotta, V. C. (1998) Suppressors of superoxide dismutase (SOD1) deficiency in Saccharomyces cerevisiae. Identification of proteins predicted to mediate iron-sulfur cluster assembly. *J Biol Chem* **273**, 31138-31144

149. Pierik, A. J., Netz, D. J., and Lill, R. (2009) Analysis of iron-sulfur protein maturation in eukaryotes. *Nat Protoc* **4**, 753-766

150. Park, E. J., Min, K. J., Lee, T. J., Yoo, Y. H., Kim, Y. S., and Kwon, T. K. (2014) beta-Lapachone induces programmed necrosis through the RIP1-PARP-AIF-dependent pathway in human hepatocellular carcinoma SK-Hep1 cells. *Cell Death Dis* **5**, e1230

151. Irani, K., Xia, Y., Zweier, J. L., Sollott, S. J., Der, C. J., Fearon, E. R., Sundaresan, M., Finkel, T., and Goldschmidt-Clermont, P. J. (1997) Mitogenic signaling mediated by oxidants in Ras-transformed fibroblasts. *Science* **275**, 1649-1652

152. Le Gal, K., Ibrahim, M. X., Wiel, C., Sayin, V. I., Akula, M. K., Karlsson, C., Dalin, M. G., Akyürek, L. M., Lindahl, P., Nilsson, J., and Bergo, M. O. (2015) Antioxidants can increase melanoma metastasis in mice. *Science Translational Medicine* **7**, 308re308

153. Piskounova, E., Agathocleous, M., Murphy, M. M., Hu, Z., Huddlestun, S. E., Zhao, Z., Leitch, A. M., Johnson, T. M., DeBerardinis, R. J., and Morrison, S. J. (2015) Oxidative stress inhibits distant metastasis by human melanoma cells. *Nature* **527**, 186-191

154. Protchenko, O., Ferea, T., Rashford, J., Tiedeman, J., Brown, P. O., Botstein, D., and Philpott, C. C. (2001) Three cell wall mannoproteins facilitate the uptake of iron in Saccharomyces cerevisiae. *J Biol Chem* **276**, 49244-49250

155. Rutherford, J. C., Jaron, S., and Winge, D. R. (2003) Aft1p and Aft2p mediate iron-responsive gene expression in yeast through related promoter elements. *J Biol Chem* **278**, 27636-27643

156. Rutherford, J. C., Ojeda, L., Balk, J., Mühlenhoff, U., Lill, R., and Winge, D. R. (2005) Activation of the iron regulon by the yeast Aft1/Aft2 transcription factors depends on mitochondrial but not cytosolic iron-sulfur protein biogenesis. *J Biol Chem* **280**, 10135-10140

157. Outten, C. E., and Culotta, V. C. (2003) A novel NADH kinase is the mitochondrial source of NADPH in Saccharomyces cerevisiae. *Embo j* **22**, 2015-2024

158. Lill, R., Diekert, K., Kaut, A., Lange, H., Pelzer, W., Prohl, C., and Kispal, G. (1999) The essential role of mitochondria in the biogenesis of cellular iron-sulfur proteins. *Biol Chem* **380**, 1157-1166

159. Poole, L. B. (2015) The basics of thiols and cysteines in redox biology and chemistry. *Free Radic Biol Med* **80**, 148-157

160. Rahman, I., Kode, A., and Biswas, S. K. (2006) Assay for quantitative determination of glutathione and glutathione disulfide levels using enzymatic recycling method. *Nat Protoc* **1**, 3159-3165

161. Orij, R., Postmus, J., Ter Beek, A., Brul, S., and Smits, G. J. (2009) In vivo measurement of cytosolic and mitochondrial pH using a pH-sensitive GFP

derivative in Saccharomyces cerevisiae reveals a relation between intracellular pH and growth. *Microbiology (Reading)* **155**, 268-278

162. McIlvaine, T. C. (1921) A BUFFER SOLUTION FOR COLORIMETRIC COMPARISON. *Journal of Biological Chemistry* **49**, 183-186

163. Outten, C. E., and Culotta, V. C. (2004) Alternative start sites in the Saccharomyces cerevisiae GLR1 gene are responsible for mitochondrial and cytosolic isoforms of glutathione reductase. *J Biol Chem* **279**, 7785-7791

164. Pierik, A. J., Netz, D. J. A., and Lill, R. (2009) Analysis of iron–sulfur protein maturation in eukaryotes. *Nature Protocols* **4**, 753-766